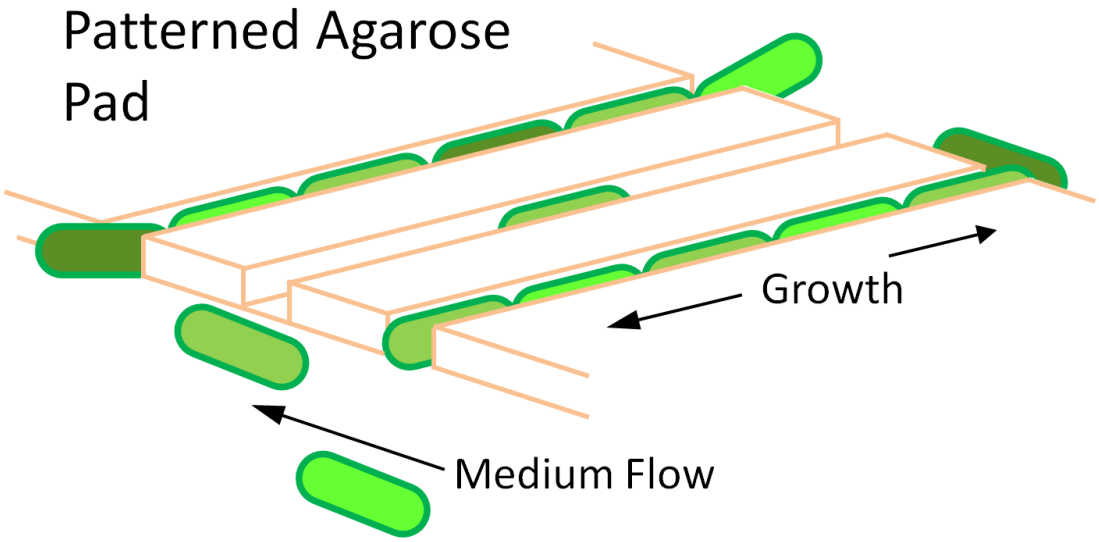

Supplementary Figure 1 | Schematic of the single-cell chemostat: an agarose-based, microfluidic device for high-throughput, single-cell studies of bacteria (43). The patterned agarose pad is depicted in light ochre lines. Printed micro-tracks in the agarose constrain the growth of E. coli cells so that they form linear colonies, depicted in green. As colonies grow, cells get pushed out from the tracks and are washed away by media that flows through gutters on the sides. Since agarose is a porous material, it allows for the free diffusion of nutrients in the media. Cells with different shades of green remind of the intrinsic stochastic nature of transcription with a hypothetical situation in which GFP is driven by a constitutive promoter.

Nature Methods: doi:10.1038/nmeth.4509

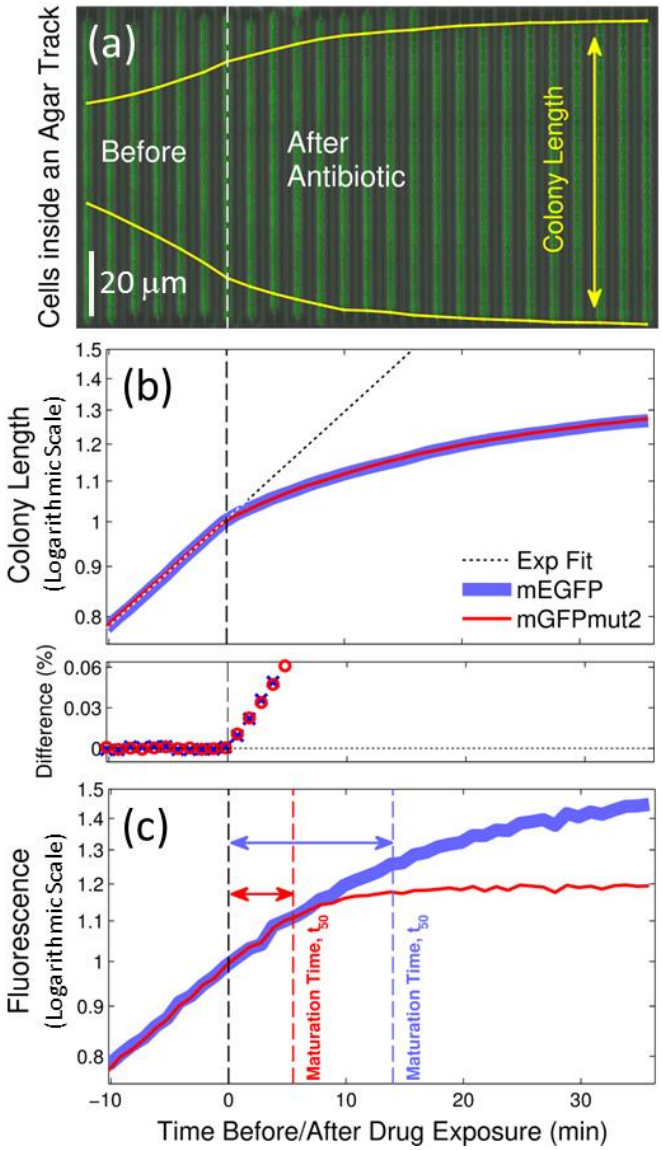

Supplementary Figure 2 | **Single-cell chemostat measurements to determine maturation time of FPs in exponentially growing *Escherichia coli* cells. (a)** Kymograph of linear colonies of *E. coli* growing along agar-printed submicron width tracks. The white dashed line indicates the moment at which chloramphenicol, an inhibitor of protein translation, reaches the cells. Yellow lines delimit cells in the linear colony that completely remain inside the agar tracks, from the start to the end of the experiment. **(b)** Mean single-cell length as a function of time obtained from 75±20 cells and normalized by its value when chloramphenicol arrives. Data for mEGFP is in blue, data for mGFPmut2 in red. Before chloramphenicol reaches the cells, growth is exponential as evidenced by the semi log plot. The start of treatment is determined by the sharp decrease in growth rate as can be seen by the sharp increase in the percentual difference between data (red circles/blue crosses) and the exponential fit (dotted line). **(c)** Mean fluorescence as a function of time normalized by its value when chloramphenicol arrives. Before chloramphenicol arrives, increase of fluorescence is due to protein synthesis and maturation. Once chloramphenicol stops translation, the increase of fluorescence is due to maturation of previously synthesized protein. It is this second part of the curve that contains the information on how the immature protein becomes fluorescent. In particular, it can be seen that for mEGFP there is more than 40% of the total protein that remains in the immature fraction when cells grow exponentially. Also, note that it is difficult to assess the time at which chloramphenicol arrives using just fluorescence.

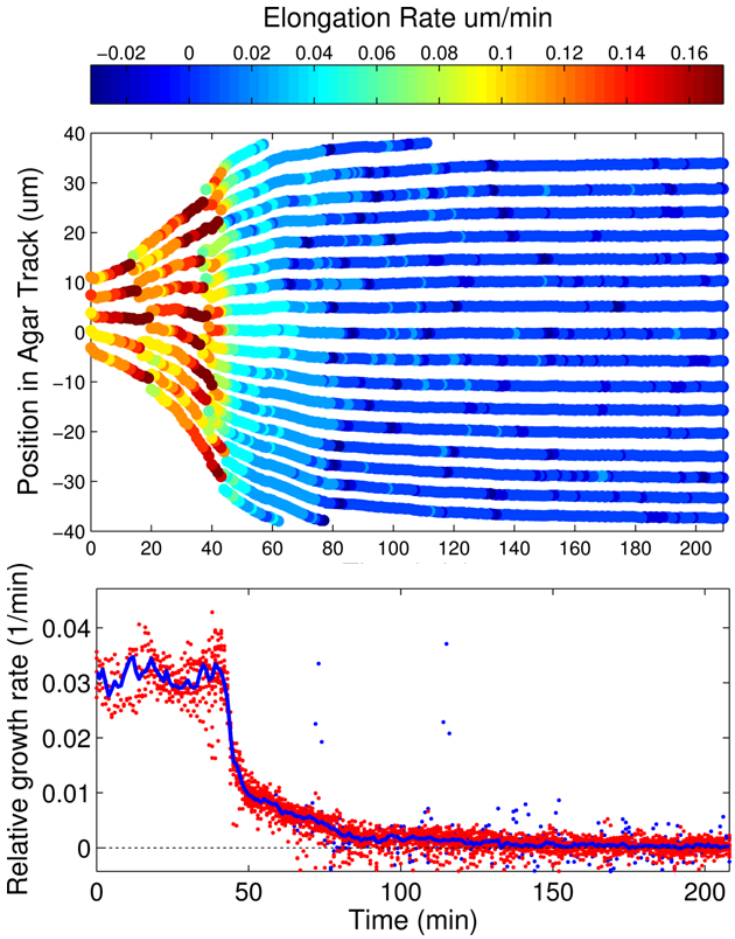

Supplementary Figure 3 | Homogeneity of chloramphenicol treatment along a linear colony. Top. Position of a cell in an agar track vs time. Every line represents the center of a cell and the coloring the elongation rate. It is readily seen that at t = 42 min there is an abrupt change in elongation rate indicating the start of the chloramphenicol treatment. Note that cells at the center of the track respond to the treatment as fast as cells at the ends of the linear colony. **Bottom.** Evolution of the relative growth rate distribution from cells on top as a function of time. The blue line indicates the average.

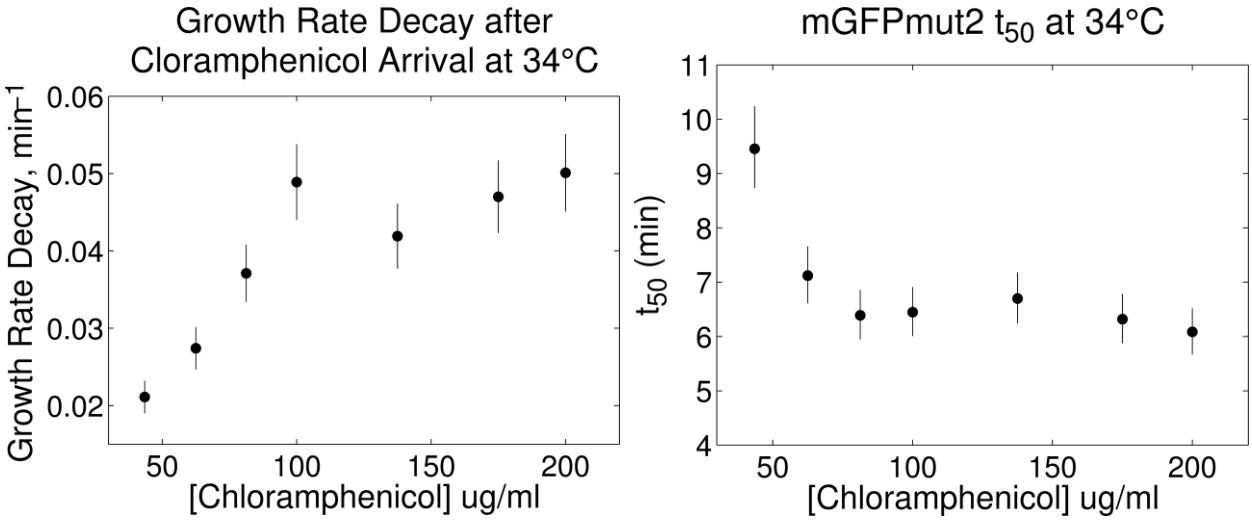

Supplementary Figure 4 | Decay in residual growth rate and maturation time as a function of chloramphenicol concentration. After chloramphenicol arrival, colony length still increases due to the fact that the drug is a protein synthesis inhibitor, not a protein activity inhibitor, see **Supplementary Figure 2** panel **(b)**. Although chloramphenicol does not inhibit the activity of previously synthesized proteins, there is still the possibility that part of the observed increase in colony length could be an indication of residual protein synthesis (FP synthesis in particular) even after the start of drug treatment. To determine whether or not there is residual synthesis, we tested how different concentrations of chloramphenicol ranging from 44 to 200ug/ml affected the observed residual growth. **Left.** As expected, we found that, in the range 44-80ug/ml the decay in residual growth rate increased with [Chlor]. However, decay in residual growth rate leveled off for [Chlor]>80mg, suggesting that the residual growth in colony length is purely due to the activity of a previously present pool of proteins at the time of drug exposure. **Right.** Similarly, estimation of mGFPmut2 maturation time decreased with [Chlor] up to ~80ug/ml. At higher concentrations, mGFPmut2 maturation time essentially did not change. In our experiments, we typically used [Chlor]=100-120ug/ml. Therefore, we ruled out in our measurements sizeable effects from residual protein synthesis on the estimation of maturation times.

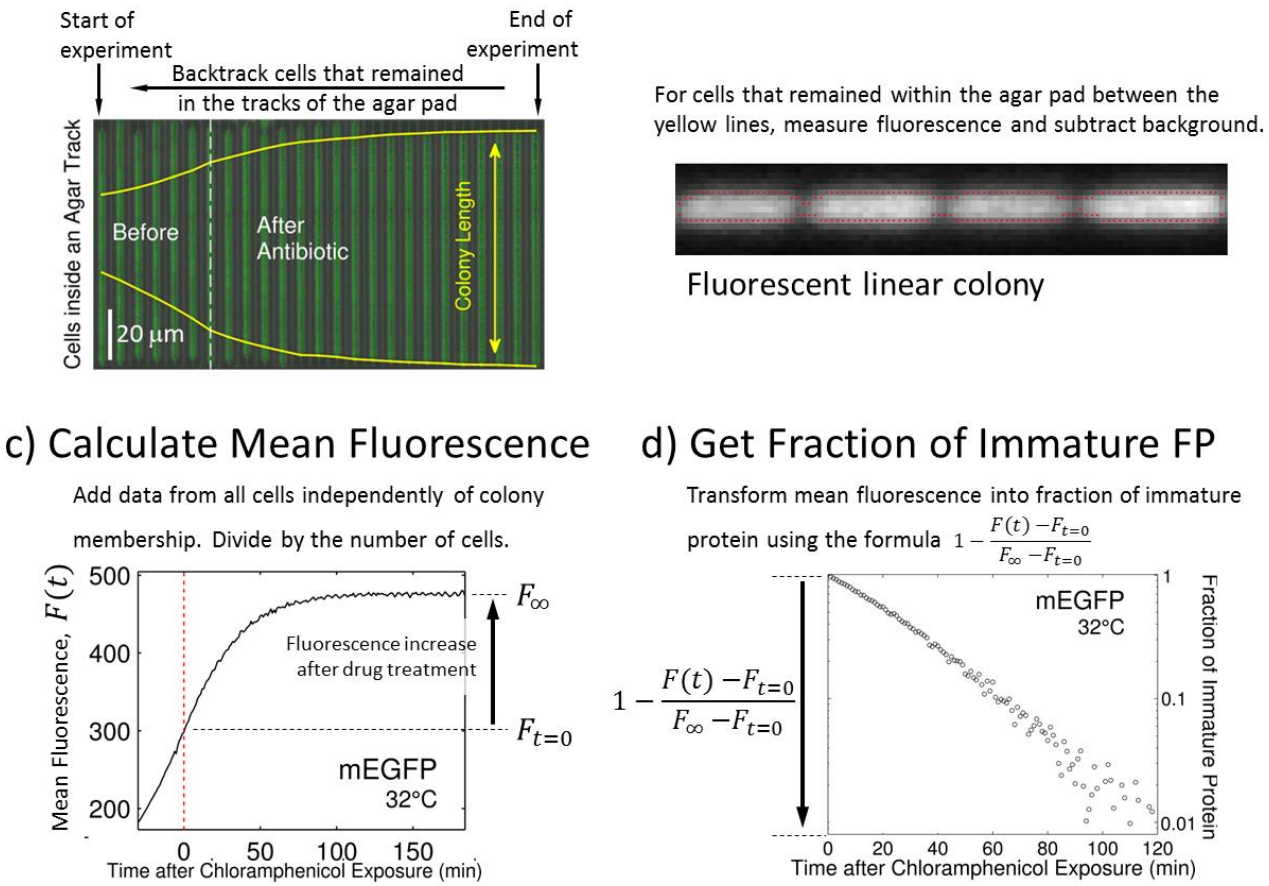

Supplementary Figure 5 | Pipeline to calculate the fraction of immature protein from single cell data. **(a)** Using a kymograph of the linear colony, we backtrack—starting from the last frame—only cells that remained in the tracks of the agar pad and that were not lysed. In this way, we avoid selecting cells being shed off the agar pad. **(b)** For every single-cell, we quantify raw fluorescence at frame t by adding signal from all pixels within a rectangular window that is twice the width of the cell in order to capture all out-of-focus light, see **Supplementary Figure 24**. To measure background fluorescence as a function of time, we construct another kymograph similar to the one shown in **(a)** but with an agar pad strip without cells. To obtain a background-corrected fluorescence value at frame t, we subtract the background quantified from the empty agar pad strip at frame $\boldsymbol{t}$ from the raw fluorescence value at frame t. **(c)** Independently of colony membership, we add fluorescence data from all cells and divide by the number of cells to obtain a mean fluorescence curve. Similarly, but with single-cell length data, we obtain a mean length curve. We use length information to determine the precise moment at which chloramphenicol arrives (red dotted line), see **Supplementary Figure 2**. **(d)** To obtain the fraction of immature protein, we transform the mean fluorescence into the fraction of immature protein using the formula $\boldsymbol{1 - (F(t) - F_{t=0})/(F_\infty - F_{t=0})}$.

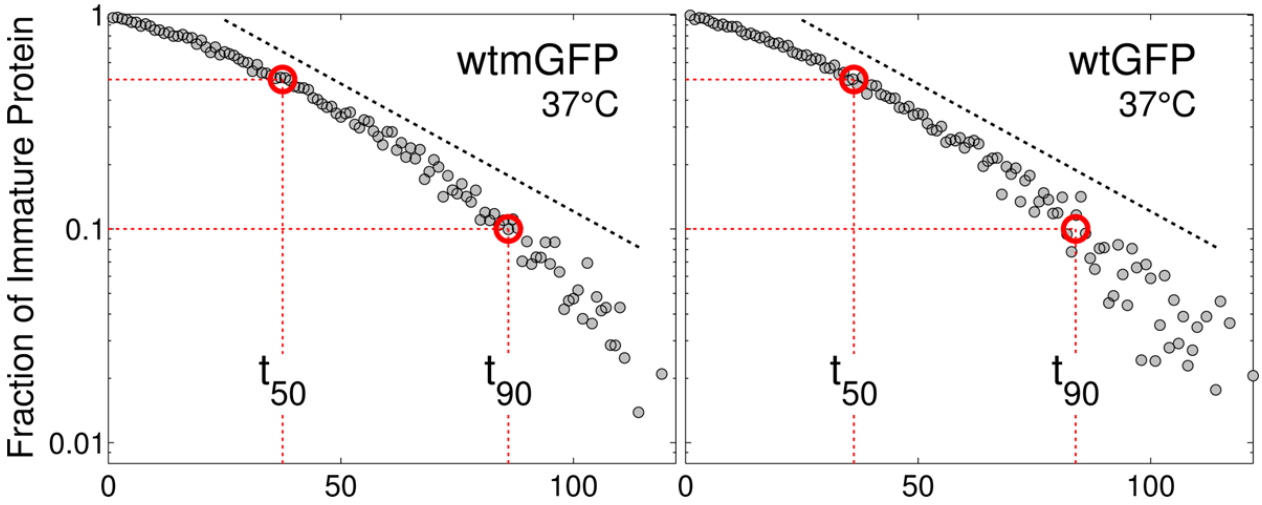

Supplementary Figure 6 | Maturation kinetics of monomeric-wtGFP and wtGFP are equal. Fraction of immature protein as a function of time after translational arrest with chloramphenicol. **Left.** Wild-type GFP with substitution A206K, wtmGFP. **Right.** wild-type GFP. The plot is the same as in Fig. 3c and it is shown here to compare, side-by-side, with the plot of wtmGFP. The black dotted line is the same in both plots. Although, the data has less experimental noise in wtmGFP, the curves are essentially equal.

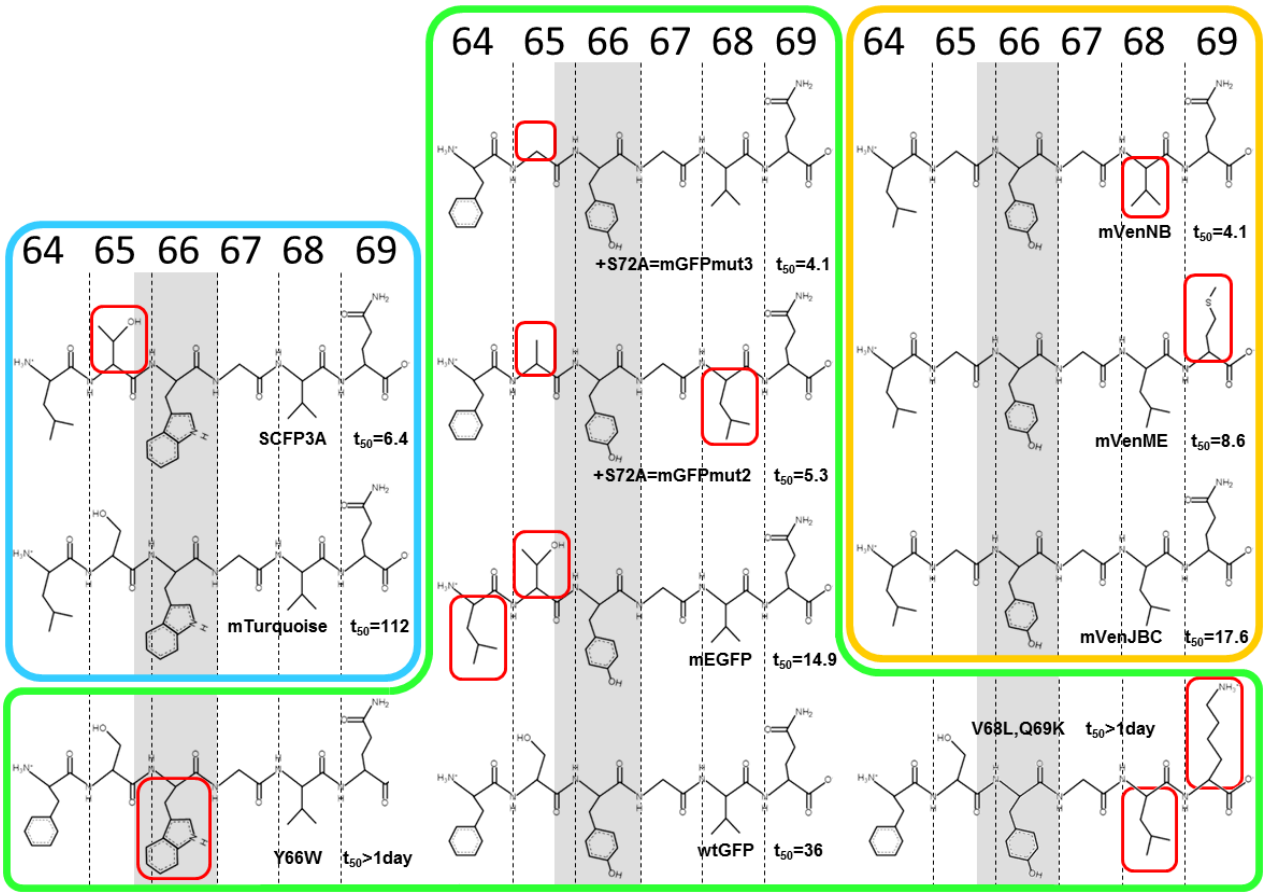

Supplementary Figure 7 | The impact of the amino acid chain context on maturation time. Numbers correspond to the numbering of amino acids in the wtGFP sequence. The limits of the grey band are the amino and carbonyl groups between which the imidazolinone ring forms. For yellow FPs, we have used the mVenJBC amino acid chain as the reference; red frames indicate differences with respect to the mVenJBC amino acid chain. For cyan FPs the reference is mTurquoise and for green FPs the reference is wtGFP. Note that mGFPmut2 and mGFPmut3 have an extra mutation not shown in position 72. Using our maturation time measurements—and given that within each box FPs have exactly the same amino acid sequence except for changes in red boxes—it is seen that amino acids next to the chromophore-forming residues strongly modulate maturation kinetics. In the examples shown, this modulation ranges from several minutes to several days. The chart suggests that torsional rearrangements to bring reacting species into the right geometry might be in some cases the rate limiting step in chromophore maturation. For mutants Y66W and {V68L, Q69K}, curves of maturation kinetics are not available because maturation is extremely slow. As a comparison, single colonies growing in agar plates expressing fast avFPs develop detectable fluorescence immediately, whereas colonies expressing Y66W and {V68L, Q69K} require several days to become fluorescent.

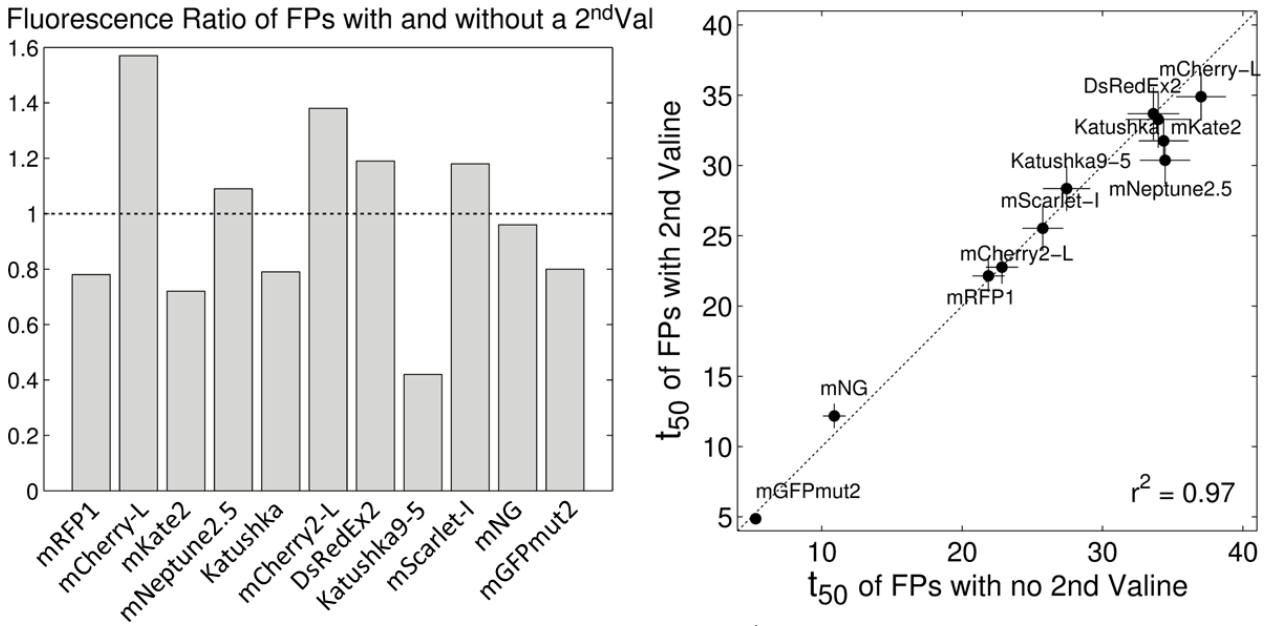

Supplementary Figure 8 | Presence or absence of Valine at 2nd position of FP amino acid sequence changes protein expression but not maturation time. Modifications of the N-terminus of coding sequences (like the addition of a 2nd Valine) alter the stability of the mRNA secondary structure (44). The change in stability has an impact on translation initiation rate and thus modifies protein levels. The effect is relevant when changes occur at the N-terminus end within the first 12 codons (45). In our library, we classified FPs such that members of each class would have the same N-terminus at least for the first 20 codons. We cloned successfully 11 FPs out of 12 N-termini classes (mRuby3 N-terminus class missing). This classification strategy allowed us to efficiently sample the FPs in our library in order to investigate the impact of a 2nd valine on maturation time. **Left. Fluorescence ratio of cells growing exponentially and expressing FPs with and without a 2nd Valine.** The spread in ratios around the identity demonstrates that the addition of a 2nd Valine at the N-terminus alter protein expression. **Right. t_{50} of FPs with and without a 2nd Valine.** The second Valine does not change the t_{50} time for the FPs representing the different 11 N-termini classes. Also, the shape of the maturation curve does not change, see SI section 3. Errors represent a confidence interval of 95%. Maturation data can be found in **Supplementary Data**.

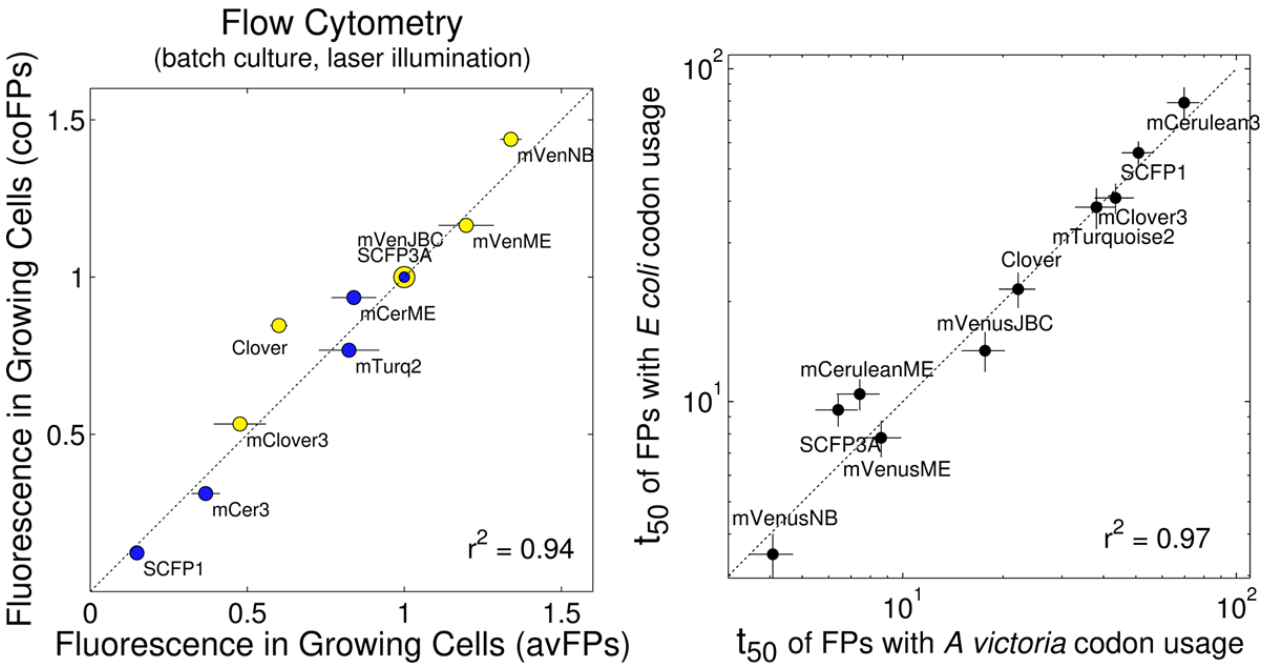

Supplementary Figure 9 | **Codon usage does not change FP maturation time.** *E. coli* codon optimized (CO) cyan FPs (GC content 48.3% vs 39.3% in *A. victoria* cyan FPs) and yellow FPs (GC content 48.7% vs 39.2 in *A. victoria* yellow FPs) were generated from previously published *E. coli* codon optimized cyan and yellow FPs (11). Note that cyan and yellow FPs have different CO sequences. The selection of cyans and yellows was such as to cover a wide range of maturation times. **Left.** Relative fluorescence of coFPs versus relative fluorescence of avFPs in growing cells; flow cytometry measurements, 37°C, M9 rich media. Although, absolute fluorescence levels in coFPs changed (yellow coFPs fluorescence 1.44 times that of avFPs; blue coFPs fluorescence 0.32 times that of avFPs), the relative fluorescence hierarchy among the two classes remained the same. Errors in avFPs are SD from three cultures. For coFPs only one replicate was measured. **Right.** Within experimental error, t_{50} is identical for FPs with *A. victoria* or *E. coli* codon usage. Finally, we observed that the shape of the maturation curve does not change, see SI section 3. Errors represent a confidence interval of 95%. Maturation data can be found in the **Supplementary Data**.

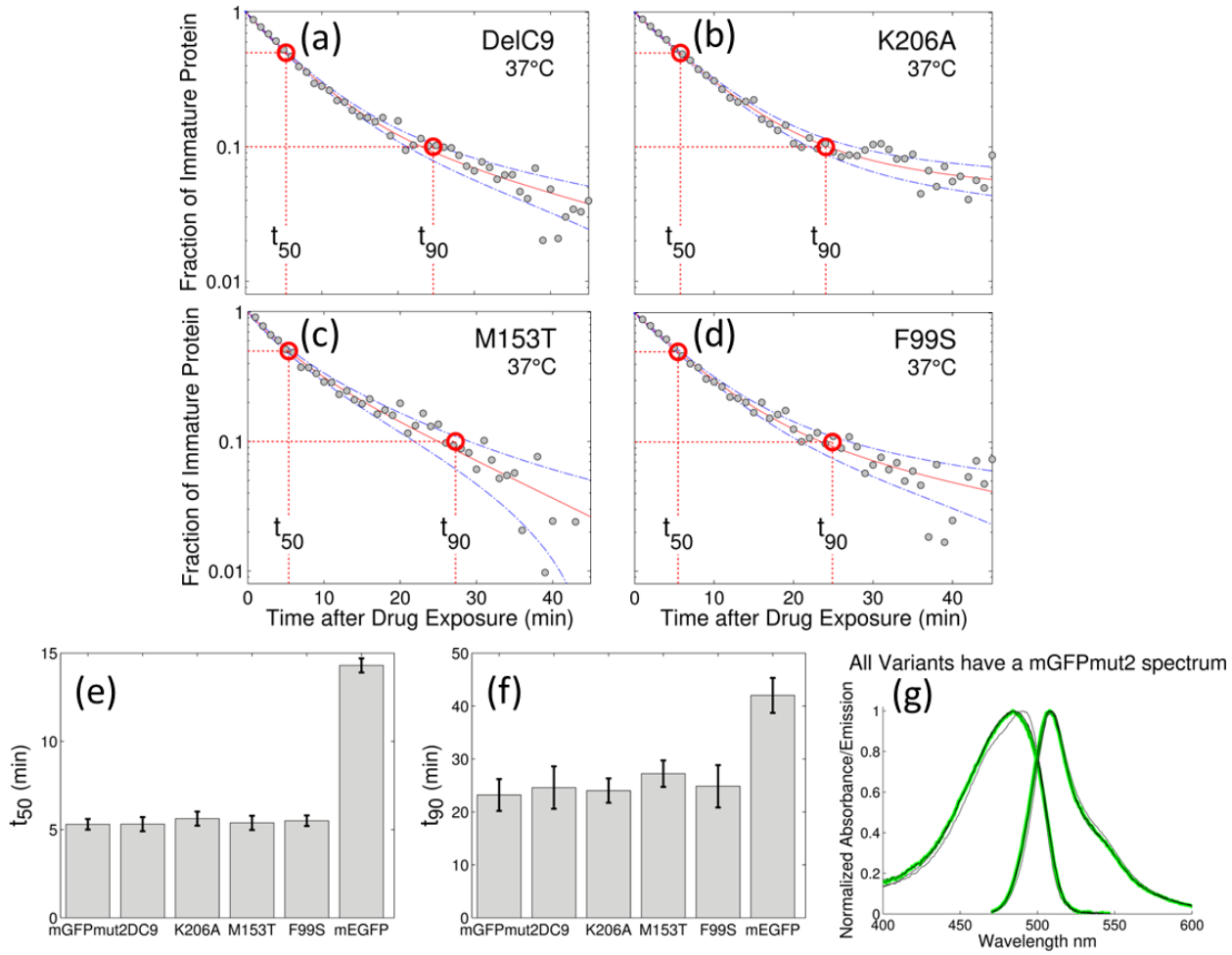

Supplementary Figure 10 | Spectroscopically silent mutations do not affect mGFPmut2 maturation. **(a)-(d).** Fraction of immature protein for mutants of mGFPmut2; **(a)** DelC9: truncation of the last 9 C-terminus amino acids; **(b)** K206A: the revertant of the monomeric substitution A206K, **(c)** M153T: M153T in the context of DelC9; **(d)** F99S. **(e)** Bar plot of t_{50} in **(a)-(d)** plus t_{50} of mGFPmut2 to the left and mEGFP to the right, shown for comparison. **(f)** Bar plot of t_{90} in **(a)-(d)** plus t_{90} of mGFPmut2 to the left and mEGFP to the right, shown for comparison. **(g)** To corroborate the spectroscopically silent nature of mutations in **(a)-(d)** we extracted and purified the mutants to obtain their absorbance and emission spectra, thin continuous black lines. In thick continuous green line, we have overlaid the mGFPmut2 abs/em spectrum. As can be seen, within experimental error, maturation kinetics of mGFPmut2 and spectroscopically silent variants are identical.

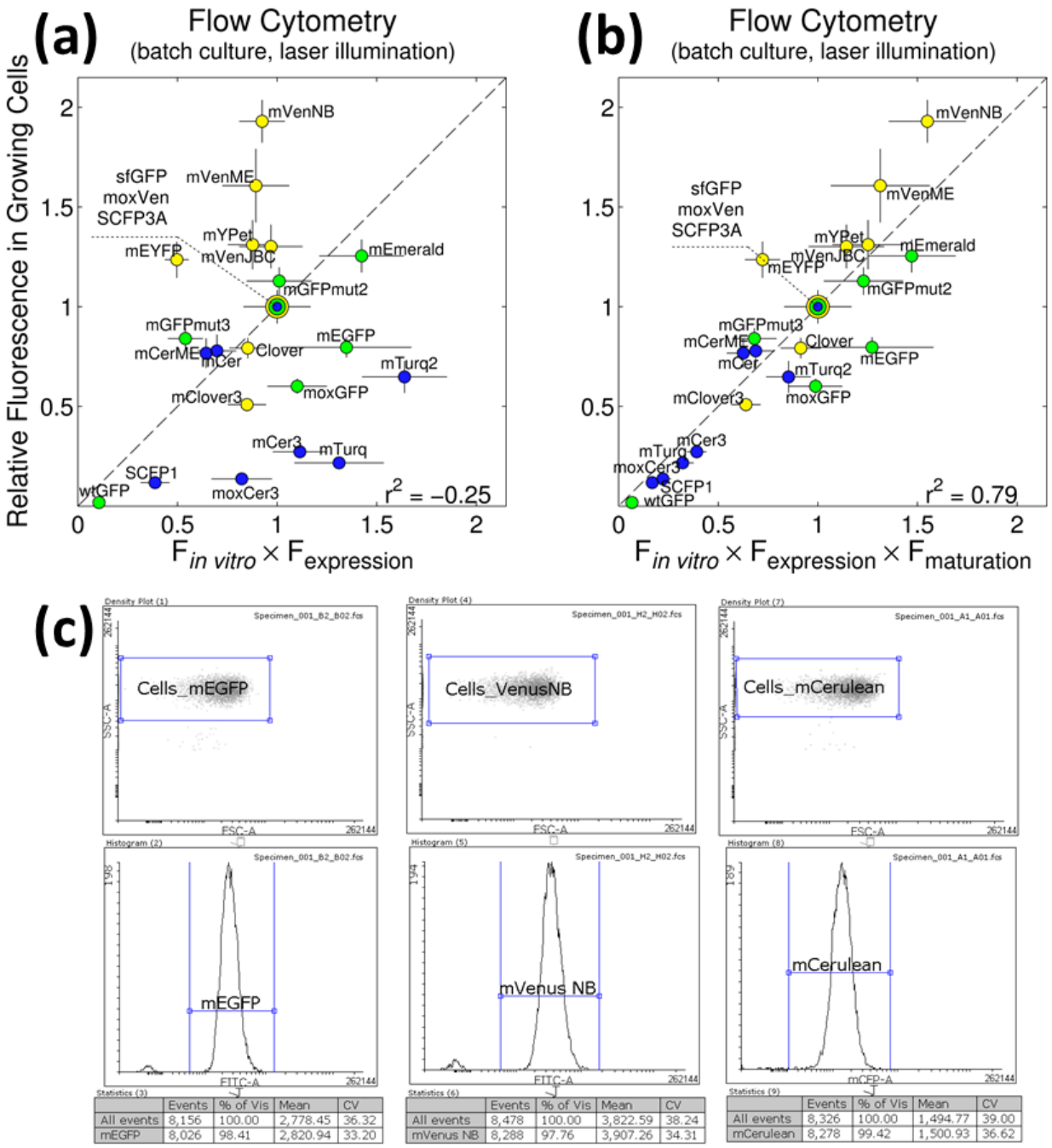

	Events	% of Vis	Mean	CV
All events	8,156	100.00	2,778.45	36.32
mEGFP	8,026	98.41	2,820.94	33.20

	Events	% of Vis	Mean	CV
All events	8,478	100.00	3,822.59	38.24
mVenus NB	8,288	97.76	3,907.26	34.31

	Events	% of Vis	Mean	CV
All events	8,326	100.00	1,494.77	39.00
mCerulean	8,278	99.42	1,500.93	36.62

Supplementary Figure 11 | Fluorescence signal in growing cells measured using flow cytometry vs *in vitro* brightness corrected for maturation. (a,b) Fluorescence in growing cells is the average fluorescence computed over a population of ~10,000 cells. Colonies were growing exponentially at 37°C in M9 rich media. Error bars are the SD calculated from three independent cell cultures. $F_{in\ vitro}$ is the product of quantum yield, QY, and molar extinction coefficient ε; $F_{mat}=1/(1+t_{50}/t_{gr})$ and $F_{expression}$= amount of protein estimated using SDS densitometry. QY, ε, and maturation times were quantified in our laboratory independently from published values (Table S1). Error bars were derived using error propagation. For green FPs, data normalized by sfGFP data; for yellow FPs, by moxVenus data; for blue FPs, by SCFP3A data. Dashed line is the identity. Dilution is given by the division rate of *E. coli* growing in rich M9 media at 37°C, t_{gr} = 28.5±2min. QY and ε were multiplied by a correction factor to account for the em/ex filter bandpass, see **Supplementary Note**. See Supplementary Figure 12 for the definition of

r^2. **(c)** Figure exemplifying the gating strategy used in flow cytometry quantification of FPs. Typical data from a yellow (mVenus NB), green (mEGFP) and cyan (mCerulean) FP. **Top plots.** We separated cell-like objects from a clear debris fraction by using the side and forward scattering. **Bottom plots.** Cell objects were identified by gating only events with yellow, green or cyan fluorescence, respectively. Statistics at the bottom show the abundance of post-sort fractions, the mean and the coefficient of variation.

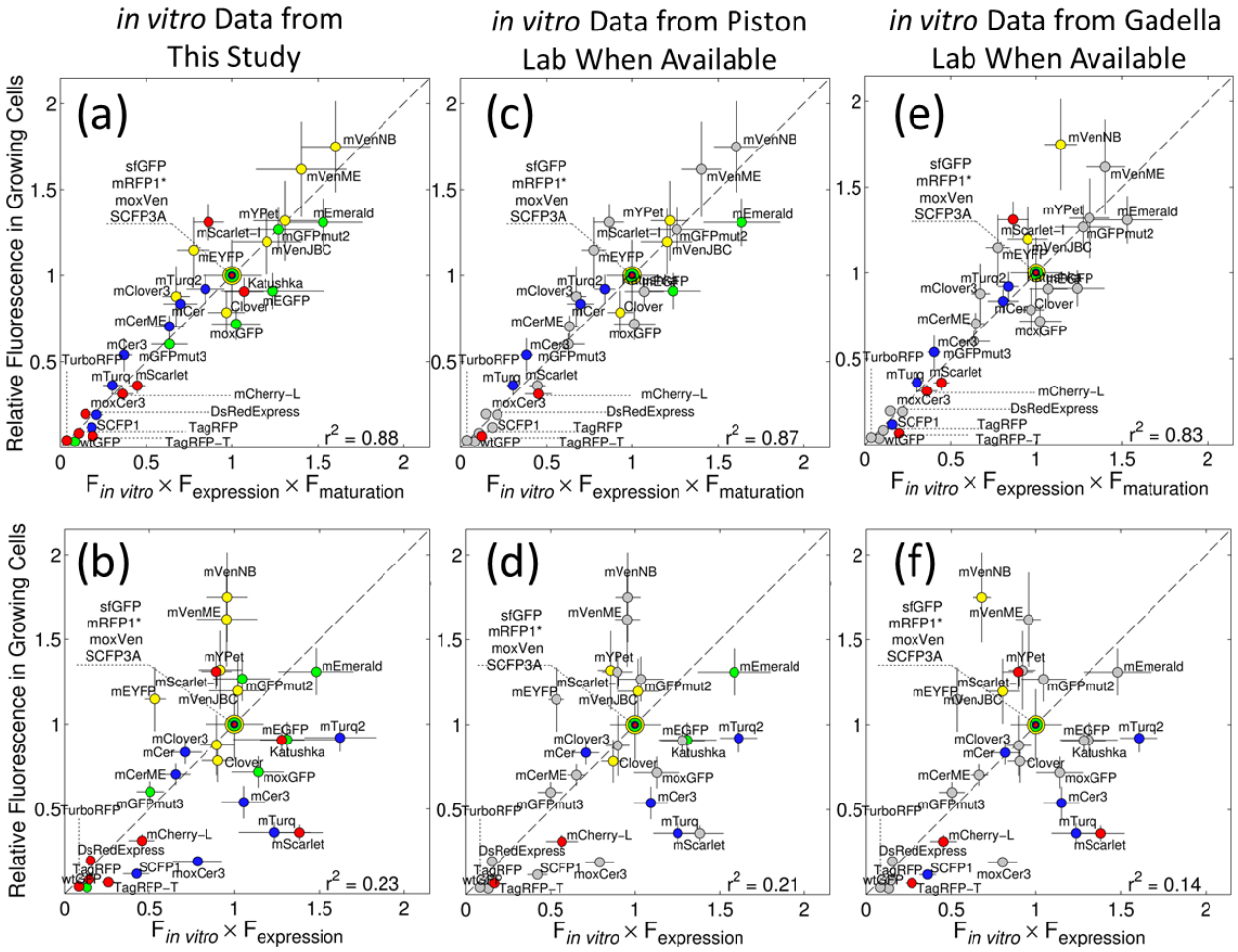

Supplementary Figure 12 | **Fluorescence signal in growing cells vs single-source *in vitro* brightness by different laboratories.** For all plots, fluorescence in growing cells was obtained from single-cell chemostat experiments. Error bars are the SEM calculated from 75± 20 cells. On top: $F_{in\ vitro}$=QY·ε multiplied by $F_{mat}=1/(1+t_{50}/t_{gr})$ and by $F_{expression}$=amount of protein estimated using SDS-PAGE gel densitometry. On bottom: $F_{in\ vitro}$ multiplied by $F_{expression}$. **(a,b)** *In vitro* brightness using data from this study (Table S1). **(a)** is the same plot as **Fig. 1e** and shown here for ease of comparison. Error bars derived using error propagation. For green FPs, data normalized by sfGFP data; for yellow FPs, by moxVenus data; for blue FPs, by SCFP3A data; and for red FPs by mRFP1*. Dashed line is the identity. **(c,d)** *In vitro* brightness using data from this study (gray circles) or obtained from the Piston laboratory when available (**Table S1** and **S2**). **(e,f)** *In vitro* brightness using data from this study (gray circles) or obtained from the Gadella laboratory when available (**Table S1** and **S2**). All *in vitro* brightness data was multiplied by a correction factor to account for the em/ex filter bandpass, see **Supplementary Note**. To calculate $\boldsymbol{r^2}$ we used $\boldsymbol{r^2 \equiv 1 - (SS_{res})/(SS_{tot})}$ (46), where $\boldsymbol{SS_{tot} = \sum(y_i - \bar{y})^2}$ is the total sum of squares and $\boldsymbol{SS_{res} = \sum(y_i - f_i)^2}$ is the sum of squares of residuals assuming model $\boldsymbol{f}$. $\boldsymbol{y_i}$ represents fluorescence signal data, $\boldsymbol{\bar{y}}$ is the mean and $\boldsymbol{f_i}$ is the corresponding modeled value, $\boldsymbol{F_{in\ vitro} \times F_{expression}}$ or $\boldsymbol{F_{in\ vitro} \times F_{expression} \times F_{maturation}}$. Note that even when substituting ~40% of the *in vitro* data by single-source data from two different laboratories, we found that maturation time was the major factor that underlied the hierarchy between the fluorescence signal of different FPs in growing cells. See **Supplementary Data** for values used to generate the plots in this figure.

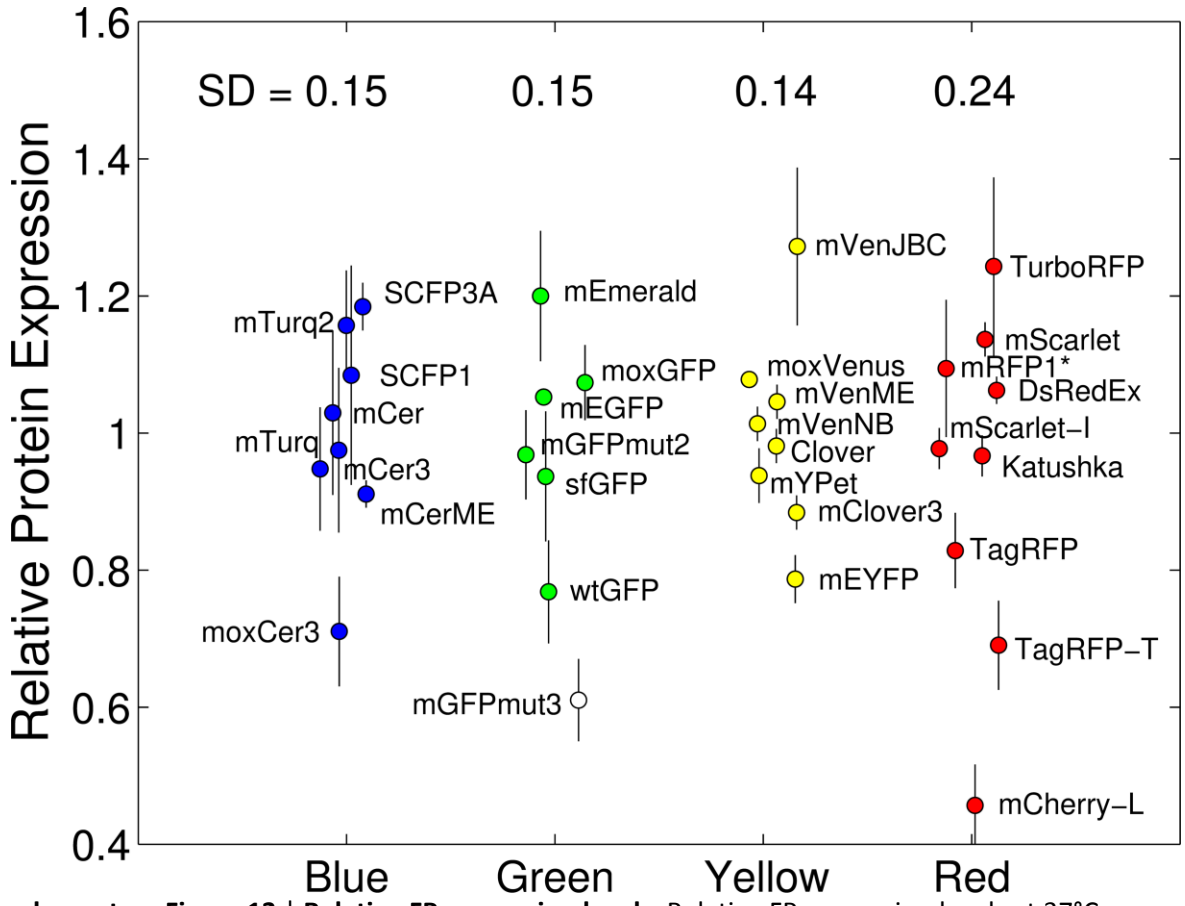

Supplementary Figure 13 | **Relative FP expression levels.** Relative FP expression levels at 37°C estimated using SDS-PAGE gel densitometry. For clarity, in each color class we have artificially added a x-axis dispersion. On top, SD values of every color class. We have single out mGFPmut3 in white to indicate that its value was left out from the SD calculation, see below. Error bars are SD values calculated from two SDS-PAGE gels, see **Supplementary Figure 18**. From the SD values on top of every cloud, it can be seen that it would be fair to assume that all avFPs variants have the same expression level when the FP expression system has the same transcription/translation signals and FPs have the same nucleotide sequence—except for mutations particular to each variant. Surprisingly, there are exceptions to this assumption like that of mGFPmut3: this green FP expression is 40% below the average of its color category. By contrast with avFPs, even when red FPs have the same transcription/translational signals, these FPs present a higher expression variability (SD=0.24). One possible source for the observed expression variability of red FPs is the differences in nucleotide sequences, in particular differences at the N-terminus, see also **Supplementary Figure 8**. Another possible source of variability is the hydrolysis of the chromophore imine linkage in RFPs that has been observed in denaturing SDS-PAGE of mRFP1 and DsRed (28, 47). The hydrolysis breaks a small fraction of red FP peptide into 19 kDa and 7 kDa fragments when the RFP peptide is boiled in Tris-HCl buffer (pH~7.0). Our analysis cannot detect those faint bands over background peptide. Thus there is, potentially, a small quantification error of red FP net expression. However, this small error is expected to have a minor impact on the estimation of signals in growing cells given that F_{mat} is the main factor responsible for increasing the correlation between observed and estimated signal from r^2=0.23 to r^2=0.88, **Supplementary Figure 12**. Yet, the small errors in the density estimation of red FPs might be enough to account for the observed higher expression variability in their color class.

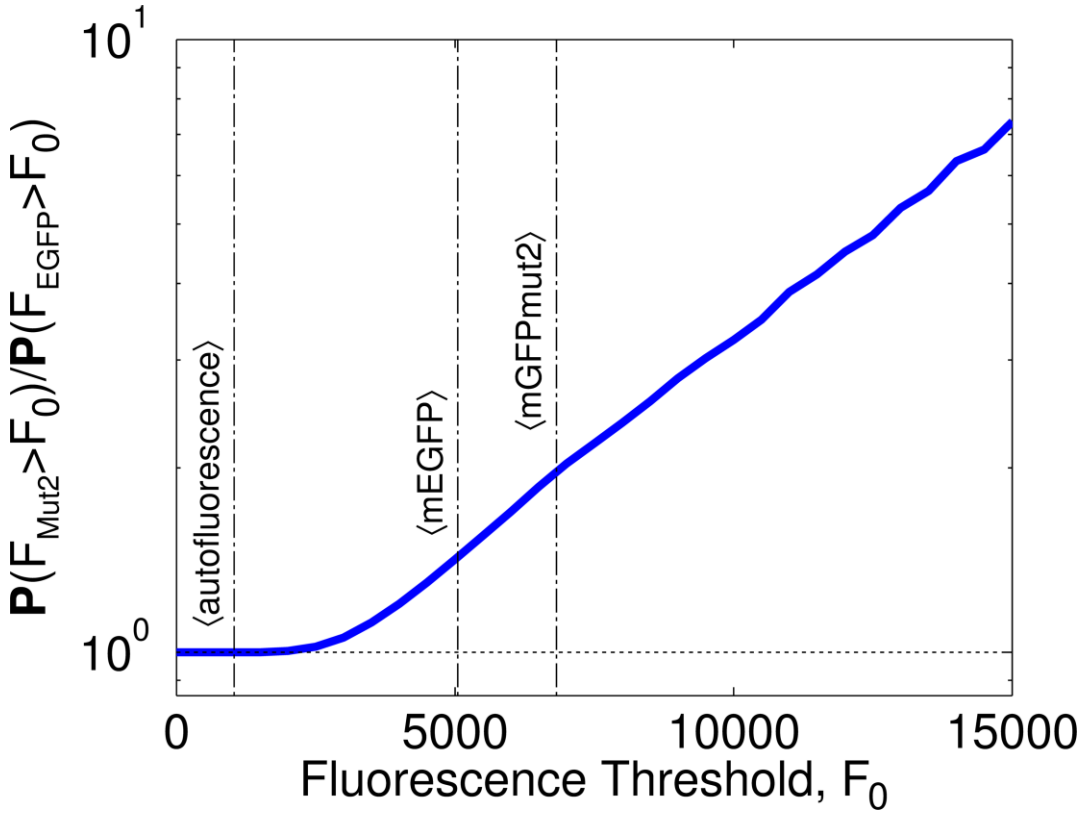

Supplementary Figure 14 | mGFPmut2 FP is brighter than mEGFP at all fluorescence signal categories above autofluorescence. Two different strains, one using mGFPmut2 the other EGFP to monitor P_{lacZ} activity, were grown in the single-cell chemostat and their fluorescence quantified. $\mathbf{P}(F_{Mut2}>F_0)$ represents the fractions of cells that had a mGFPmut2 fluorescence signal higher than a fluorescence signal threshold F_0. When a similar quantity for mEGFP was compared to that of mGFPmut2 by means of their ratio, we saw that mGFPmut2 had a much greater fraction of cells that presented a fluorescence signal higher than the set threshold. This difference in signal could easily reach 2X and reach 8X for the brightest cell categories. As a reference, the mean fluorescence signal of auto-fluorescence, mEGFP and mGFPmut2 is shown.

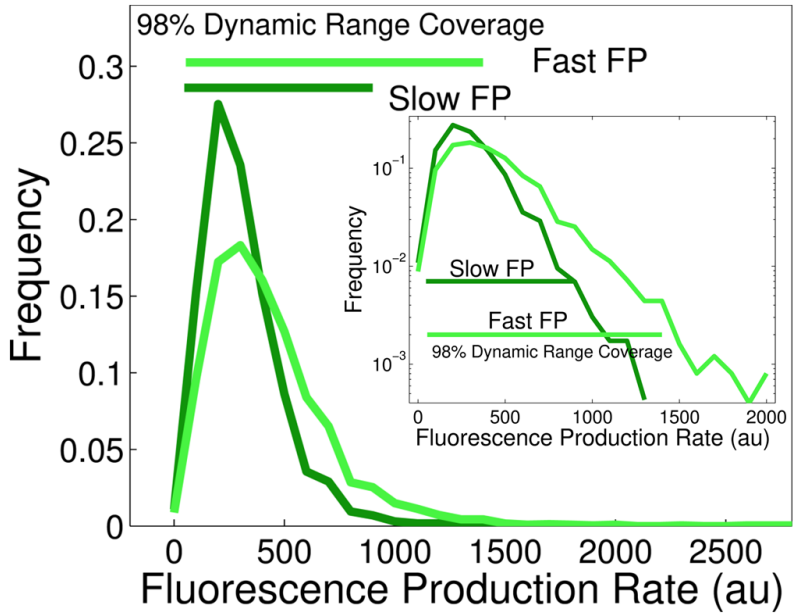

Supplementary Figure 15 | Distribution of the average fluorescence production rate per cell for mEGFP (slow FP) and mGFPmut2 (fast FP) controlled by the repressed P_{lacZ} promoter. The distribution of the average production rate per cell for the fast FP (light blue) has an 60% greater dynamic range (n_{cells}=2581 slow, n_{cells}=2489 fast). We defined dynamic range as the length of the range necessary to cover 98% of the central mass of the distribution. In general, when the expression of both proteins is controlled by the repressed P_{lacZ}, we observed that the fast FP yields indeed a better signal to noise ratio: the fast green variant showed consistently higher promoter activity levels than the slow variant**. Inset.** Same data displayed in a semi logarithmic plot.

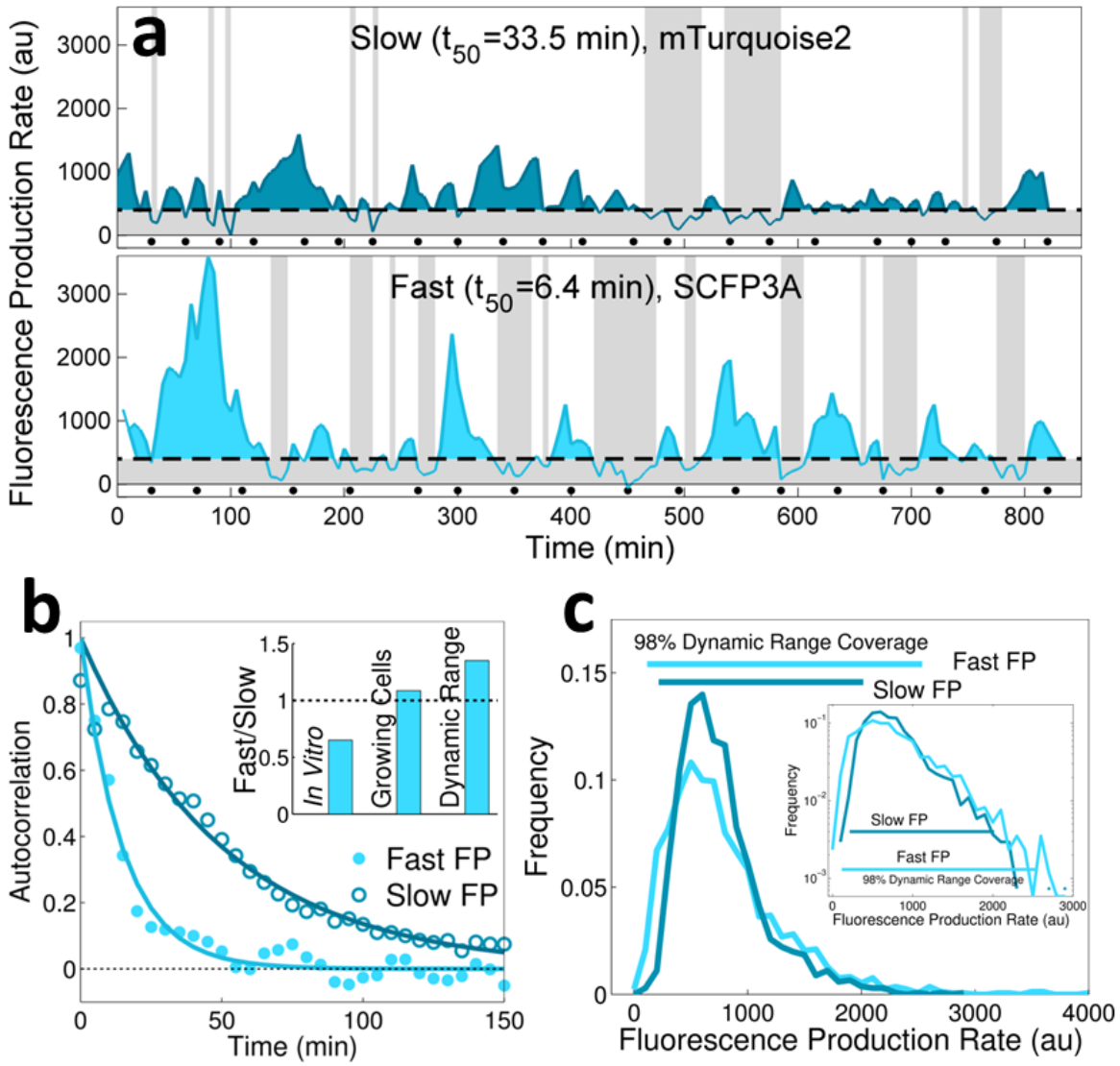

Supplementary Figure 16 | Activity of the repressed P_{lacZ} as reported by the fastest blue FP, SCFP3A, or the *in vitro* 1.66 times brighter blue FP, mTurquoise2. (a) Time traces of the fluorescence production rate of the repressed P_{lacZ} using the fast (SCFP3A) or the slow FP (mTurquoise2). The detection limit (dashed line) is 3σ units above autofluorescence production; black dots indicate cell division, t_{div}=33min at 37 °C. The fast FP displays greater transcriptional bursts and clear periods of promoter inactivity (shaded bands). By contrast, the slow FP smears out the fluorescence signal, which alters the true activity of P_{lacZ}. **(b)** Autocorrelation of fluorescence production rate for the slow and the fast FP variants (characteristic decay times t_{slowFP}=34min and t_{fastFP}=12min). Both FPs are driven by the same promoter thus using the fast FP increases the temporal resolution. **Inset.** Bar plot showing the advantage of fast over slow FPs by means of the *in vitro* brightness ratio, signal in growing cells ratio, and dynamic range ratio. Note that mTurquoise2 is *in vitro* 1.66 times brighter than SCFP3A. **(c)** The distribution of the average production rate per cell for the fast FP (light blue) has a 40% greater dynamic range (n_{cells}=1360 slow, n_{cells}=1711 fast). We defined dynamic range as the length of the range necessary to cover 98% of the central mass of the distribution. Note, in particular, that the activity reported by the slow FP never reaches values as low as those evidenced by the fast FP. In general, when the expression of both proteins is controlled by the repressed P_{lacZ} promoter, we observed that the fast FP yields indeed a better signal to noise ratio: the fast blue variant showed consistently higher promoter activity levels than the slow variant. **Inset.** Same data in semi-log.

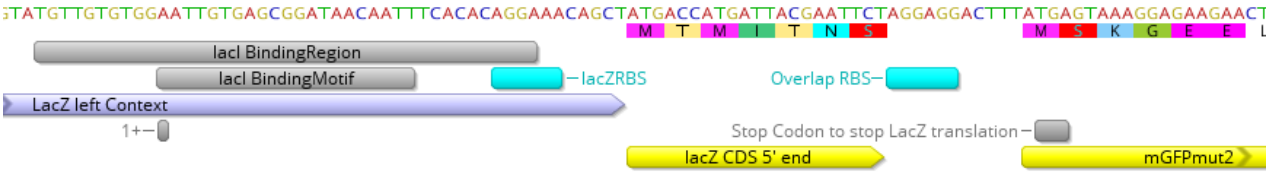

Supplementary Figure 17 | DNA sequence context of the reporter fluorescent protein inserted in the lacZ locus. The region upstream the FP is the wild type lacZ region up to amino acid Ser7, after it a strong RBS is inserted. A few bases downstream, there is a stop codon between Met1 and Ser2 of the FP sequence which truncates the LacZ peptide. This overlap RBS design is from (49).

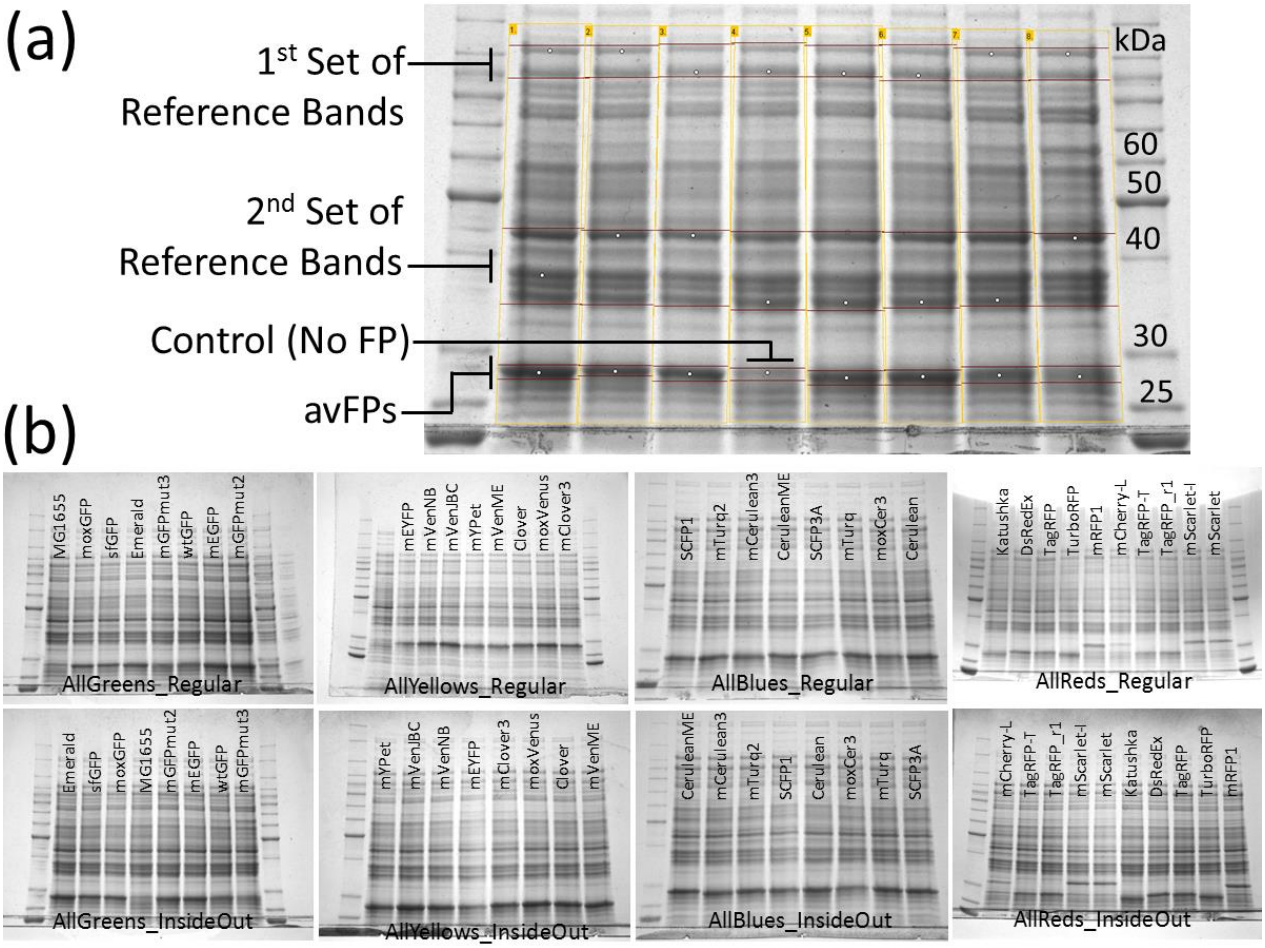

Supplementary Figure 18 | **SDS-PAGE gel densitometry of FP expression from *E. coli* total lysate. (a)** Example of densitometry analysis using the software GelAnalyzer 2010a. Each lane was background corrected using the rolling ball method with a radius of 60 points. We estimated the density contribution from total protein at the FP migration size by using the background strain MG1655 without an FP expression system; note that the contribution from total protein was low compared to FP expression. To correct for variations in the amount of loaded sample, we used two sets of stereotypical bands as loading references: *1st Set of Reference Bands* and *2nd Set of Reference Bands*. To correct for systematic gel distortions, we ran every set of samples in two different gels, with samples in the second gel loaded in an inside-out fashion with respect to the first gel; see **(b)** for specific sample loading order. For every lane, we used the reference bands as a proportionality factor to backcalculate the density contribution from total protein at the FP migration size. To calculate FP density, we estimated density at the FP migration size, then we subtracted the backcalculated total protein contribution and, finally, we corrected for loading variations by multiplying with the factor needed to make the density of one set of reference bands equal. The reported relative FP density is the median from four measurements: (2 estimations using either set of reference bands) X (2 gels: one in which samples were loaded in a regular fashion and one in an inside-out fashion). **(b)** Annotation of all total protein gels. Note that avFPs migrated at the expected length. However, some red DsRed variants (mRFP1, mCherry-L, mScarlet-I and mScarlet) had an anomalous migration effectively appearing as ~32 kDa peptide chains. This anomalous migration has been observed in other studies for mCherry (see Fig. 4, lanes 4 and 8 in (48)) and mRFP1 (see Supporting Figure 7 in (28)). For these four red FPs the density contribution from MG1655 protein, after bakcground correction with the rolling ball method, was essentially equal to zero. See **Supplementary Data** for calculations.

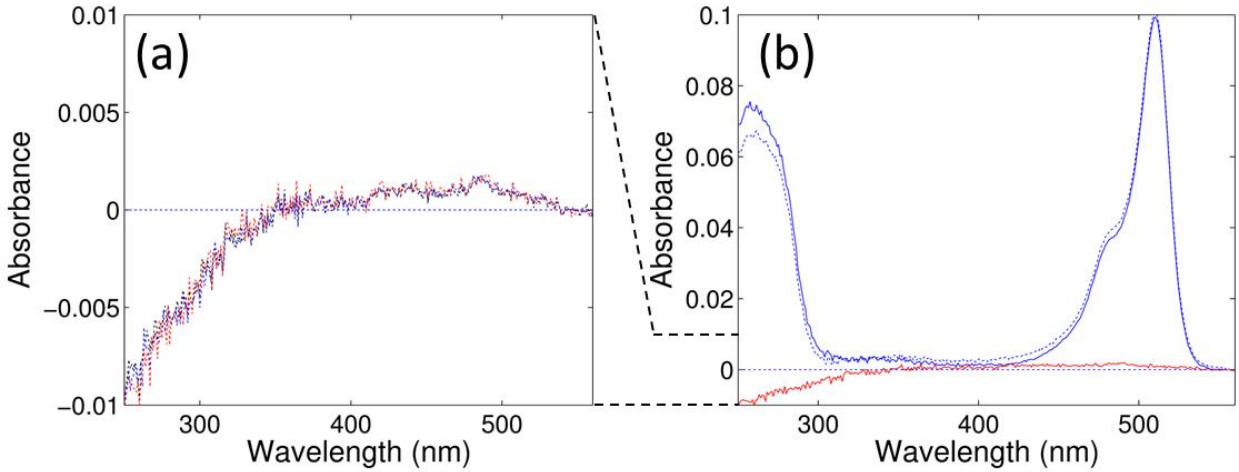

Supplementary Figure 19 | Typical acquisition and correction of an absorbance spectrum using PMMA plastic cuvettes. (a) Absorbance spectra variability of a sample of 3 cuvettes made from the same mold cavity filled with Tris-HCl buffer, pH 8.0. (b) Absorbance spectra of mVenNB before correction (dotted blue line) and after correction (solid blue line). The red line is the average absorbance of the three spectra in (a).

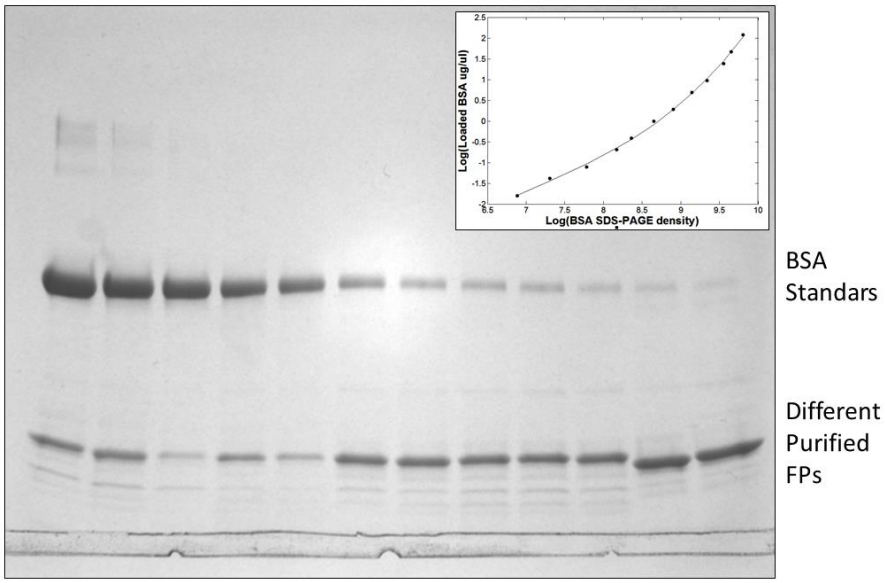

Supplementary Figure 20 | **Typical SDS-PAGE Analysis to determine FP concentration by the use of BSA standards**. A 4-20% SDS-PAGE loaded with samples of different purified FPs and BSA standards. As an inset, the standard curve derived from the BSA standards.

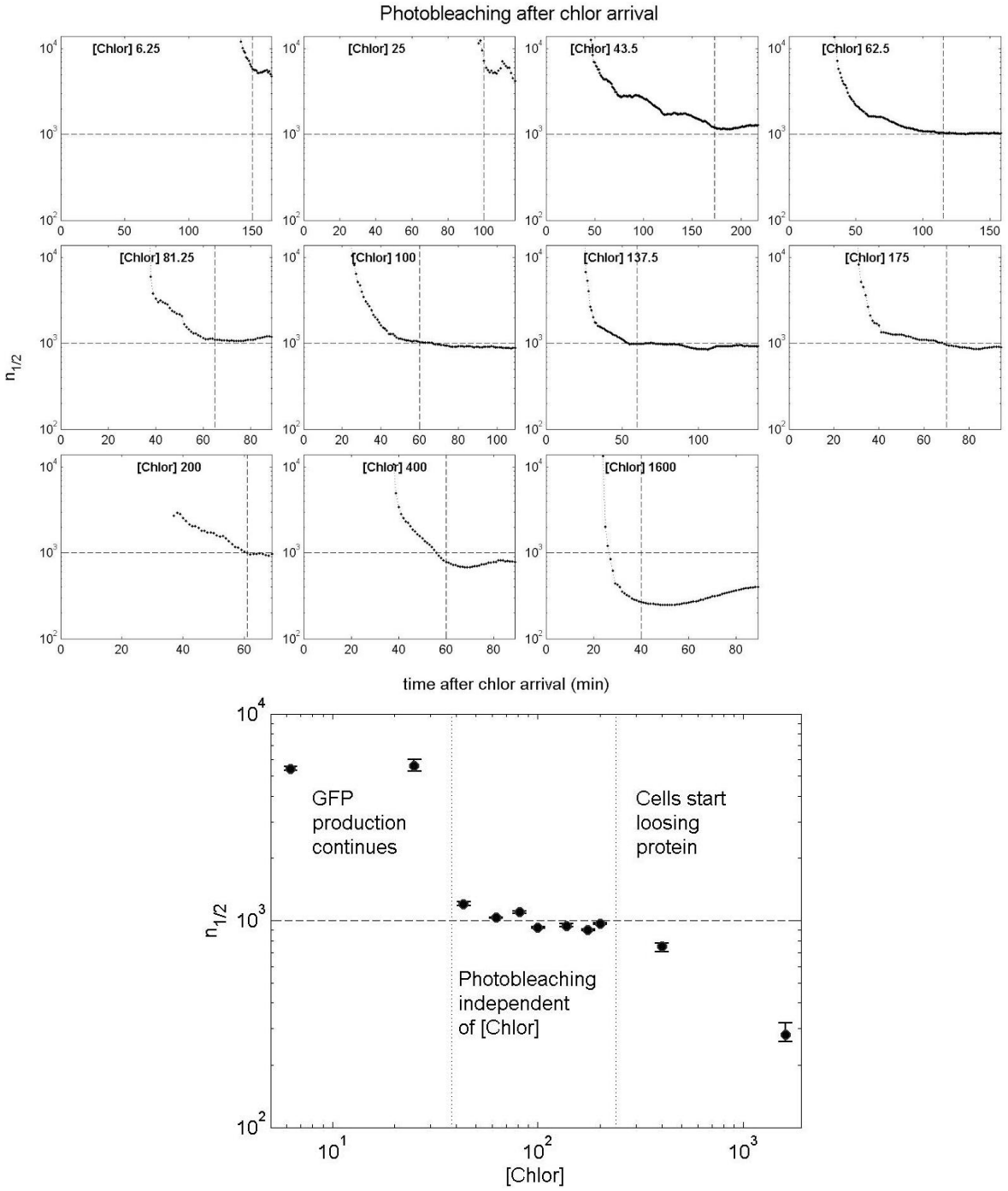

Supplementary Figure 21 | Photobleaching rate during chloramphenicol treatment for different [Chlor]. Top. Semi log plot of the number of exposures needed to lose half of the initial fluorescence $n_{1/2}$ in a linear colony expressing mGFPmut2 as a function of chloramphenicol treatment duration. From top to bottom, left to right. For the lowest chloramphenicol concentration, the photobleaching rate does not reach a stationary state even after more than two hours of treatment. This might be an indication of residual translation that obscures the real rate. Around [Chlor] = 43.5 ug/ml onwards, the photobleaching rate reaches a stationary value that is kept up to 200 ug/ml. At higher concentrations, the apparent photobleaching rate increases again. This seemingly strong photbleaching is caused by leaks of the cytoplasmic content, including GFP. **Bottom.** Data reduction from (a) showing the apparent photobleaching rate as a function of [Chlor].

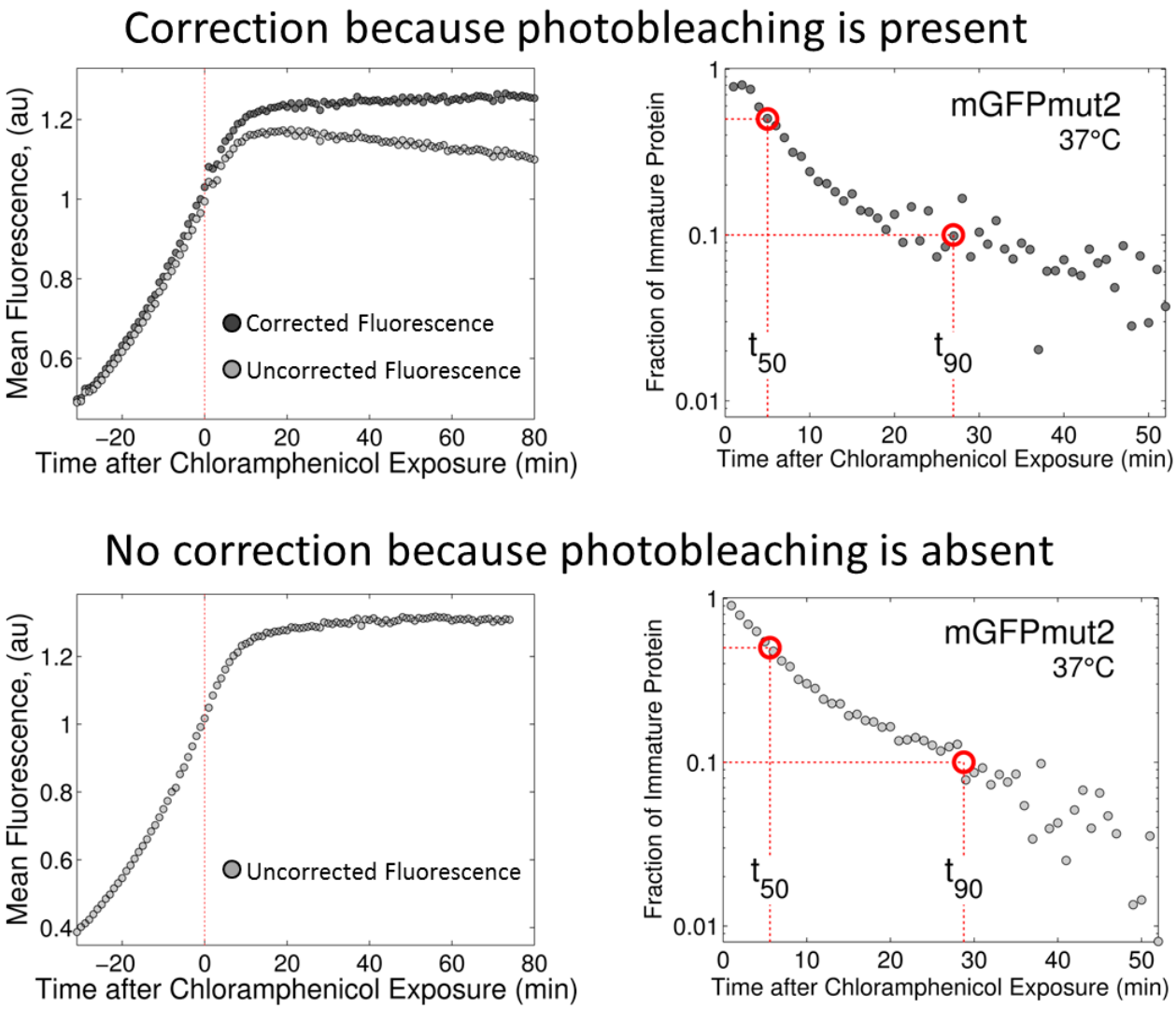

Supplementary Figure 22 | **Photobleaching correction of maturation curves.** Figures on the left. Mean fluorescence intensity uncorrected (light gray) and corrected (dark grey) for photobleaching, see section Photobleaching Correction. The mean fluorescence is from cells expressing mGFPmut2. Figures on the right. Fraction of immature protein obtained from (top) the corrected mean fluorescence curve or from (bottom) the uncorrected mean fluorescence curve. As can be seen, mGFPmut2 characteristic 2-step kinetics is present in both cases (i) when photobleaching is detected and corrected and (ii) when photobleaching is absent.

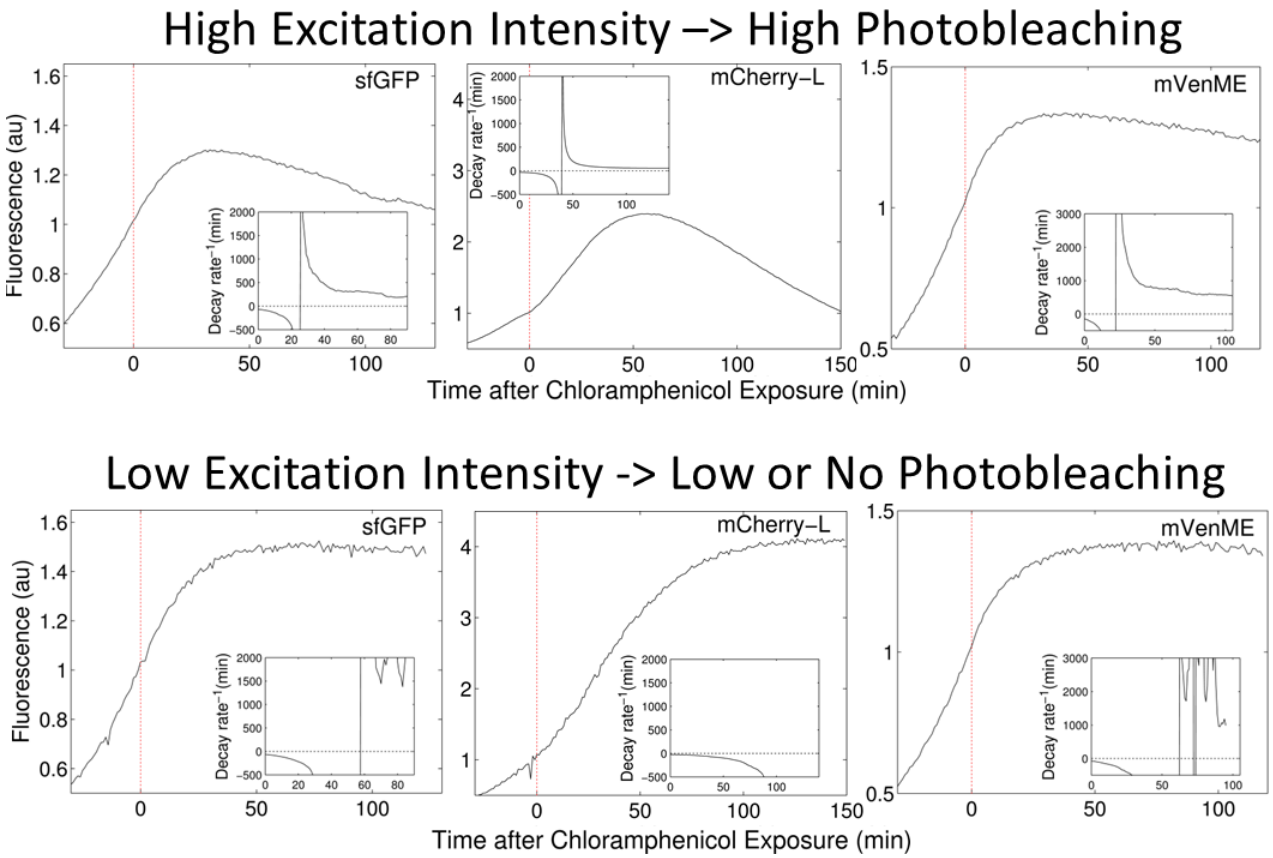

Supplementary Figure 23 | Test experiments where high intensity illumination photobleaches the sample and the subsequent experiments, with low intensity illumination, with no detectable photobleaching. Top row. Illumination intensity is so high that, soon after FP production stops due to chloramphenicol (start of treatment indicated by red line), photobleaching becomes the main feature of the fluorescence curves, completely obscuring maturation kinetics. **Insets.** Local decay rate as a function of time after chloramphenicol exposure. The local decay rate was estimated by fitting the measured fluorescence with a single exponential in a 20 to 40 min sliding window; the window was slided in one minute steps. Right after chloramphenicol arrival, the decay rate is negative indicating that fluoresce is still increasing. After the discontinuity due to the presence of a fluorescence maximum, the decay rate starts to decrease until it reaches a stationary value. This value is the characteristic photobleaching rate inside *E. coli* cells arrested with chloramphenicol. For some cyan, yellow and green FPs, we have reported this stationary decay rate in **Supplementary Table 1**. **Bottom row**. By reducing exposure time and excitation intensity it is possible to practically eliminate sizeable effects of photobleaching and fluorescence curves reach a clear saturation value.

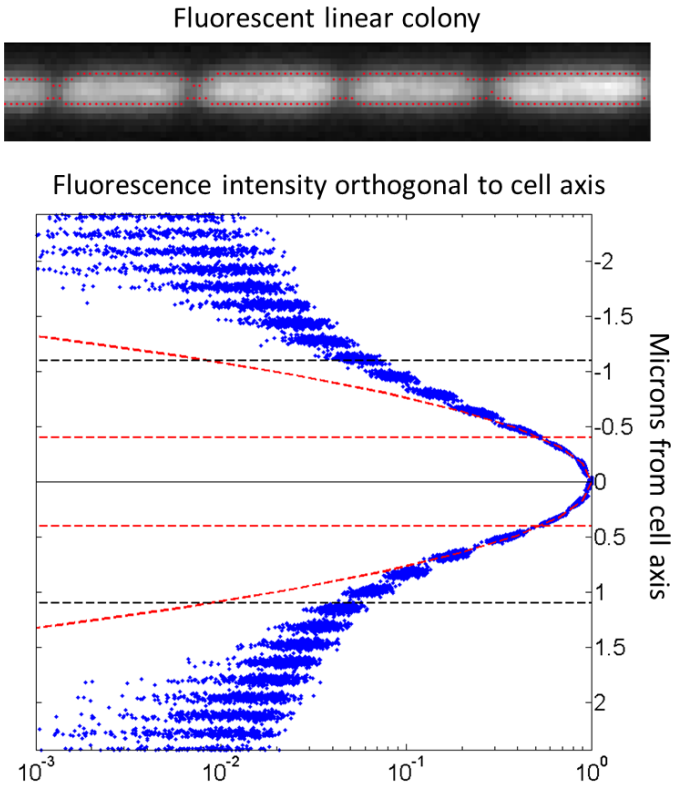

Supplementary Figure 24 | Quantifying out-of-focus fluorescence light in linear colonies. Top. Fluorescence image of a linear colony showing in red the limits of masks obtained by thresholding the phase contrast image, note that there is light outside the mask boundaries. Bottom. Blue scatter dots: normalized fluorescence intensity orthogonal to the cell axis (black line at center) of 234 cells. In comparison to a Gaussian profile (red parable), the fluorescence profile has longer tails. The red horizontal lines are one cell diameter apart (0.8 um) and contain 60% of the emitted light. Light within the black dotted lines (2.2 um apart from each other) accounts for 95% of the total fluorescence. In our analysis we add this out-of-focus light to the total fluorescence.

Nature Methods: doi:10.1038/nmeth.4509

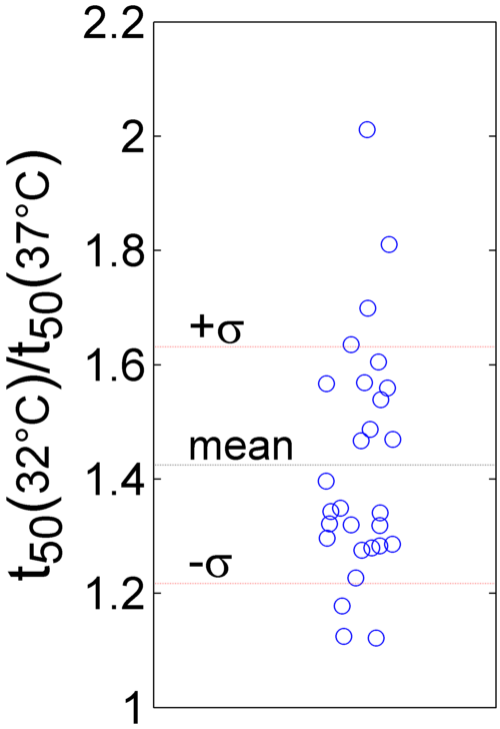

Supplementary Figure 25 | Ratio of maturation times at 32°C and 37°C for all FPs for which experimental data is available. The dispersion in the x axes is artificial and serves to better visualize the distribution of the ratio between the two maturation times. As can be seen, almost all ratios (~85%) are smaller than one standard deviation above the mean.

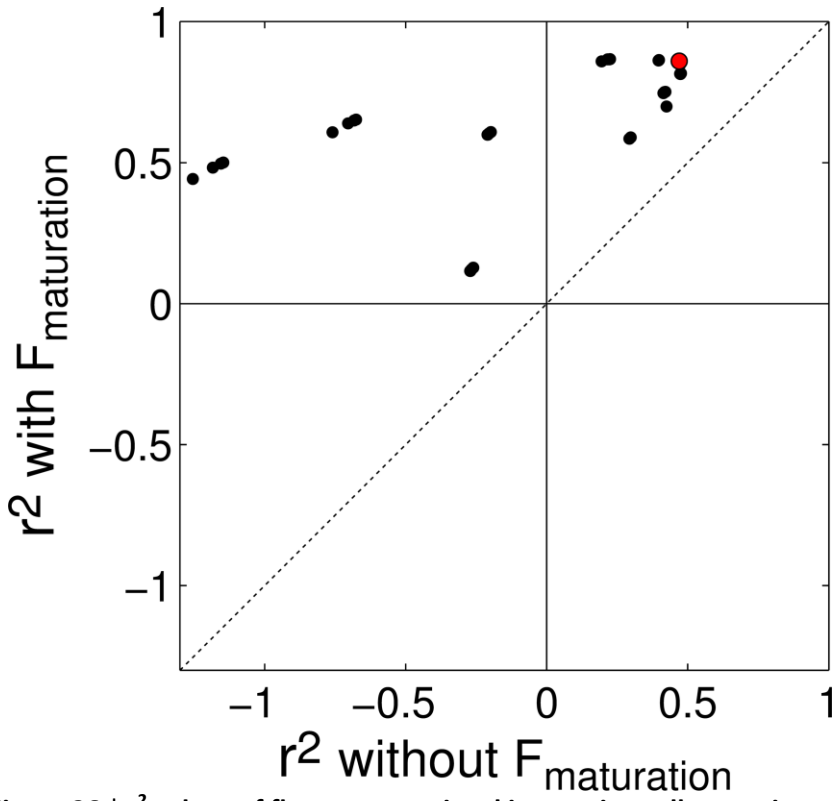

Supplementary Figure 26 | r^2 values of fluorescence signal in growing cells *vs* estimated fluorescence signal using single-source *in vitro* brightness of different red FPs, multiplying with or ignoring the maturation factor. We generated all different sets of *in vitro* values from same-laboratory characterizations for the nine red FPs listed in **Supplementary Table 2**. Also, for every set, we normalized by every red FP in the set. With each set of *in vitro* values thus generated, we estimated fluorescence signal in growing cells by multiplying the *in vitro* brightness with the expression factor and with or without the maturation factor. The dotted line is the identity line. As can be seen, in every possible set of *in vitro* values, taking into account the maturation factor increases considerably the r^2 between estimated FP signal and observed signal in growing cells. The red dot corresponds to the r^2 of the set of *in vitro* values in bold face in **Supplementary Table 2** normalized by the value of mRFP1. See **Supplementary Figure 12** for the definition of r^2.

1 Coding Sequences of Fluorescent Proteins

For cyan, UV-excitable green, green, and yellow FPs, mutations are relative to the avGFP (GenBank: M62653.1) sequence. Following the wtGFP amino acid sequence, our library constructs do not have a valine (codon GTG) usually added at the second position of the amino acid sequence. The purpose of this valine is to increase translation efficiency in eukaryotes (1). The lack or addition of the 2nd valine does not alter maturation kinetics as demonstrated in **Supplementary Figure 8.**

moxFPs present the neutral mutations H231L and Q80R (2), which we ignored in our constructs.

For mCerulean, we used the sequence defined in (3, 4) given that the definition in the original publication (5) is ambiguous: Cerulean is defined as (ECFP/S72A/Y145A/H148D) with the definition of ECFP given in reference (6). However, this last reference only contains sequence definitions of ECFP ancestors. The earliest definition of ECFP that we could find is in (7). Using this reference, mCerulean would contain an extra mutation, N164H, not included in the modern version of mCerulean (3, 4). However, this extra mutation N164H appears in what we have called mCerulean ME (8).

The version of mEmerald that we characterized appears in (2). This version differs from the original mEmerald sequence by one mutation, F64L (8).

We call Venus NB the original Venus FP described by Miyawaki *et al.*(9). When first published, the fast *in vitro* refolding/oxidation of Venus NB was highlighted. In a subsequent study, Miyawaki *et al.* reported the crystal structure of Venus(10). In that study, they added a new substitution, V68L; we call this variant Venus JBC. Four years later, Kremers *et al.*(3) took Venus JBC and reverted L68 back to V68 to get Venus NB again. Kremers *et al.* called this revertant SYFP2. mVenus ME is mVenusJBC with the extra mutation Q69M. Venus SX is Venus JBC with extensive substitutions in the C-terminus (9).

In DsRed-Express, DsRed-Express2, mRFP1, mScarlet, mScarlet-I, mCherry, mCherry2, and E2-Crimson, mutations are relative to the wild-type DsRed protein sequence (13). In TurboRFP, TagRFP, TagRFP-T, mKate2, mNeptune2, mNeptune2.5, Katushka, and Katushka-9-5, mutations are relative to the eqFP578 protein sequence (14). Finally, in mRuby3 and mRuby3 Addgene mutations are relative to the eqFP611 protein sequence (15). mRuby3 Addgene is mRuby3 (16) minus T40V and is the sequence deposited by the authors in Addgene (#74252).

The development of mCherry included the addition of the N- and C- termini of avGFP to mRFP1 (a DsRed variant). Thus, there is a shift in the mCherry alignment to the DsRed sequence. We decided to indicate the mutations with respect to the DsRed core and add, at the beginning and at the end of the sequence, the avGFP N- and C- termini used in blue. Note that, at the N-terminus, there is a leucine in red to indicate that we changed the original methionine to a leucine given that this downstream methionine works as an alternative translation start site. Thus every mCherry mRNA transcript might produce a mixture of two kinds of proteins, both of them fluorescent (17). To characterize solely the maturation time of the species intended to be mCherry or mCherry2 we decided to eliminate translation from the second start site by mutating the methionine into a leucine; we indicate this change by appending an “L”

to the name of the FPs: mCherry-L or mCherry2-L. Also, note that mRFP1 is the regular mRFP1 and mRFP1* is mRFP1 plus the N- and C-termini of avGFP.

FP Name	Mutations relative to corresponding FP ancestor	Ref.
mCerulean	F64L, S65T, Y66W, S72A, Y145A, N146I, H148D, M153T, V163A, A206K	(3-5)
SCFP1	F64L, S65T, Y66W, V68L, S72A, N146I, M153T, V163A, S175G, A206K	(3)
SCFP3A	F64L, S65T, Y66W, S72A, N146I, H148D, M153T, V163A, S175G, A206K	(3)
mCerulean ME	F64L, S65T, Y66W, S72A, Y145A, N146I, H148D, M153T, V163A, N164H, A206K	(11)
mTurquoise	F64L, Y66W, S72A, N146I, H148D, M153T, V163A, S175G, A206K	(18)
mCerulean3	F64L, Y66W, S72A, Y145A, N146I, S147H, H148G, M153T, V163A, K166G, I167L, R168N, H169C, A206K	(4)
mTurquoise2	F64L, Y66W, S72A, N146F, H148D, M153T, V163A, S175G, A206K	(19)
moxCerulean3	S30R, Y39N, C48S, F64L, Y66W, C70S, S72A, N105T, Y145A, N146I, S147H, H148G, M153T, V163A, K166G, I167L, R168N, H169C, I171V, A206K	(20)
Sapphire	S72A, Y145F, T203I	(8)
T-Sapphire	Q69M, C70V, S72A, Y145F, V163A, S175G, T203I	(21)
mEGFP	F64L, S65T, A206K	(1)
mGFPmut2	S65A, V68L, S72A, A206K	(22)
mGFPmut3	S65G, S72A, A206K	(22)
mEmerald	F64L, S65T, S72A, N149K, M153T, I167T, A206K	(2)
sfGFP	S30R, Y39N, F64L, S65T, F99S, N105T, Y145F, M153T, V163A, I171V, A206V	(23)
moxGFP	S30R, Y39N, C48S, F64L, S65T, C70S, F99S, N105T, Y145F, M153T, V163A, I171V, A206K	(20)
mEYFP	S65G, V68L, S72A, T203Y, A206K	(2)
mVenus NB	F46L, F64L, S65G, S72A, M153T, V163A, S175G, T203Y, A206K	(9)
mVenus JBC	F46L, F64L, S65G, V68L, S72A, M153T, V163A, S175G, T203Y, A206K	(10),(3)
mYPet	F46L, I47L, F64L, S65G, S72A, M153T, V163A, S175G, T203Y, A206K, S208F, V224L, H231E, D234N	(24)
mVenus ME	F46L, F64L, S65G, V68L, Q69M, S72A, M153T, V163A, S175G, T203Y, A206K	(11)
Venus SX	F46L, F64L, S65G, V68L, S72A, M153T, V163A, S175G, T203Y, T230D, H231L, G232Q, M233F, D234E, E235V, L236P, Y237I, K238L	(12)
Clover	S30R, Y39N, S65G, Q69A, F99S, N105T, Y145F, M153T, V163A, I171V, T203H	(25)
moxVenus	S30R, Y39N, F46L, C48S, F64L, S65G, V68L, C70S, S72A, N105T, Y145F, M153T, V163A, I171V, S175G, T203Y, A206K, F223R	(20)

mClover3	S30R, Y39N, S65G, Q69A, F99S, N105T, Y145F, N149Y, M153T, G160C, V163A, I171V, T203H, A206K	(16)
DsRed-Express	R2A, K5E, N6D, T21S, H41T, N42Q, V44A, C117S, T217A	(13)
TurboRFP	R32G, T68A, L79F, L110F, S131P, L138R	(14)
TagRFP	R32G, K42R, K67R, L79F, I93V, N112D, I115L, N122R, S131P, R155E, H157R, Q159D, Y169H, H171I, S173N, F192V, H193Y, F194Y, M216V, K220R, R231K	(14)
TagRFP-T	R32G, K42R, K67R, L79F, I93V, N112D, I115L, N122R, S131P, R155E, H157R, S158T, Q159D, Y169H, H171I, S173N, F192V, H193Y, F194Y, M216V, K220R, R231K	(26)
DsRed-Express2	R2D, S4T, K5E, E10P, R17H, T21S, R36K, H41T, N42Q, V44A, K47Q, C117T, K121H, M141L, A145P, D169G, Q188K, I210V, T217A, G219A, L225Q	(27)
mRFP1*	**MSKGEE NNLA VIKEF**… T21S, H41T, N42Q, V44A, V71A, K83L, C117E, F124L, I125R, V127T, L150M, R153E, V156A, H162K, K163M, A164R, L174D, V175A, F177V, S179T, I180T, Y192A, Y194K, V195T, S197I, T217A, H222S, L223T, F224G … **EGRHSTG GMDELYK**	(28)
mRFP1	R2A, K5E, N6D, T21S, H41T, N42Q, V44A, V71A, K83L, C117E, F124L, I125R, V127T, L150M, R153E, V156A, H162K, K163M, A164R, L174D, V175A, F177V, S179T, I180T, Y192A, Y194K, V195T, S197I, T217A, H222S, L223T, F224G	(28)
mCherry-L	**MSKGEE DNLA IIKEF**… V7I, R17H, T21S, H41T, N42Q, V44A, Q66M, V71A, K83L, C117E, F124L, I125R, V127T, T147S, L150M, R153E, V156A, H162K, K163Q, A164R, L174D, V175A, F177V, S179T, I180T, M182K, Y192A, Y194N, D196N, S197I, T217A, H222S, L223T, F224G … **EGRHSTG GMDELYK**	(29)
mCherry2-L	**MSKGEE NNLA IIKEF**… V7I, R17H, T21S, H41T, N42Q, V44A, Q66M, V71A, K83L, K92N, C117E, F124L, I125R, V127T, K138C, K139R, L150M, R153E, V156A, H162K, K163Q, A164R, L174D, V175A, F177V, S179T, I180T, M182K, Y192A, Y194N, S197I, T202L, T217A, H222S, L223T, F224G … **EGRHSTG GMDELYK**	(30)
mRuby3	**MSKGEE LIKENMRMKVVMEG…** M12K, Y22H, D31E, N33R, M36E, T38V, T40V, V46I, K67R, H72Y, T73P, K74A, G75D, F102V, M105T, C114E, H118N, A119V, T122R, A131P, L147M, S158T, Q159D, M160I, N163K, Y169H, S171H, S173N, E175V, E185G, F187I, F192V, F194A, L202I, K207N, M209T, F210Y, H214R, H216V, F221Y, C222S, D223N **… AVAKYSNLGG GMDELYK**	(16)

mRuby3 Addgene	**MSKGEE LIKENMRMKVVMEG…** M12K, Y22H, D31E, N33R, M36E, T38V, V46I, K67R, H72Y, T73P, K74A, G75D, F102V, M105T, C114E, H118N, A119V, T122R, A131P, L147M, S158T, Q159D, M160I, N163K, Y169H, S171H, S173N, E175V, E185G, F187I, F192V, F194A, L202I, K207N, M209T, F210Y, H214R, H216V, F221Y, C222S, D223N **… AVAKYSNLGG GMDELYK**	(16)
mScarlet	**MSKGE AVIKEF…** N6A, R17H, T21S, V22M, H41T, N42Q, V44A, A57S, Q66M, K70R, V71A, Y72F, V73T, K83Y, L85Q, V104A, S111T, Q114E, C117T, F118L, F124L, I125R, V127T, S131P, R153E, E160D, H162K, K163M, K166R, H172R, V175A, E176D, S179T, I180T, M182K, L189M, Y192A, Y194N, S197R, I210V, T217S, H222S, L223T, F224G **… EGRHSTG GMDELYK**	(31)
mScarlet-I	**MSKGE AVIKEF…** N6A, R17H, T21S, V22M, H41T, N42Q, V44A, A57S, Q66M, K70R, V71A, Y72F, V73I, K83Y, L85Q, V104A, S111T, Q114E, C117T, F118L, F124L, I125R, V127T, S131P, R153E, E160D, H162K, K163M, K166R, H172R, V175A, E176D, S179T, I180T, M182K, L189M, Y192A, Y194N, S197R, I210V, T217S, H222S, L223T, F224G **… EGRHSTG GMDELYK**	(31)
Katushka	E3V, K6T, N21D, R32G, L79F, I115L, S131P, N143S, G152S, F174L, H193Y, H197R, K220R, R231S	(32)
mKate2	R32G, K42R, V45A, L79F, I93V, N112D, I115L, N122R, S131P, N143S, M146T, R155E, H157R, S158A, Q159D, Y169H, H171I, S173N, F174L, F192V, H193Y, F194Y, H197R, M216V, K220R	
E2-Crimson	R2D, S4T, K5E, E10P, R17H, T21S, E32V, R36K, H41T, N42Q, V44A, K47Q, Q66F, V71A, V73I, K83L, L85Q, C117T, F118L, K121H, M141L, A145P, L150N, I161N, K163M, D169G, V175C, Q188K, Y193H, S197Y, I210V, T217A, G219A, L225Q	(33)
Katushka-9-5	K6S, N21D, R32G, L79F, I115L, S131P, N143S, G152S, F174L, H193Y, H197R, R198K, K220R, R231S	(34)
mNeptune2	**MSKGEE LIKENM…** R32G, M41G, K42R, S61C, L79F, I93V, A104V, N112D, I115L, I121L, N122R, S131P, N143S, M146T, R155E, H157R, S158C, Q159D, Y169H, S173N, F174L, F192V, H193Y, H197R, K207N, M216V, K220R, R231K **… SKLGHK LN GMDELYK**	(35)
mNeptune2.5	**MSKGEE LIKENM…** M11T, S28H, R32G, M41N, K42R, S61C, L79F, I93V, A104V, N112D, I115L, I121L, N122R, S131P, N143S, M146T, R155E, H157R, S158C, Q159D, Y169H, S173N, F174L, F192V, H193Y, H197R, K207N, M216V, K220R, R231K **… SKLGHK LN GMDELYK**	(35)

2 Temperature Calibration for Single-Cell Microfluidics Experiments

Given the strong dependence of maturation time on temperature, we made sure temperature was correctly controlled inside the microfluidics device. Our main concern was to know if flown-in media at 22°C would equilibrate at the desired temperature before reaching the cells. We took advantage that our microscopy setup was encaged inside an acrylic box with a temperature controller. Besides the necessary tubing between the peristaltic pump with the media and the microfluidics device, we added 1m of tubing in excess to be inside the acrylic box. The excess tubing inside the thermally controlled box allows the media to reach the desired temperature before entering the microfluidic device. To measure the actual temperature inside the device, we ran a microfluidics experiment introducing a thermocouple between the bottom coverslip and the agarose pad. 1 m excess tubing was enough to deliver media at the desired temperature $\pm$ 0.5°C in a flow rate range from 0ul/sec to 70ul/sec and in a temperature range from 30 to 37°C.

3 Correction Factors to Take into Account the Use of the Same Ex/Em Filters with Proteins That Have Different Ex/Em Spectra

In order to compare the brightness of different FPs of the same color category but with different ex/em spectra, we adjusted the measured *in vitro* brightness with two compensating factors: one for the molar extinction coefficient (ϵ), and another one for the quantum yield (QY). The emission factor was equal to the fraction of the emission spectrum covered by the emission filter. The excitation factor was equal to

$$f_{ex} = \frac{\int_{Ex1}^{Ex2} 1 - 10^{-Abs(\lambda_{ex})} d\lambda_{ex}}{\int_{\lambda_{max}-0.5}^{\lambda_{max}+0.5} 1 - 10^{-Abs(\lambda_{ex})} d\lambda_{ex}} \approx \frac{\int_{Ex1}^{Ex2} 1 - 10^{-Abs(\lambda_{ex})} d\lambda_{ex}}{1 - 10^{-\epsilon}},$$

with Ex_1 and Ex_2 equal to the limits of the excitation filter, Abs the absorption spectrum and $\lambda_{\max}$ the wavelength of maximum absorption. Note that the numerator is just the fraction of absorbed light between the limits of the filter because $1 - 10^{-Abs(\lambda_{ex})} = 1 - T(\lambda_{ex})$, where T is the transmittance. Thus f_{ex} quantifies how many times more the FP absorbs light from a broader excitation window with respect to absorption at the maximum, $1 - 10^{-\epsilon}$. In the case of flow cytometry, we modeled the width of the laser as a bandpass of 2 nm. See **Online Methods** for filters used in microscopy and in flow cytometry.

	Flow Cytometry		Microscopy	
	QY factor	**ε factor**	**QY factor**	**ε factor**
SCFP3A	0.22	2.89	0.41	24.00

Nature Methods: doi:10.1038/nmeth.4509

SCFP1	0.19	2.94	0.39	24.13
mCerulean	0.21	2.91	0.40	24.00
mCeruleanME	0.21	2.91	0.40	24.02
mTurquoise2	0.22	2.89	0.41	23.76
mCerulean3	0.23	2.94	0.41	24.15
mTurquoise	0.23	2.93	0.41	24.00
moxCerulean3	0.23	2.92	0.41	24.10
mEGFP	0.60	2.98	0.60	17.45
mGFPmut2	0.57	2.96	0.57	18.44
mGFPmut3	0.61	2.61	0.61	14.67
sfGFP	0.60	2.99	0.60	18.00
wtGFP	0.52	0.86	0.52	6.42
moxGFP	0.59	2.96	0.59	18.14
mEmerald	0.57	2.92	0.57	18.28
mVenJBC	0.47	1.02	0.47	13.24
mVenNB	0.47	1.08	0.47	13.79
mVenME	0.46	1.03	0.46	13.57
mEYFP	0.46	1.13	0.46	14.96
mYPet	0.47	0.99	0.47	12.77
Clover	0.33	1.47	0.33	19.80
moxVenus	0.45	1.09	0.45	12.87
mClover3	0.33	1.46	0.33	19.61
mScarlet	–	–	0.36	8.64
mScarlet-I	–	–	0.36	8.10
mRFP	–	–	0.45	19.41
TagRFP	–	–	0.28	2.35
TagRFP-T	–	–	0.30	4.28
mCherry-L	–	–	0.46	19.62
DsRedExpress	–	–	0.30	4.36
Katushka	–	–	0.55	19.88
TurboRFP	–	–	0.22	0.89

4 Impact of Photobleaching on Maturation Time Experiments

Photobleaching of FPs is a complex process. For example, it has been shown that EYFP, Citrine and ECFP present reversible photobleaching (19, 36). Also, there are FPs that do not photobleach with a single rate, e.g. Emerald (2) or FPs that increase their brightness after an initial exposure to excitation light (32, 37). In order to try to avoid the previous effects from complicating the interpretation of our maturation curves, we set illumination power and exposure time to the lowest experimental possible value. We ran test experiments to determine the minimum illumination that would still give us quantifiable data. The result of these pilot experiments was that FPs practically did not photobleach during the data acquisition process except for mCerulean, SCFP1, SCFP3A, mCeruleanME, mGFPmut3. For these FPs we corrected the maturation curves using the procedure described in the section

Photobleaching Correction. Additionally, for mEGFP(32°C), mGFPmut2(32°), sfGFP(32°C), mVenusME (32°C) and mVenusNB (32°C) we did not perform low illumination experiments, but we corrected the maturation curves also following the procedure in section *Photobleaching Correction*.

The initial illumination in some pilot experiments was too high and photobleaching was easily quantifiable. Thus, we were able to determine, for a subset of FPs, a relative photobleaching rate in living cells that we report in Table S1 (for photobleaching quantification, see *Photobleaching Rate as a Function of Chloramphenicol Concentration*). See **Supplementary Figure 23** for examples of photobleaching test experiments.

5 Photobleaching Correction

In a few cases, we corrected photobleaching from maturation curves as follows. We assume a general fluorescent protein dynamics

$$p_i = p_{i-1} + dp(t, p_{i-1}),$$

with p the total number of proteins (fluorescent and photobleached proteins) and dp the, in general non-autonomous, change in total protein number between measurements $i-1$ and i. If we assume that photobleaching does not affect protein dynamics and that proteins are not degraded—i.e. dp always contributes positively to fluorescence—then the number f of fluorescent proteins follows

$$f_i = \big(f_{i-1} + dp(t, p_{i-1})\big)(1-\beta),$$

with β the photobleaching factor. If we iteratively solve the previous two equations for the total protein, p, in terms of f, we obtain

$$p_n = \frac{f_n}{1-\beta} + \frac{\beta}{1-\beta}\sum_{i=1}^{n-1} f_i\,.$$

In our experiments, when maturation has ceased and there is only photobleaching, we fit an exponential decay to obtain the decay rate λ_c. Note that λ_c –a continuous decay rate—is not equal to the discrete β of the previous equation in which fluorescence is measured *instantaneously* by exposing cells to light and then waiting a dark interval Δ before measuring again. The relationship between β and λ_c is

$$\lambda_c = -\frac{1}{\Delta}\log(1-\beta).$$

In **Supplementary Figure 22**, we show an example of a FP for which we acquired two experiments one in which the mean fluorescence curve photobleaches and another one in which photobleaching is not detectable. After correcting the fluorescence decay from the curve presenting photobleaching, we see that the curve presents the same maturation kinetics as the curve that does not present photobleaching.

6 Photobleaching Rate as a Function of Chloramphenicol Concentration

After chloramphenicol exposure, photobleaching and maturation happen simultaneously. To solely determine the photobleaching rate, we fitted, in a 20 to 40 min window, a single exponential to the measured fluorescence and slided the window in one-minute steps. Then, we estimated the photo-bleaching decay rate as the stationary value of the single exponent in the fit throughout these time windows.

We observed that mGFPmut2 photobleaching rate reaches a stationary value that is independent of chloramphenicol concentration in the range from 40ug/ml to 200ug/ml in M9+CA+Glu, **Supplementary Figure 21**. For [Chlor]≤25ug/ml, we detected residual GFP production—even after two hours of treatment. Whereas above a concentration of 200ug/ml—for which photobleaching appeared to be more pronounced—a few cells lysed inside the agar tracks and a few others steadily lost all their fluorescence after few minutes. At [Chlor] = 400 and after 1 hr. of treatment, the lysis was so dramatic that most linear colonies would have lost several cells. Thus, we observed that the increased loss of fluorescence signal at high [Chlor] is not due to the drug affecting the photobleaching rate, but rather to cells losing fluorescent proteins—presumably—to cell wall or cell membrane damage. Given the previous observations, all experiments were performed at [Chlor] = 100-120ug/ml.

7 Homogeneity of Chloramphenicol Treatment in a Linear Colony

Even though start of chloramphenicol treatment is evident by the change in elongation rate of a linear colony (see **Supplementary Figure 2**), it is not clear if the potency of the treatment is independent of cell position in the agar track. To answer this question, we show in **Supplementary Figure 3** a typical response of a linear colony to chloramphenicol treatment. As can be seen, all cells –including those at the center of the agar track– respond with no delay as it is evident from the identical decay in elongation rate for all cells along the track.

8 Experimental Observations where $F_{expression}$ affects FP Fluorescence Signal in Growing Cells

In general, FPs derived from the same backbone, if coded with identical codons (except where they differ), will have a similar net expression F_{ne}. However, some exceptions exist. For example, although mScarlet-I differs from mScarlet by just one residue, Bindels *et al*.(31) found that in the cytoplasm of mammalian cells, the net expression of mScarlet-I was 50% higher than that of mScarlet's. Interestingly, we find that in *E. coli* both mScarlets have similar net expression levels. We note that Bindels *et al.*, like

us in *E. coli*, find that t_{50} (Scarlet-I) << t_{50} (Scarlet). Thus, this discrepancy likely arises from organism specific effects on the net expression.

In addition, we find in *E. coli* that while expression systems are the same across the whole FP library, mGFPmut3 has 40% lower net expression than other green-avFPs. These examples signal that even when variations in transcription and translation are reduced/eliminated at the sequence level, there can be unexpected variations in net expression ($F_{expression}$), e.g. differential protein degradation. In such cases, the resulting fluorescence signal cannot be solely accounted by $F_{in\ vitro}$ and F_{mat}, but we also need to take into account $F_{expression}$.

Name of Fluorescent Protein	Photostability in *E. coli*[a]	This Study					Original Reference				Gadella Lab (3, 18, 19)			Piston Lab (38)		
		λ_{Abs}	ε[b]	λ_{Em}	QY[b]	ε QY	ε	QY	εQY[e]	Ref.	ε	QY	εQY[f]	ε	QY	εQY[f]
mCerulean	1.00 ± 0.12	435	31.2 ± 2.3	476	0.46 ± 0.01	14.3 ± 1.1	43.0	0.62	26.6	(5)	33.0	0.49	16.2	28.0	0.51	14.3
SCFP1	5.13 ± 2.77	435	36.3 ± 7.5	478	0.23 ± 0.01	8.26 ± 1.7	29.0	0.24	7.0	(3)	29.0	0.24	7.0	—	—	—
SCFP3A	1.00 ± 0.09	435	32.6 ± 4.9	476	0.53 ± 0.02	17.1 ± 2.6	30.0	0.56	16.8	(3)	30.0	0.56	16.8	—	—	—
mCerulean ME	1.00 ± 0.06	435	31.2 ± 4.5	476	0.48 ± 0.03	14.9 ± 2.3	—	—	—	(11)	—	—	—	—	—	—
mTurquoise	ND	435	37.3 ± 7.3	476	0.69 ± 0.04	25.7 ± 5.2	30.0	0.84	25.2	(18)	30.0	0.84	25.2	31.0	0.84	26.0
mCerulean3	ND	435	32.9 ± 4.3	476	0.68 ± 0.04	22.4 ± 1.4	40.0	0.87	34.8	(4)	30.0	0.80	24.0	29.0	0.80	23.2
mTurquoise2	2.86 ± 0.66	435	36.6 ± 5.7	475	0.78 ± 0.04	28.7 ± 4.7	30.0	0.93	27.9	(19)	30.0	0.93	27.9	31.0	0.92	28.5
moxCerulean3	ND	435	33.6 ± 8.6	475	0.66 ± 0.04	22.2 ± 5.8	41.0	0.87	35.7	(20)	—	—	—	—	—	—
wtGFP[c]	ND	398	24.1 ± 2.6	504-10	0.82 ± 0.05	19.7 ± 2.4	27.6	0.80	22.1	(39, 40)	—	—	—	—	—	—
mEGFP	1.00 ± 0.14	488	64.6 ± 25.1	510	0.70 ± 0.03	45.5 ± 17.8	56.0	0.60	33.6	(1)	—	—	—	62.0	0.74	45.9
mGFPmut2[d]	0.45 ± 0.07	485	53.9 ± 8.3	508	0.73 ± 0.04	39.3 ± 6.5	—	—	18.2	(22)	—	—	—	—	—	—
mGFPmut3[d]	0.19 ± 0.07	500	89.4 ± 6.7	513	0.39 ± 0.01	35.3 ± 2.9	—	—	20.2	(22)	—	—	—	—	—	—
mEmerald	ND	484	59.0 ± 3.7	509	0.77 ± 0.02	45.3 ± 3.1	57.5	0.68	39.1	(2)	—	—	—	62.0	0.79	49.0
sfGFP	0.41 ± 0.14	488	59.2 ± 6.0	510	0.64 ± 0.02	37.8 ± 4.0	83.3	0.65	54.2	(23)	—	—	—	53.0	0.72	38.2
moxGFP	ND	485	57.4 ± 3.5	510	0.65 ± 0.02	37.3 ± 2.6	87.0	0.58	50.5	(20)	—	—	—	—	—	—
mEYFP	>0.80	515	98.6 ± 4.2	528	0.66 ± 0.05	65.2 ± 5.3	83.4	0.61	50.9	(2)	—	—	—	—	—	—
mVenusNB	0.44 ± 0.05	515	135.3 ± 17.1	529	0.71 ± 0.01	96.5 ± 12.3	92.2	0.57	52.6	(9)	101.0	0.68	68.7	—	—	—
mVenusJBC[g]	1.00 ± 0.07	515	133.2 ± 20.9	529	0.64 ± 0.03	85.2 ± 14.0	105.0	0.64	67.2	(10)	105.0	0.64	67.2	127.0	0.67	85.1
mYPet	0.29 ± 0.04	515	153.4 ± 11.8	528	0.70 ± 0.08	107.9 ± 15.4	104.0	0.77	80.1	(24)	—	—	—	132.0	0.76	100.3
mVenus ME	0.34 ± 0.06	515	142.6 ± 42.6	528	0.68 ± 0.07	96.8 ± 30.7	—	—	—	(11)	—	—	—	—	—	—
Clover	0.80 ± 0.17	505	116.5 ± 2.6	518	0.83 ± 0.01	96.2 ± 2.7	111.0	0.76	84.4	(25)	—	—	—	105.0	0.88	92.4
moxVenus	ND	513	135.3 ± 17.1	528	0.73 ± 0.05	101.5 ± 14.5	89.0	0.49	43.6	(20)	—	—	—	—	—	—
mClover3	ND	505	122.3 ± 7.6	518	0.88 ± 0.02	107.0 ± 7.1	109.0	0.78	85.0	(16)	—	—	—	—	—	—

Supplementary Table 1 | ***In vitro* characteristics of avFPs considered in this work and references to previous characterizations. (a)** Amount of time to lose half of the initial fluorescence after the maturation process has finished; errors are SD from stationary decay rates, see **Supplementary Figure 23**. Bleaching relative to that of SCFP3A, mEGFP and mVenJBC. See **Supplementary Note** for a description of filters used. **(b)** Extinction coefficient reported in $mM^{-1}cm^{-1}$ units. Mean ± SD derived from three independent extractions except for moxCerulean, mEmerald, moxGFP, moxVenus. For these FPs only 2 independent extractions were performed. We used propagation of errors to calculate the error of brightness, $\varepsilon \cdot QY$.

See **Online Methods** for a description of fluorescent molecules used as references in QY estimation. **(c)** For wtGFP, we noticed a dependence of emission spectrum on excitation wavelength. In particular, when exciting at 398 nm, the maximum emission is at 510 nm, a value reported in (39); and, when exciting at 488 nm, the maximum is at 504, a value reported in (40). This small shift in emission maximum might have a more important impact on QY and might be the source of some discrepancies in previous work. Due to this observation, we list for further reference the excitation wavelengths used to calculate the QY. Blue FPs were excited at 425nm, greens at 455nm and yellows at 482nm. **(d)** Cormack et al. (22) report molecular brightness in arbitrary units for EGFP (or GFPmut1), GFPmut2 and GFPmut3. Here we scaled mGFPmut2 and mGFPmut3 values with respect to the molecular brightness value of mEGFP found in (1). **(e)** Brightness data used to generate **Figure 1d**. **(f)** Brightness data used to generate **Supplementary Figure 12**. **(g)** Note that Kremers *et al.* (3) performed the *in vitro* characterization of mVenusJBC (therein mVenus) and mVenusNB (therein SYFP2). Also, we believe mVenJBC is the most popular version of mVenus. Thus, we have associated to mVenJBC the *in vitro* measurement of mVenus done by Cranfill *et al.* (38).

FP Name	Original Ref				Gadella Lab (31)			Piston Lab (38)			Chudakov Lab (41)		
	ε	QY	εQY[a]	Ref	ε	QY	εQY[b]	ε	QY	εQY[b]	ε	QY	εQY[b]
mScarlet	100.0	0.70	71	(31)	**100.0**	**0.70**	**71**	—	—	—	—	—	—
mScarlet-I	104.0	0.54	57	(31)	**104.0**	**0.54**	**57**	—	—	—	—	—	—
mRFP1	44.0	0.25	11	(28)	—	—	—	**55.0**	**0.35**	**19**	—	—	—
TagRFP	100.0	0.48	48	(14)	—	—	—	—	—	—	**100.0**	**0.48**	**48**
TagRFP-T	81.0	0.41	33	(26)	**110**	**0.48**	**55**	106.0	0.32	34	—	—	—
mCherry	72.0	0.22	16	(29)	**88.0**	**0.23**	**20**	85.0	0.30	25	78.0	0.22	17
DsRedExpress	30.1	0.42	13	(42)	—	—	—	—	—	—	**39.5**	**0.51**	**20**
Katushka	65.0	0.34	22	(41)	—	—	—	—	—	—	**65.0**	**0.34**	**22**
TurboRFP	92.0	0.67	62	(14)	—	—	—	—	—	—	**92.0**	**0.67**	**62**

Supplementary Table 2 | **Original *in vitro* characterization of selected red FPs together with single-source characterization by different laboratories. (a)** Brightness data used to generate **Figure 1d. (b)** In bold face**,** brightness data used to generate **Figure 1e** and **Supplementary Figure 12**, see **Supplementary Figure 26** for the rationale behind the selection of *in vitro* values.

9 Fraction of Immature Protein for All Analyzed FPs

In every figure, the inset plot is the mean single cell fluorescence throughout the complete duration of the experiment, i.e. every curve was obtained by adding the fluorescence of all tracked cells, then dividing by the number of tracked cells. Similarly, we obtained a mean cell length curve by adding the length of all tracked cells, then dividing by the number tracked of cells, see **Supplementary Figure 2**. The maturation time data presented in Table 1 was extracted from curves obtained by tracking 75+/-20 cells. For codon optimized FPs and FPs with a 2nd valine the average number of cells was approximately 25. The vertical red line indicates the moment of chloramphenicol arrival, which was estimated using the abrupt deviation from an exponential elongation rate in the mean cell length curve (**Supplementary Figure 2**). We estimated the fraction of immature protein by subtracting the mean fluorescence value from the final mean fluorescence value. Then, we normalized the result by dividing with the increase of mean fluorescence after chloramphenicol arrival. For some FPs, fluorescence does not saturate within the experimental limit of our setup. In those cases, we estimated the last part of the maturation kinetics with a single exponential, using a rate equal to the rate of the last recorded hour of data. Those estimations are clearly indicated with a solid red line.

All fluorescence and length curves can be found in **Supplementary Data**. We also report (1) the estimated chloramphenicol arrival time; (2) the number of tracked cells; (3) the elongation rate; (4) the experimental error of the mean fluorescence curve (coefficient of variation (CV) at two intensities: high intensity or 100% and low intensity or 25%; the CV was estimated by first smoothing the mean fluorescence curve, Flscnc(t), with the function `filtfilt` in Matlab to obtain the smoothed curve, FlscncFilt(t). Then, we calculated the standard deviation of the difference (Flscnc(t)-FlscncFilt(t)) within a 10 minute window around 25% or 100% intensities; finally we divided the standard deviations by the corresponding intensity at 25% or 100%); (5) the fluorescence signal at the moment of chloramphenicol arrival (this is the value used in the y-axes of Fig. 1d-e and in **Supplementary Figure 12**); (6) a proportionality factor equal to the ratio of fluorescence signal between the FP of interest and a reference FP (this factor only applies to the y-axes of Fig. 1d-e in order to make fluorescence signal comparable given that not all FPs were taken in the same experiment but in different experiments that contained a common reference FP); and (7) the estimated biological variability quantified as the standard error of the mean (SEM) of the single cell fluorescence intensities at the moment of chloramphenicol arrival (this is the error used in the y-axes of **Fig. 1d-e** and in **Supplementary Figure 12**). Finally, we obtained the t_{50} and t_{90} values by smoothing the log transformed data using the function `csaps` in MATLAB R2013a with the smoothing parameter equal to `0.01`. The maturation time errors were estimated assuming errors in the mean cell fluorescence of $\pm$3%. Given the experimental noise (CV 25% and CV 100%, see reported values for different mean cell fluorescence curves in **Supplementary Data**), the assumed error gives at least a confidence interval of 66%, and typically it is a confidence interval of 95%.

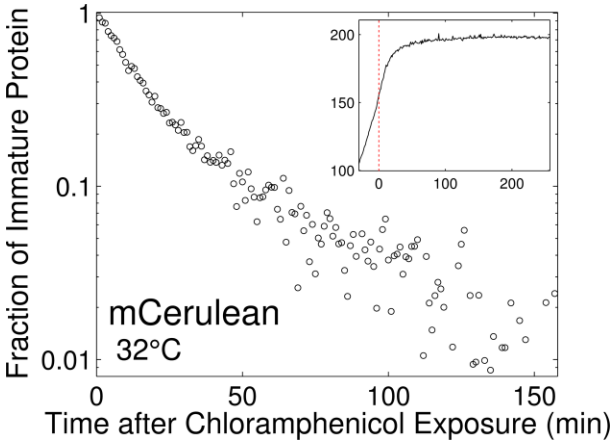
Fraction of Immature Protein
mCerulean
32°C
Time after Chloramphenicol Exposure (min)

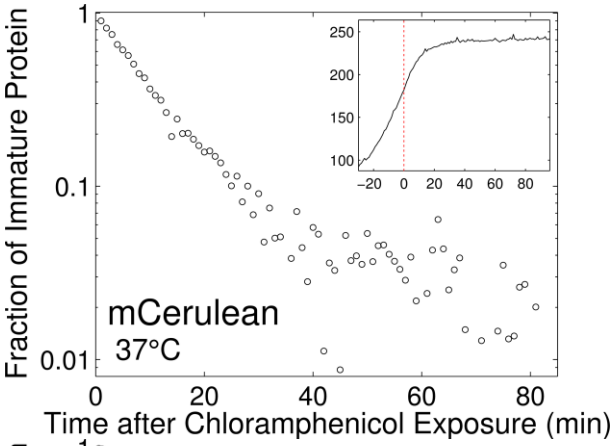
Fraction of Immature Protein
mCerulean
37°C
Time after Chloramphenicol Exposure (min)

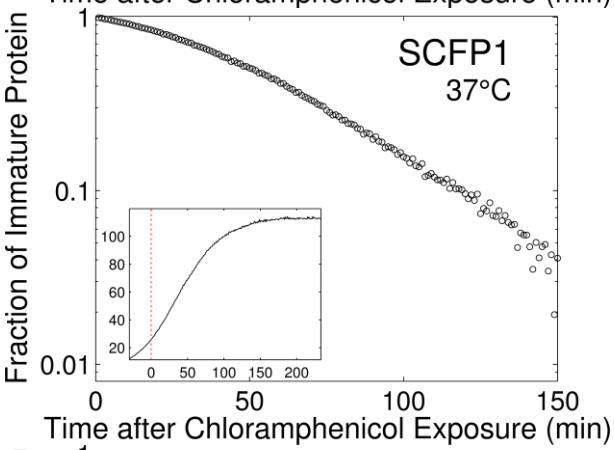
Fraction of Immature Protein
SCFP1
37°C
Time after Chloramphenicol Exposure (min)

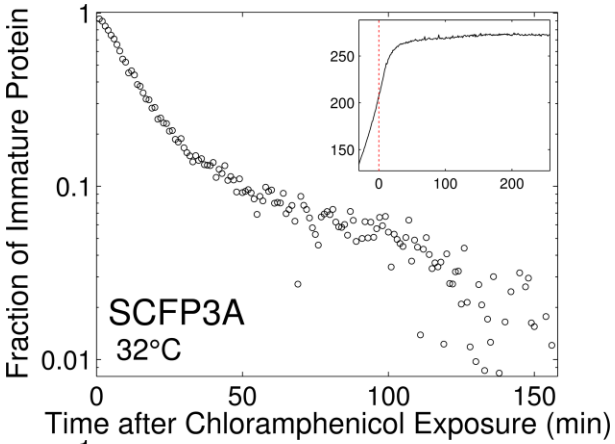
Fraction of Immature Protein
SCFP3A
32°C
Time after Chloramphenicol Exposure (min)

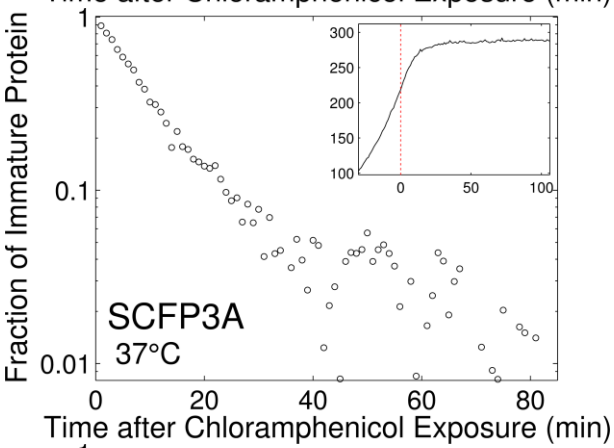
Fraction of Immature Protein
SCFP3A
37°C
Time after Chloramphenicol Exposure (min)

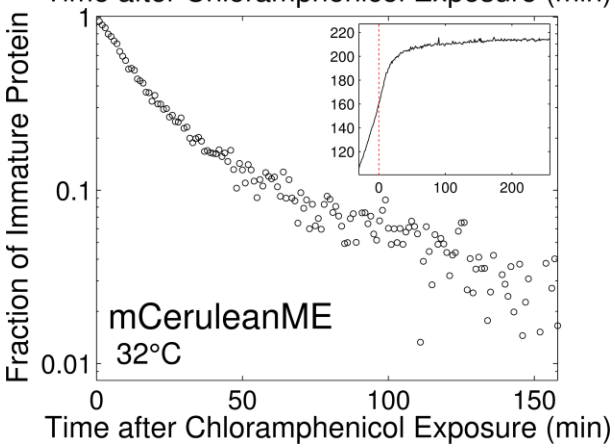
Fraction of Immature Protein
mCeruleanME
32°C
Time after Chloramphenicol Exposure (min)

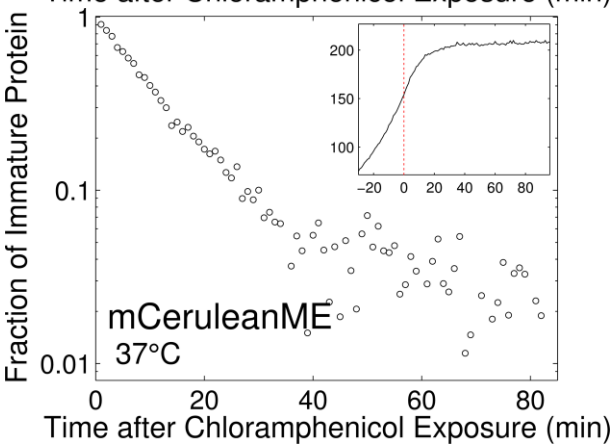
Fraction of Immature Protein
mCeruleanME
37°C
Time after Chloramphenicol Exposure (min)

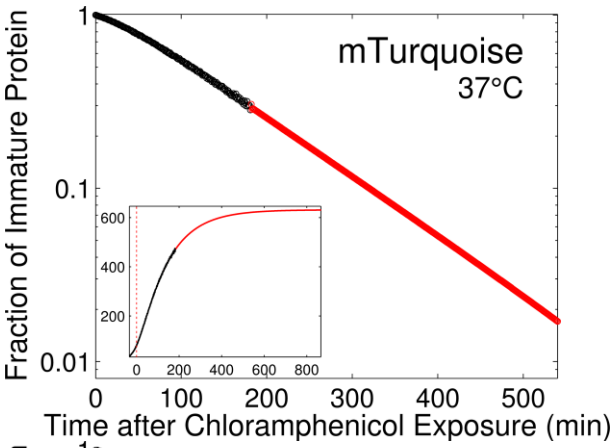
mTurquoise
37°C
Fraction of Immature Protein
Time after Chloramphenicol Exposure (min)

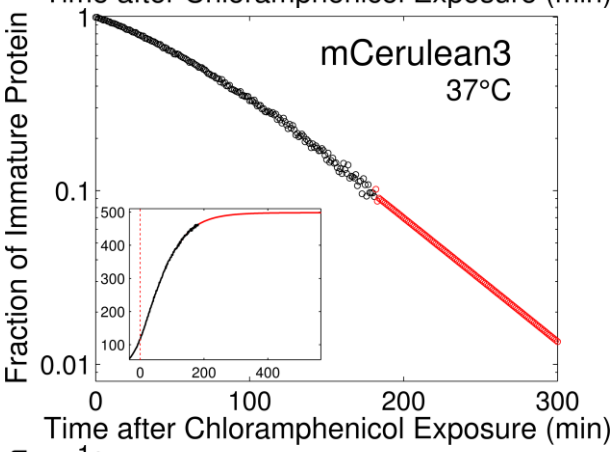
mCerulean3
37°C
Fraction of Immature Protein
Time after Chloramphenicol Exposure (min)

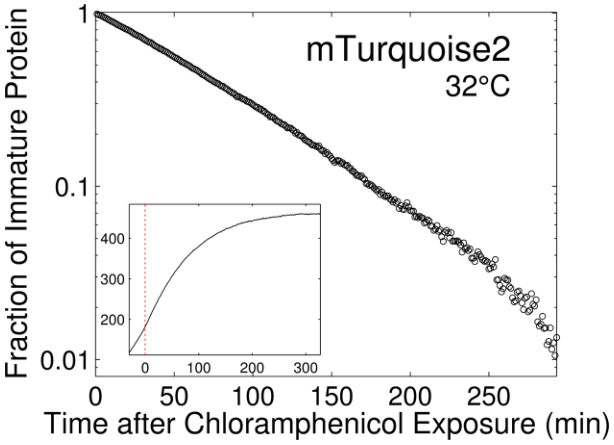
mTurquoise2
32°C
Fraction of Immature Protein
Time after Chloramphenicol Exposure (min)

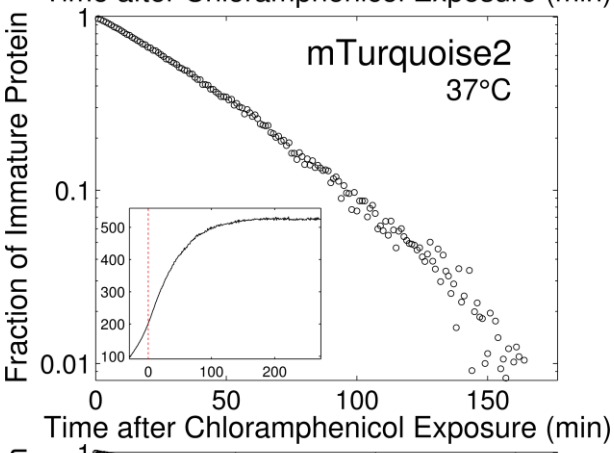
mTurquoise2
37°C
Fraction of Immature Protein
Time after Chloramphenicol Exposure (min)

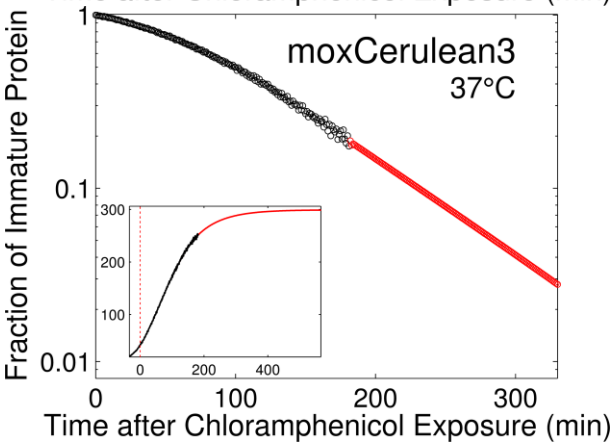
moxCerulean3
37°C
Fraction of Immature Protein
Time after Chloramphenicol Exposure (min)

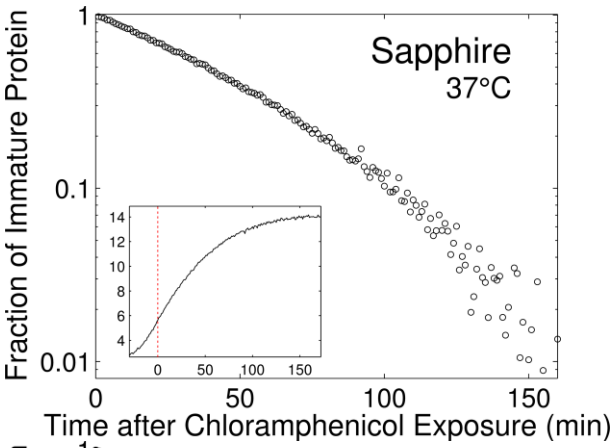
Sapphire
37°C
Fraction of Immature Protein
Time after Chloramphenicol Exposure (min)

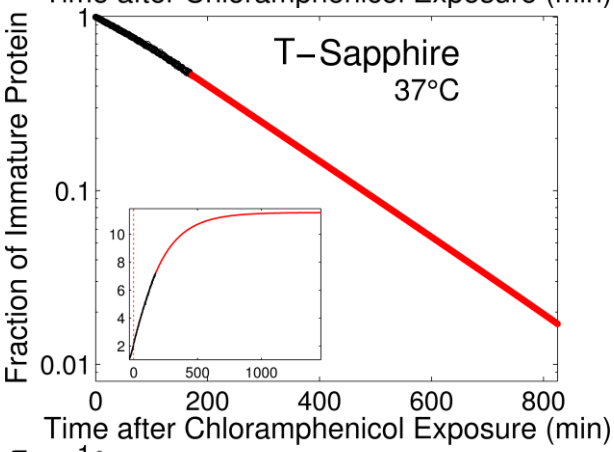
T−Sapphire
37°C
Fraction of Immature Protein
Time after Chloramphenicol Exposure (min)

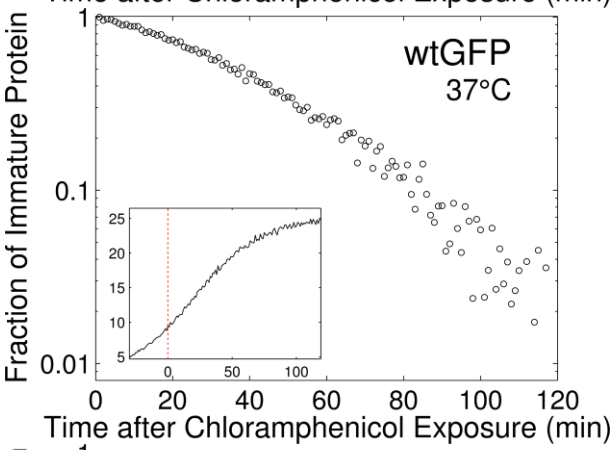
wtGFP
37°C
Fraction of Immature Protein
Time after Chloramphenicol Exposure (min)

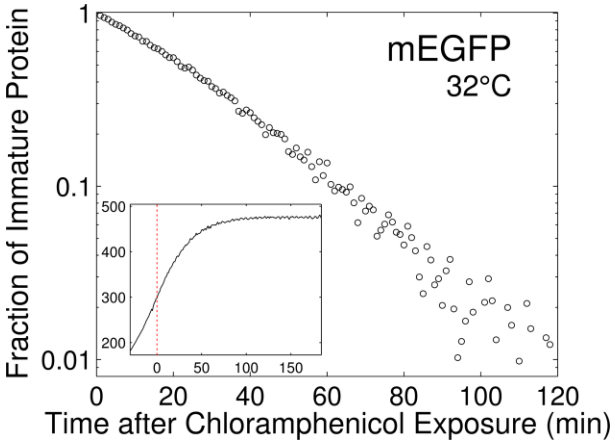
mEGFP
32°C
Fraction of Immature Protein
Time after Chloramphenicol Exposure (min)

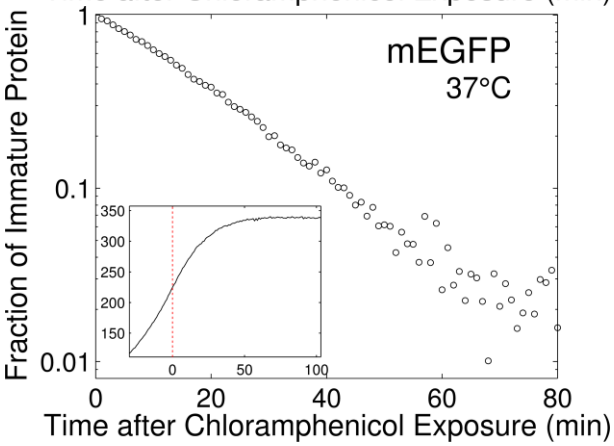
mEGFP
37°C
Fraction of Immature Protein
Time after Chloramphenicol Exposure (min)

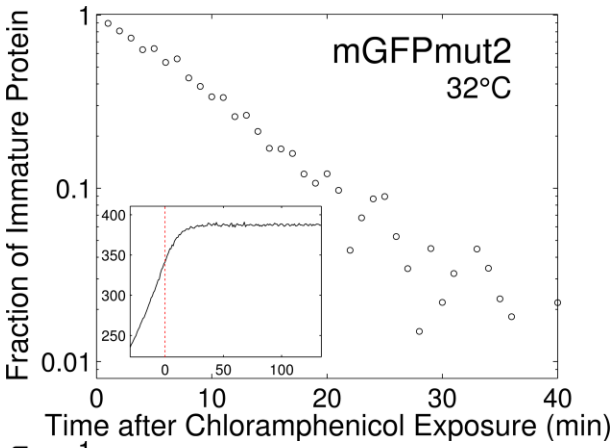

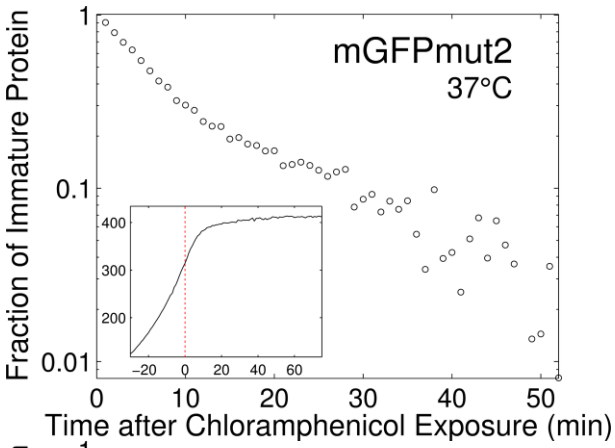

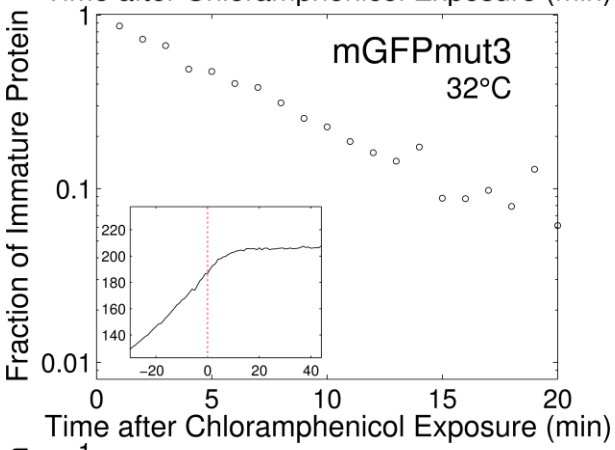

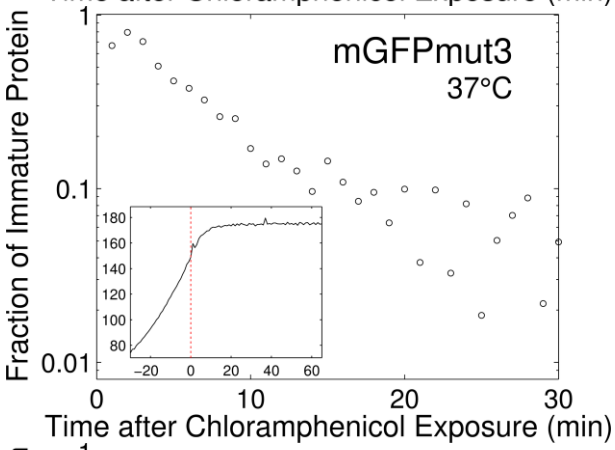

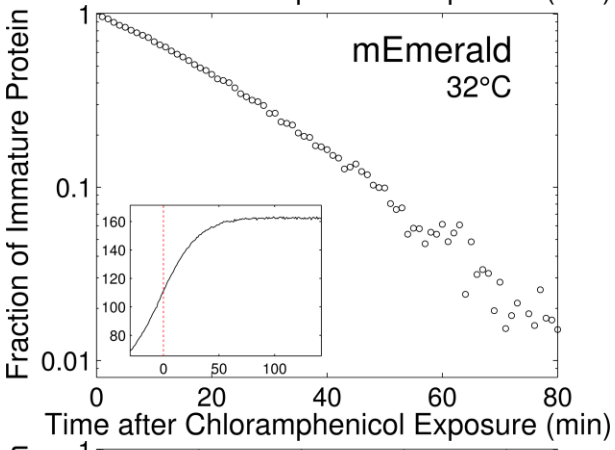

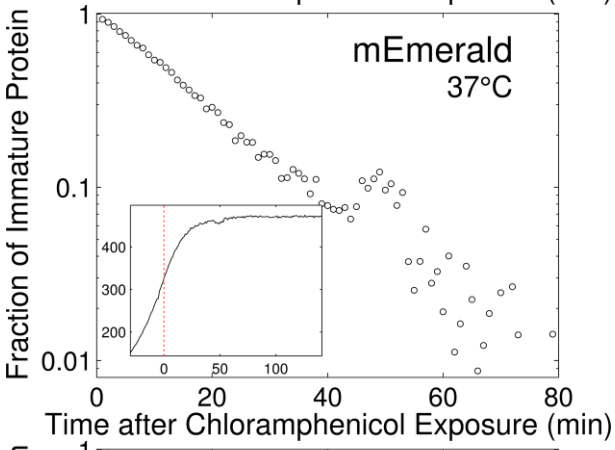

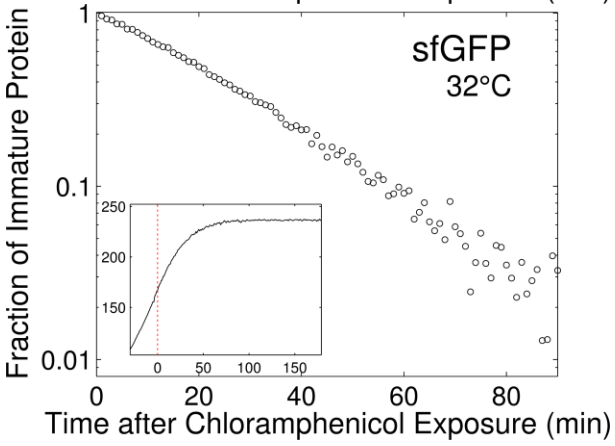

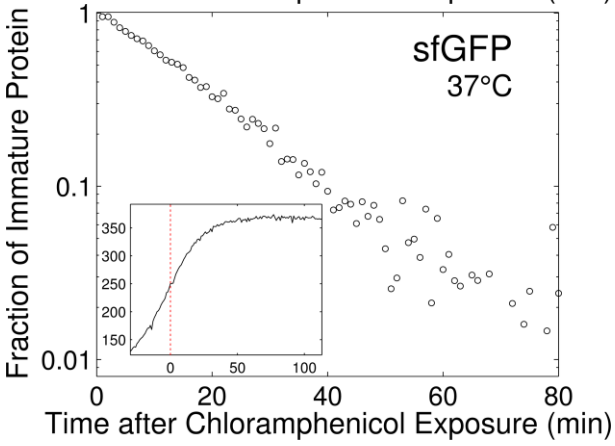

Nature Methods: doi:10.1038/nmeth.4509

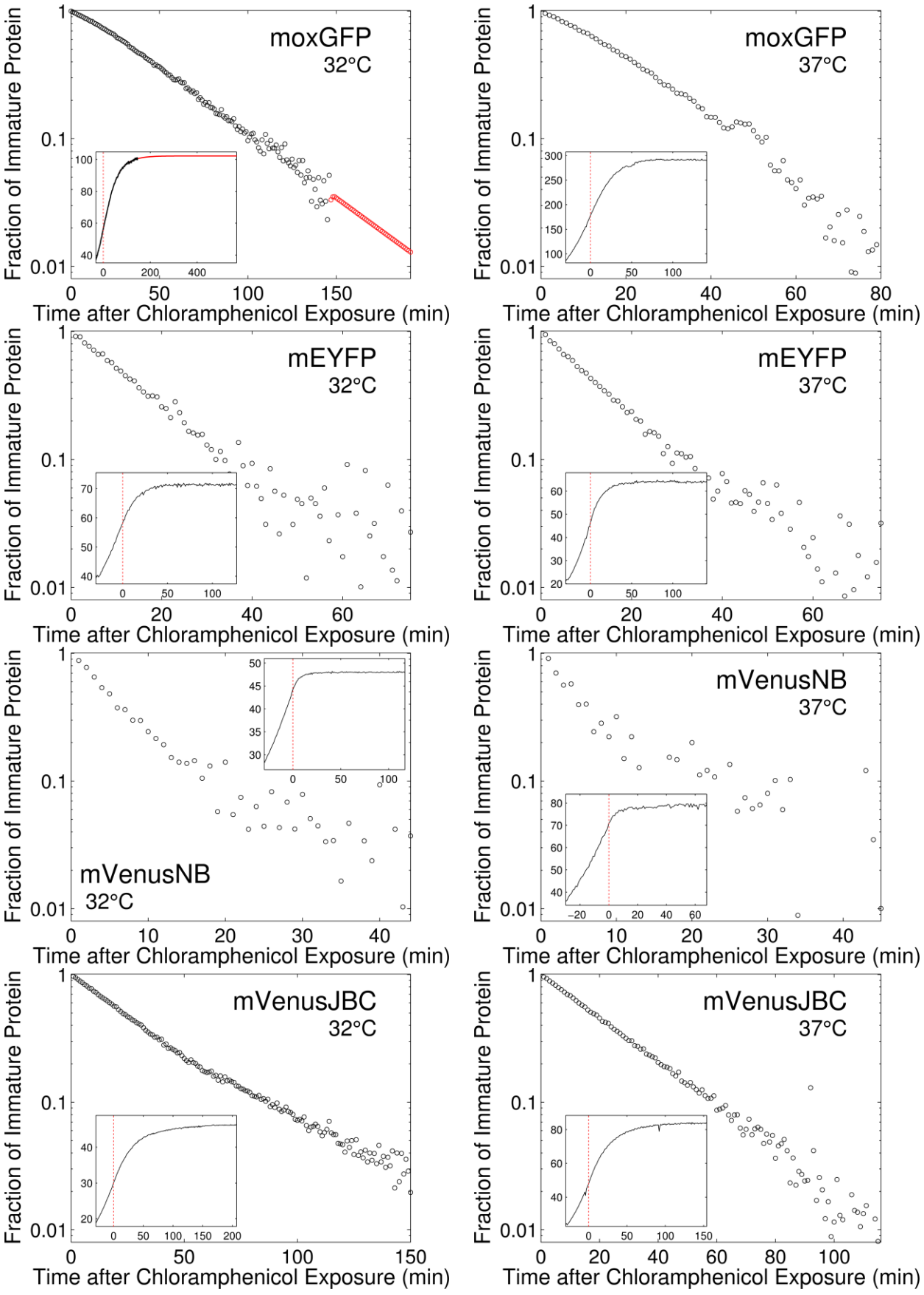
moxGFP
32°C
moxGFP
37°C
mEYFP
32°C
mEYFP
37°C
mVenusNB
32°C
mVenusNB
37°C
mVenusJBC
32°C
mVenusJBC
37°C
Fraction of Immature Protein
Time after Chloramphenicol Exposure (min)

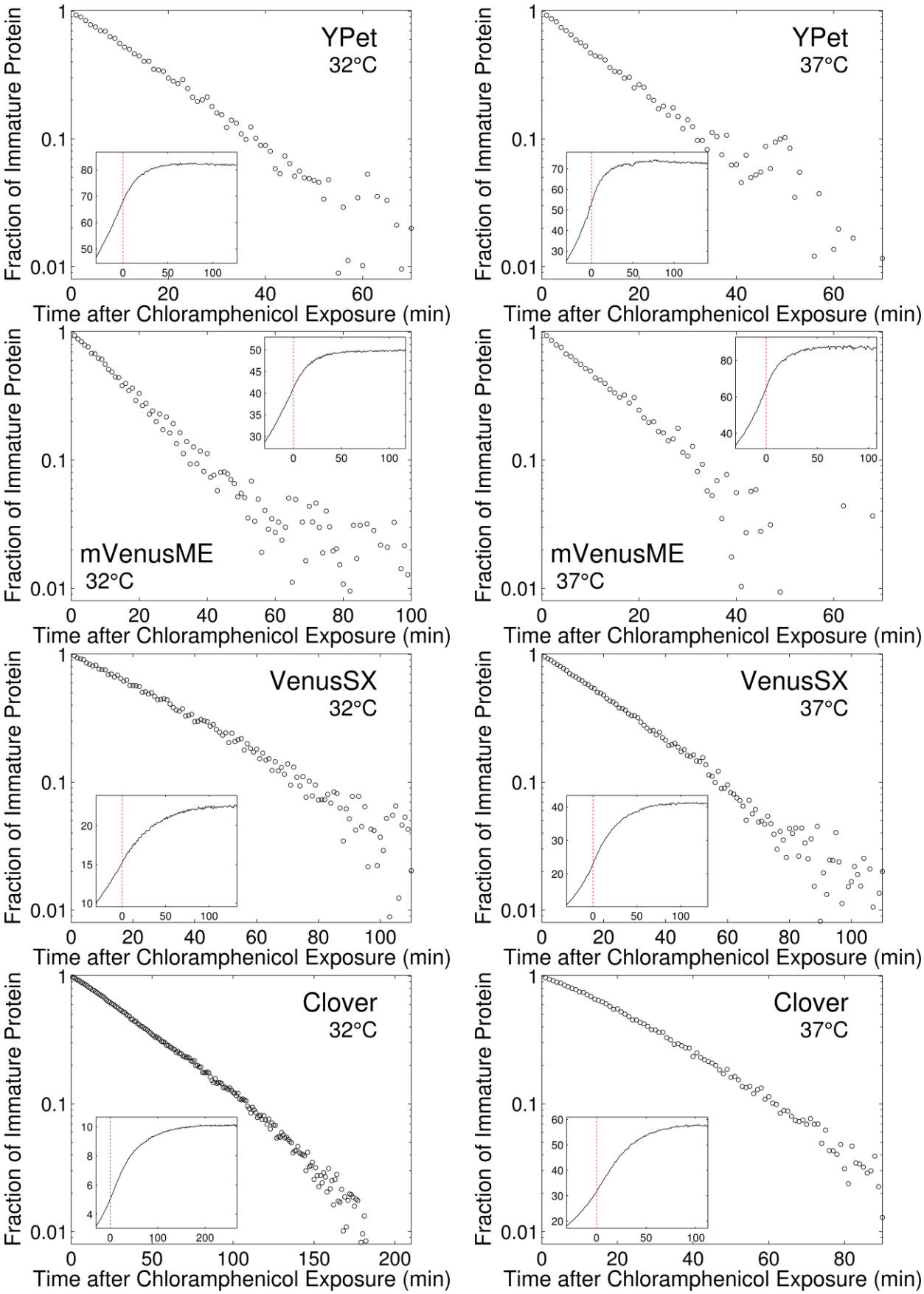

Nature Methods: doi:10.1038/nmeth.4509

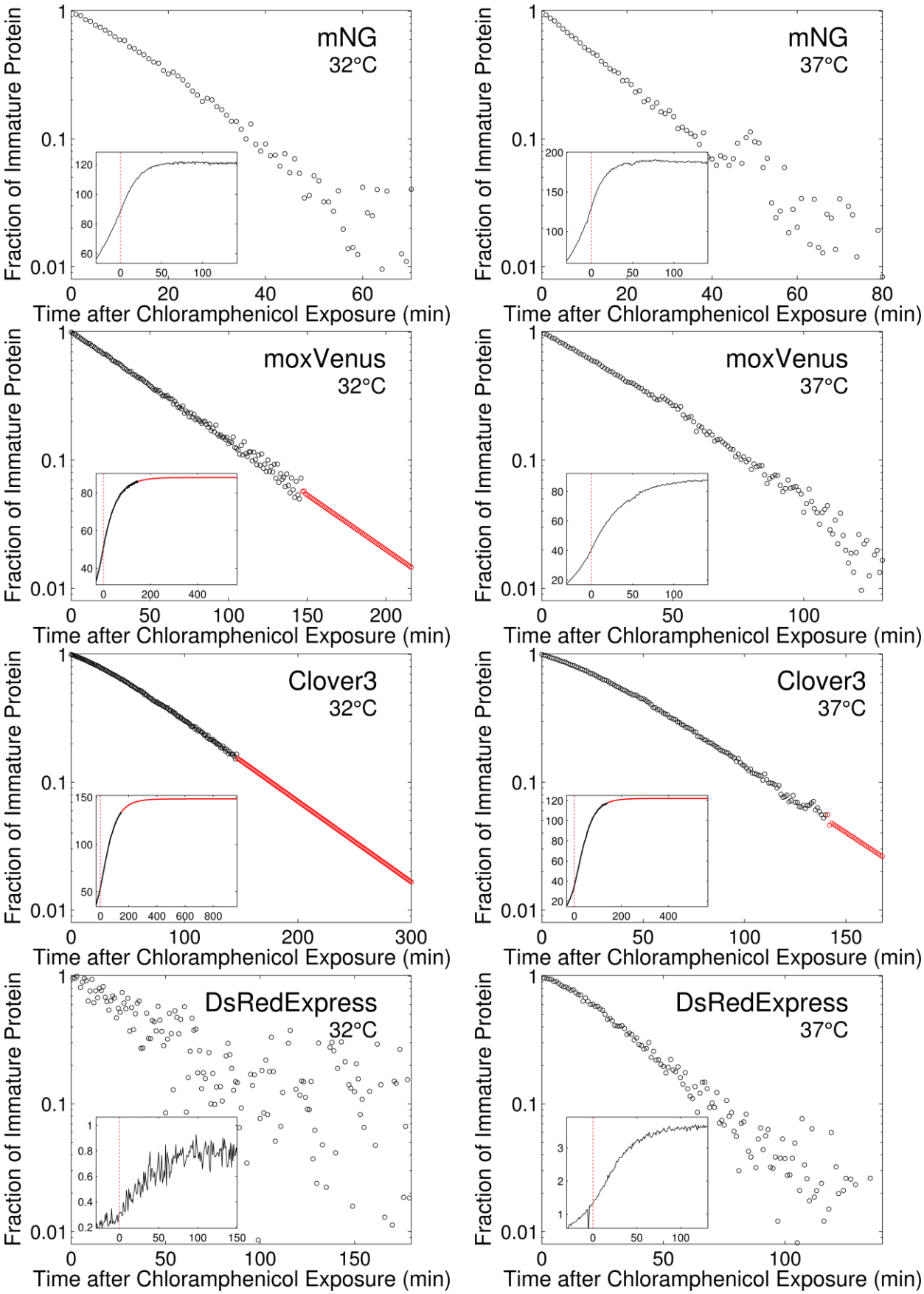
mNG
32°C
mNG
37°C
moxVenus
32°C
moxVenus
37°C
Clover3
32°C
Clover3
37°C
DsRedExpress
32°C
DsRedExpress
37°C
Fraction of Immature Protein
Time after Chloramphenicol Exposure (min)

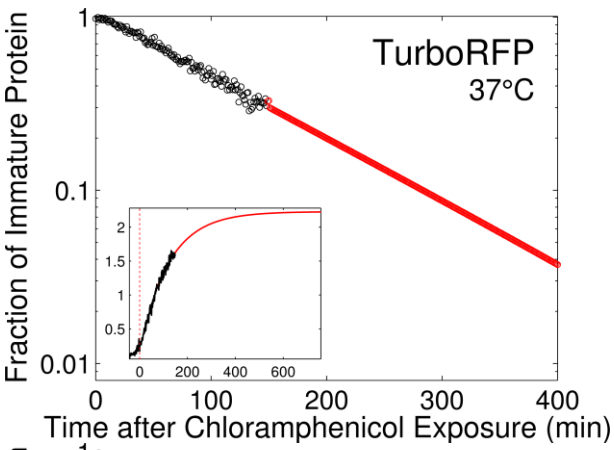
TurboRFP
37°C
Fraction of Immature Protein
Time after Chloramphenicol Exposure (min)

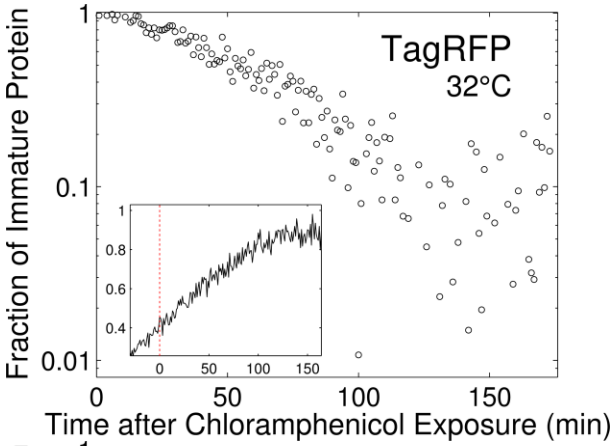
TagRFP
32°C
Fraction of Immature Protein
Time after Chloramphenicol Exposure (min)

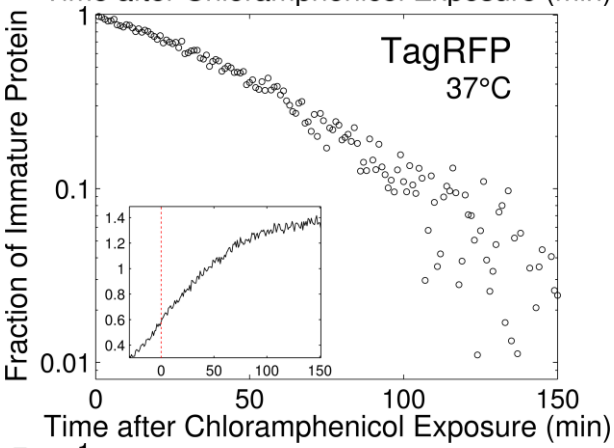
TagRFP
37°C
Fraction of Immature Protein
Time after Chloramphenicol Exposure (min)

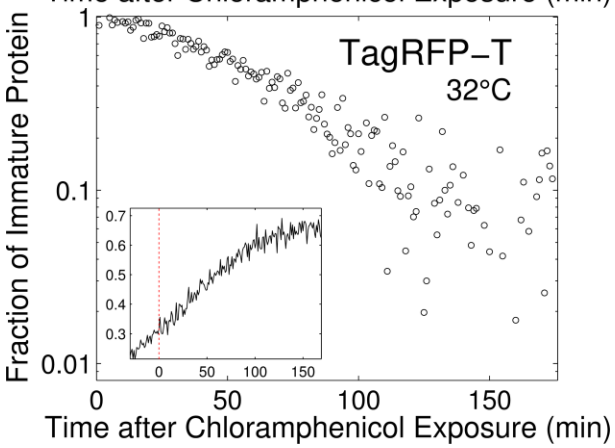
TagRFP−T
32°C
Fraction of Immature Protein
Time after Chloramphenicol Exposure (min)

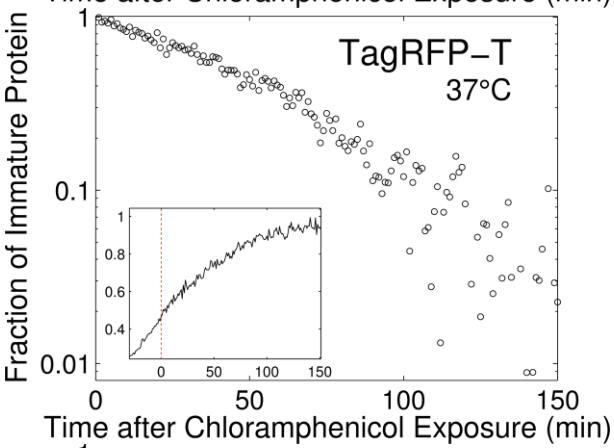
TagRFP−T
37°C
Fraction of Immature Protein
Time after Chloramphenicol Exposure (min)

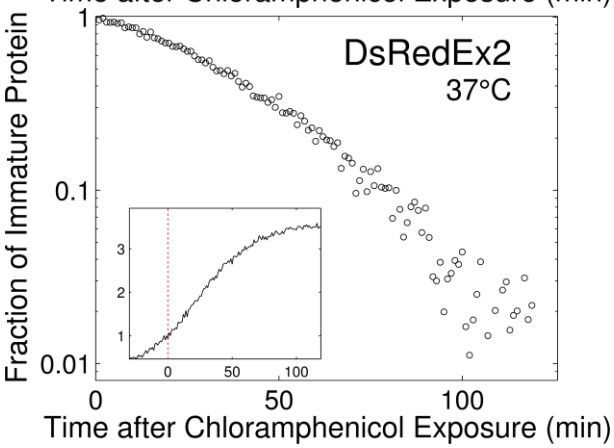
DsRedEx2
37°C
Fraction of Immature Protein
Time after Chloramphenicol Exposure (min)

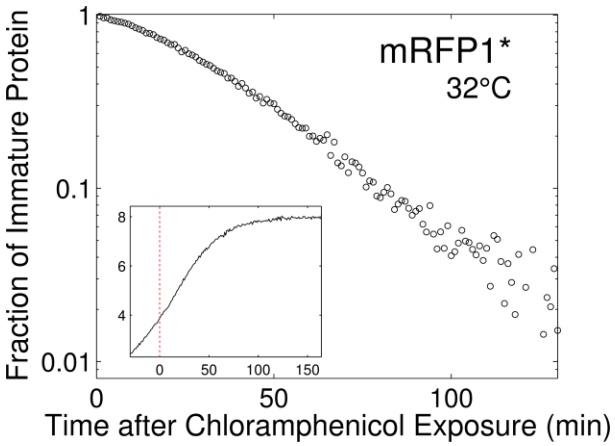
mRFP1*
32°C
Fraction of Immature Protein
Time after Chloramphenicol Exposure (min)

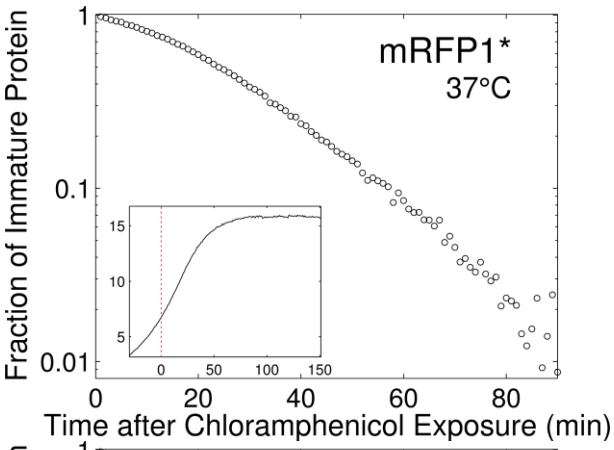
mRFP1*
37°C
Fraction of Immature Protein
Time after Chloramphenicol Exposure (min)

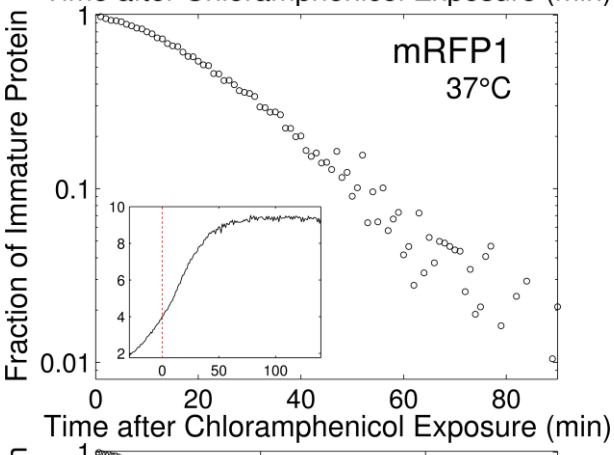
mRFP1
37°C
Fraction of Immature Protein
Time after Chloramphenicol Exposure (min)

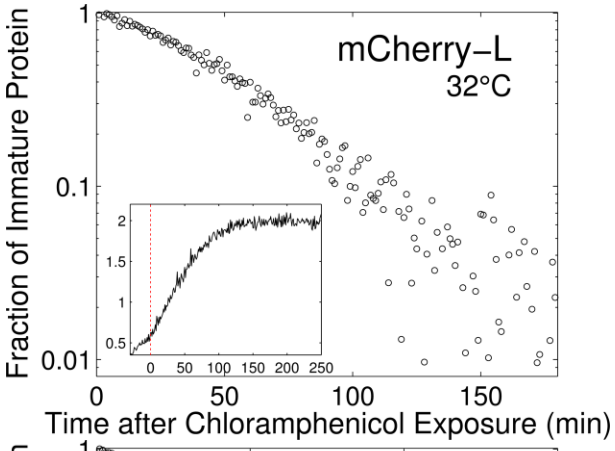
mCherry−L
32°C
Fraction of Immature Protein
Time after Chloramphenicol Exposure (min)

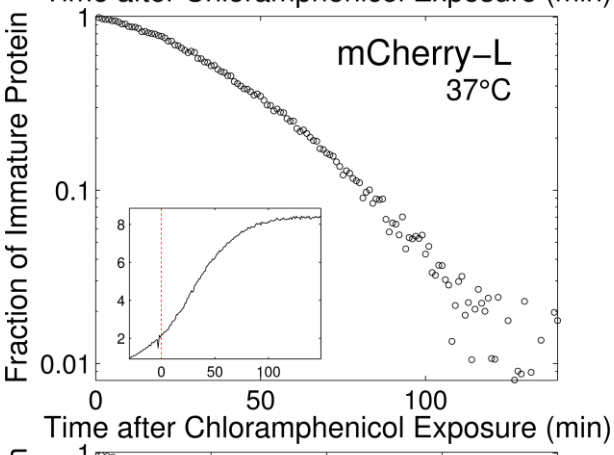
mCherry−L
37°C
Fraction of Immature Protein
Time after Chloramphenicol Exposure (min)

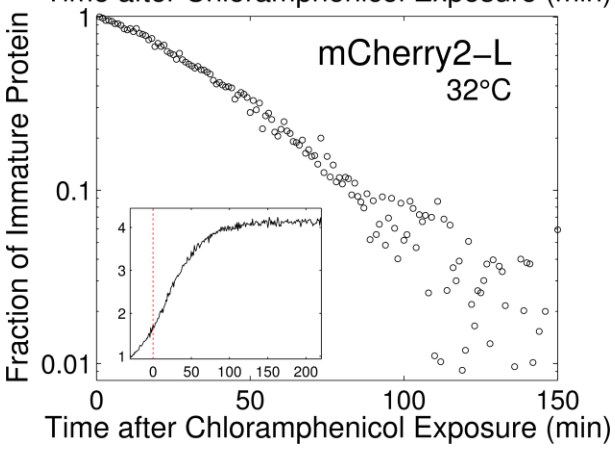
mCherry2−L
32°C
Fraction of Immature Protein
Time after Chloramphenicol Exposure (min)

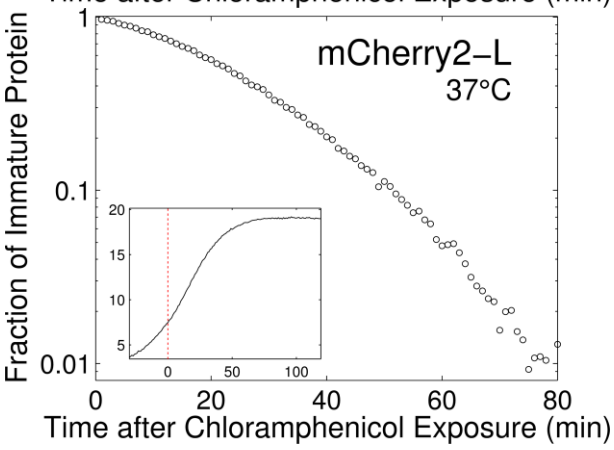
mCherry2−L
37°C
Fraction of Immature Protein
Time after Chloramphenicol Exposure (min)

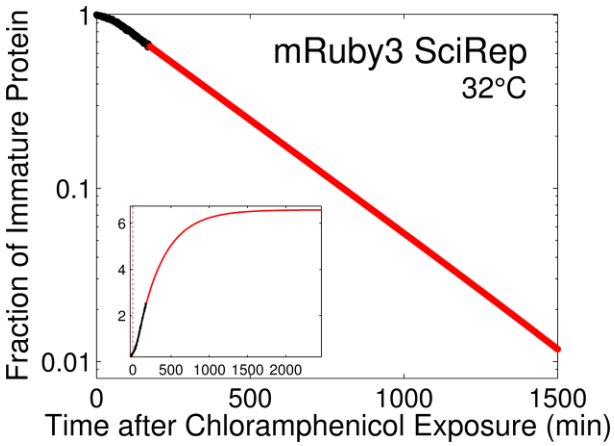
mRuby3 SciRep
32°C
Fraction of Immature Protein
Time after Chloramphenicol Exposure (min)

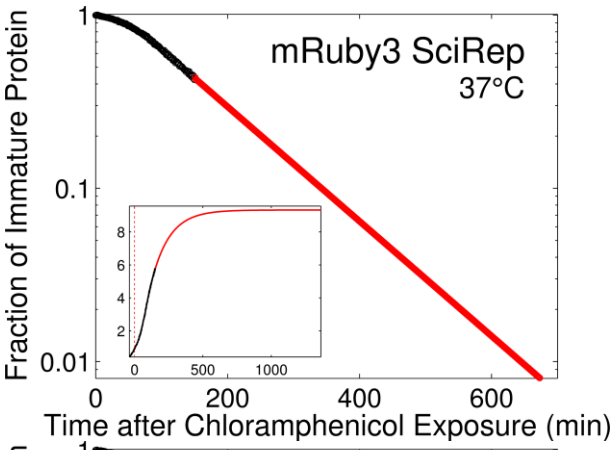
mRuby3 SciRep
37°C
Fraction of Immature Protein
Time after Chloramphenicol Exposure (min)

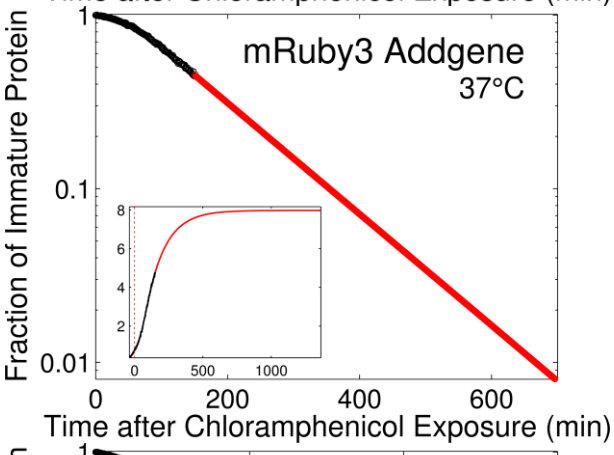
mRuby3 Addgene
37°C
Fraction of Immature Protein
Time after Chloramphenicol Exposure (min)

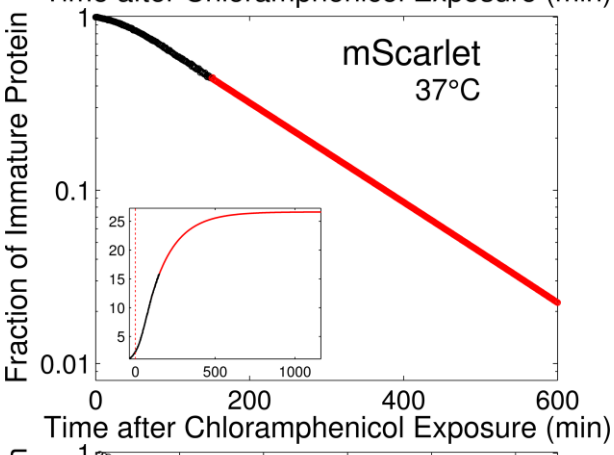
mScarlet
37°C
Fraction of Immature Protein
Time after Chloramphenicol Exposure (min)

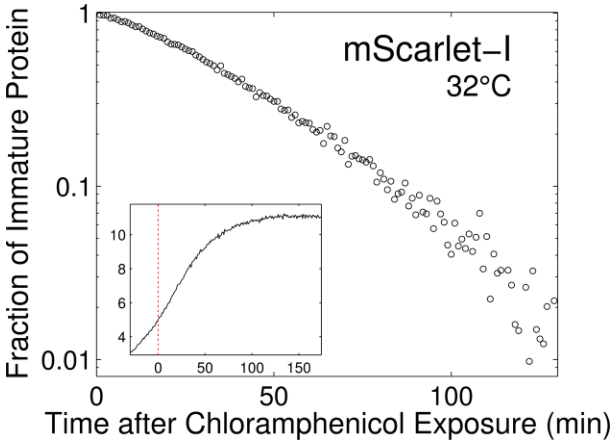
mScarlet–I
32°C
Fraction of Immature Protein
Time after Chloramphenicol Exposure (min)

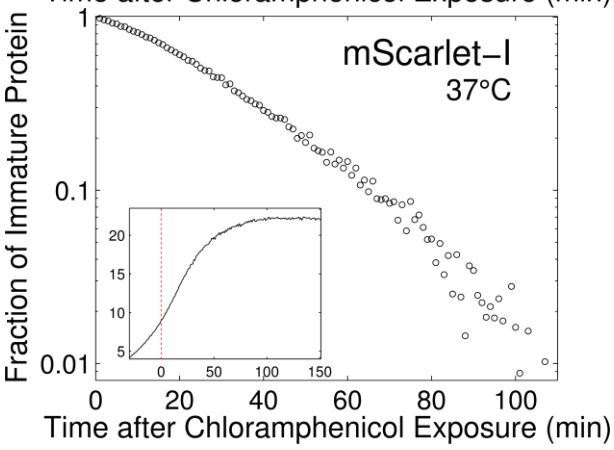
mScarlet–I
37°C
Fraction of Immature Protein
Time after Chloramphenicol Exposure (min)

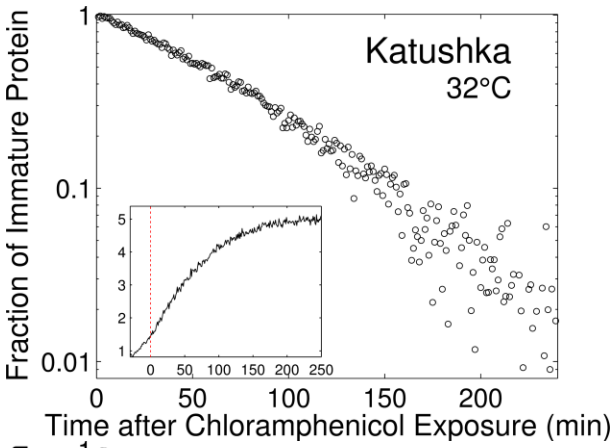
Katushka
32°C
Fraction of Immature Protein
Time after Chloramphenicol Exposure (min)

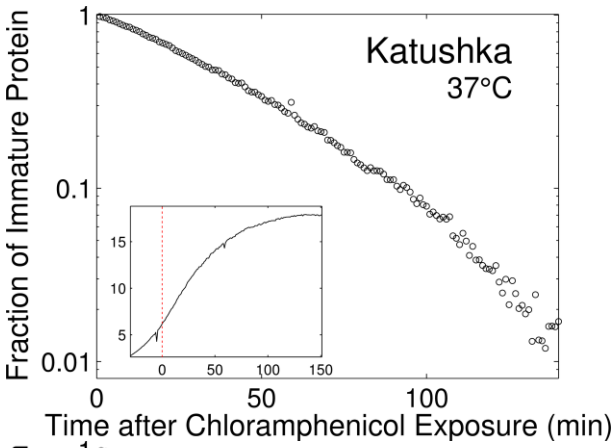
Katushka
37°C
Fraction of Immature Protein
Time after Chloramphenicol Exposure (min)

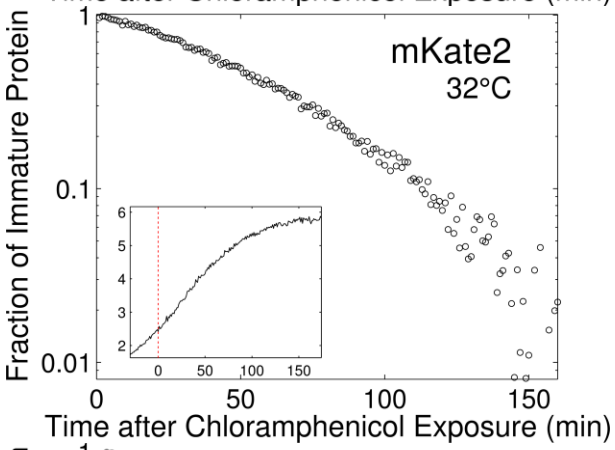
mKate2
32°C
Fraction of Immature Protein
Time after Chloramphenicol Exposure (min)

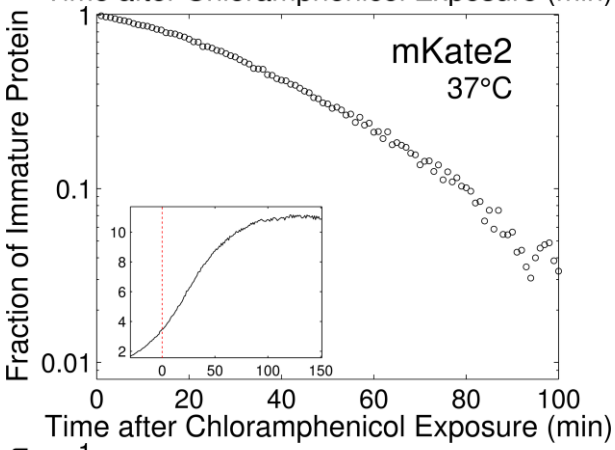
mKate2
37°C
Fraction of Immature Protein
Time after Chloramphenicol Exposure (min)

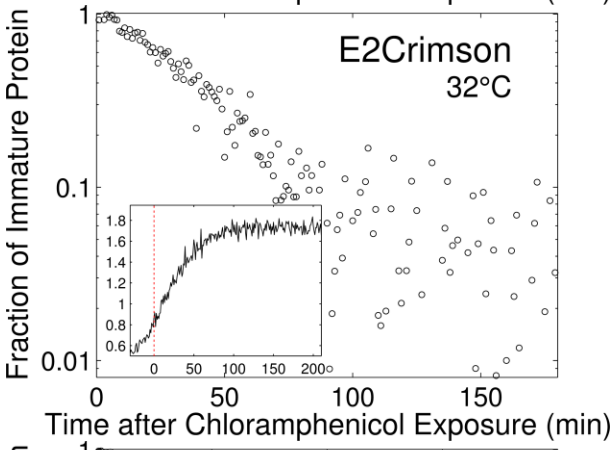
E2Crimson
32°C
Fraction of Immature Protein
Time after Chloramphenicol Exposure (min)

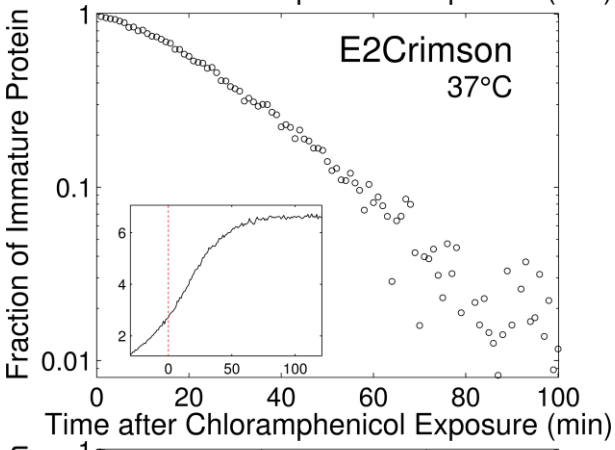
E2Crimson
37°C
Fraction of Immature Protein
Time after Chloramphenicol Exposure (min)

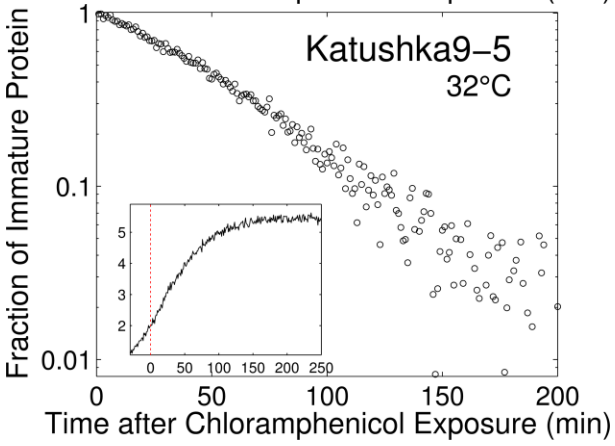
Katushka9−5
32°C
Fraction of Immature Protein
Time after Chloramphenicol Exposure (min)

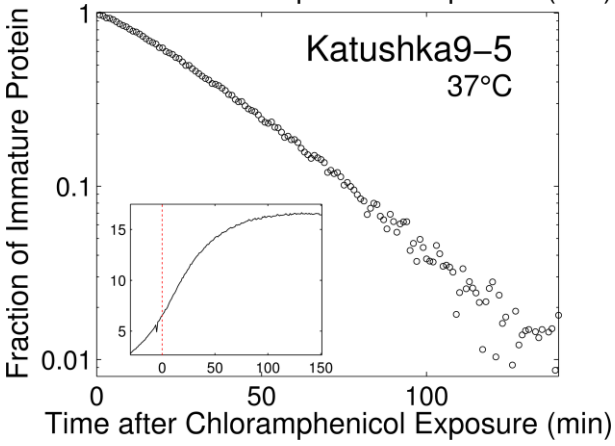
Katushka9−5
37°C
Fraction of Immature Protein
Time after Chloramphenicol Exposure (min)

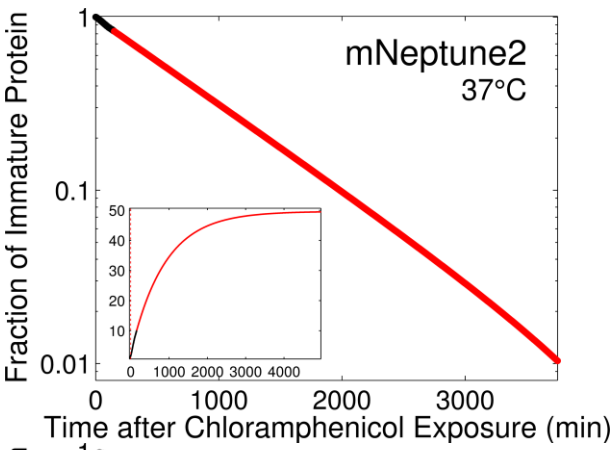

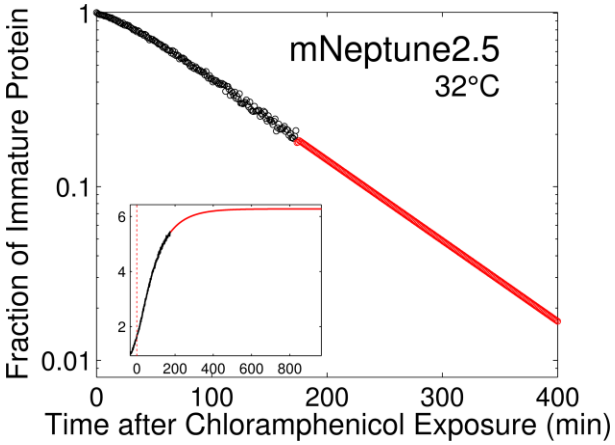

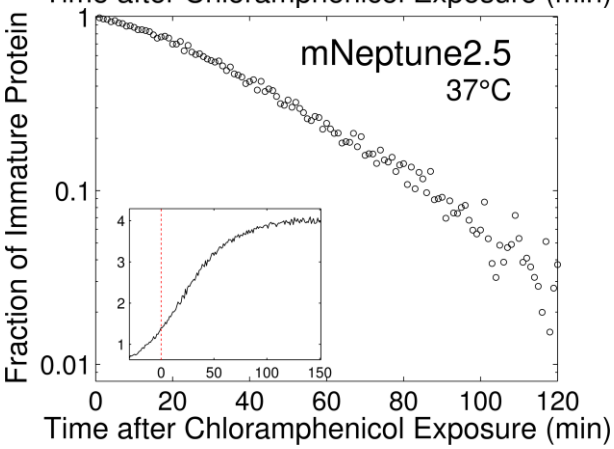

Fraction of Immature Protein for codon optimized and 2nd Valine FPs

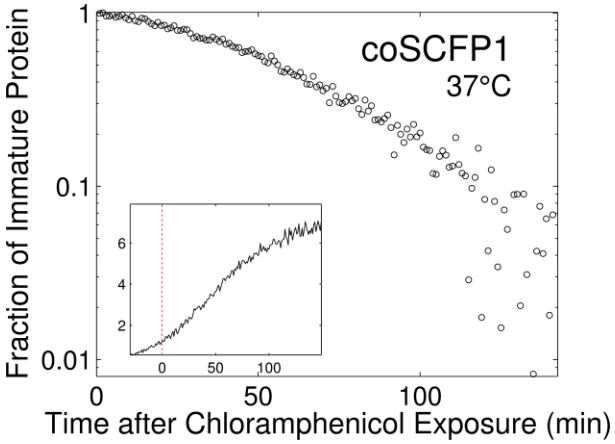

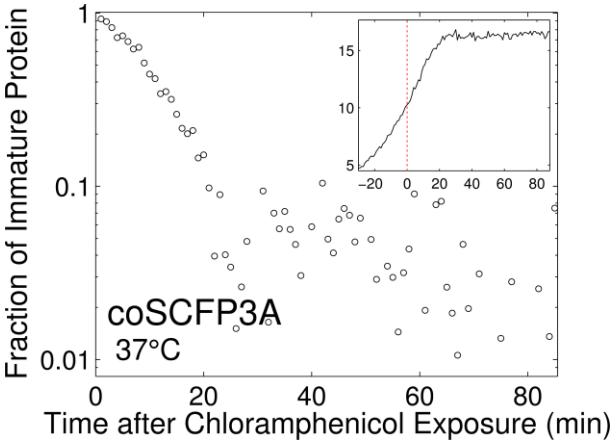

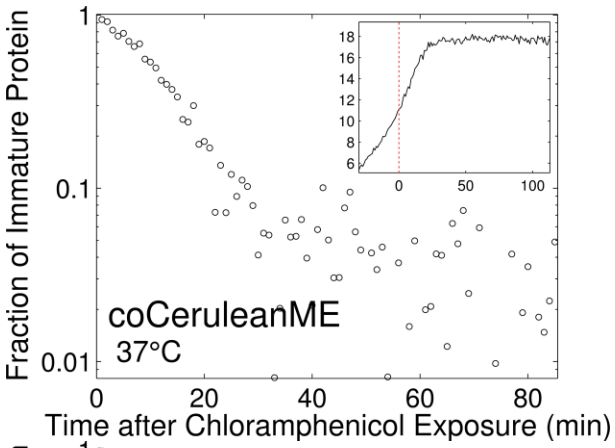

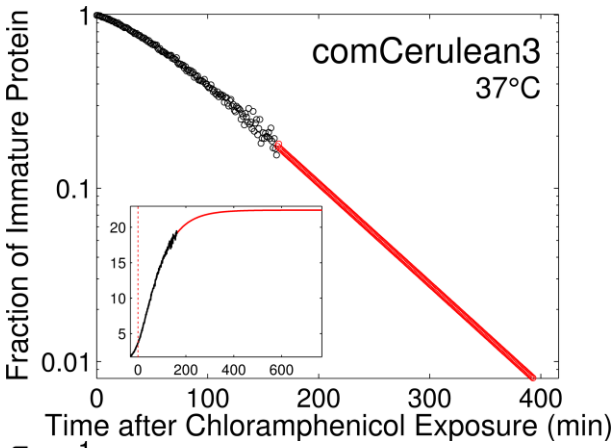

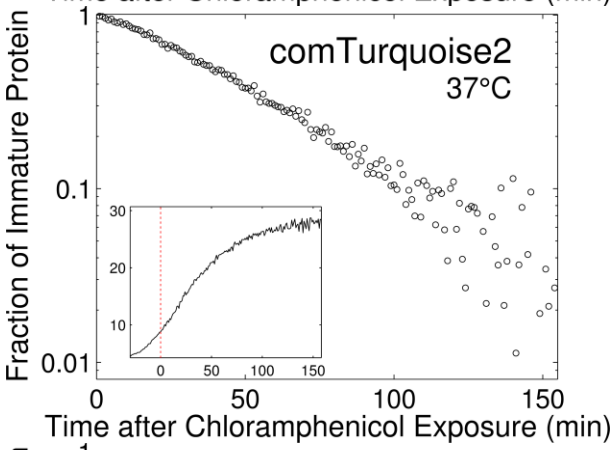

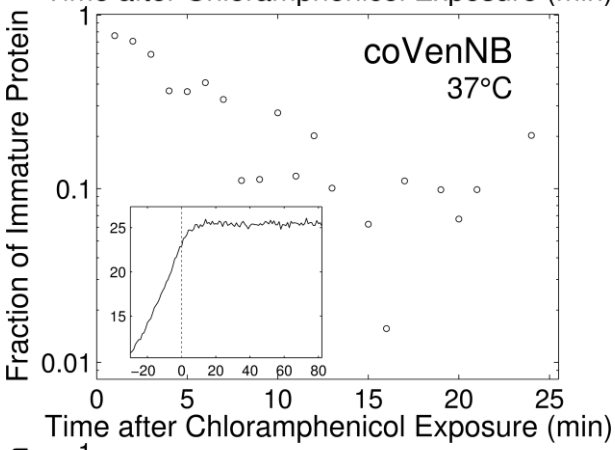

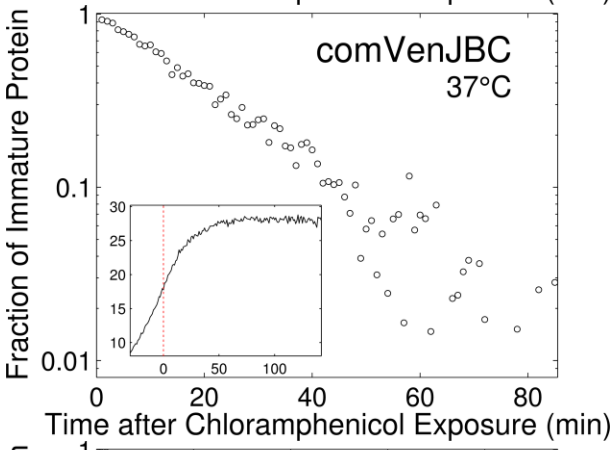

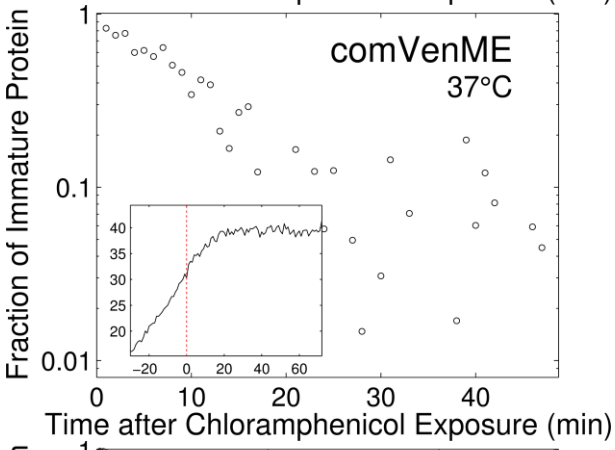

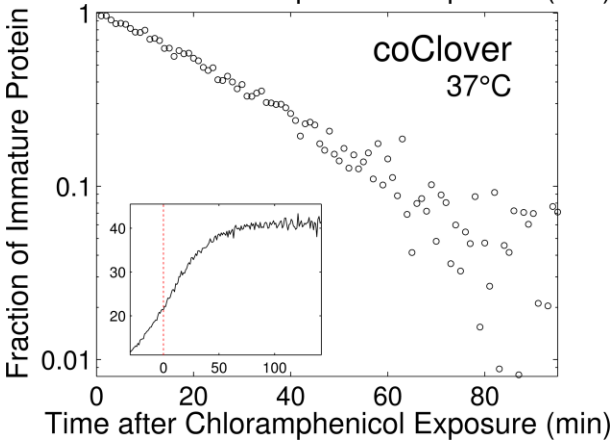

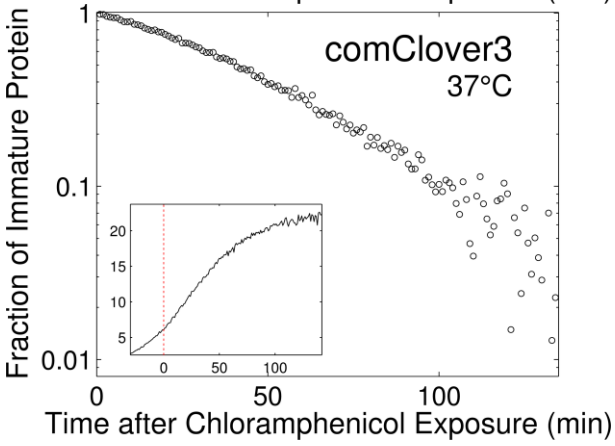

Nature Methods: doi:10.1038/nmeth.4509

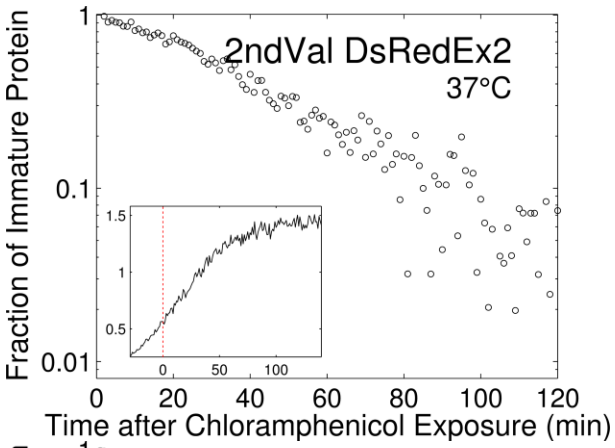
2ndVal DsRedEx2
37°C
Fraction of Immature Protein
Time after Chloramphenicol Exposure (min)

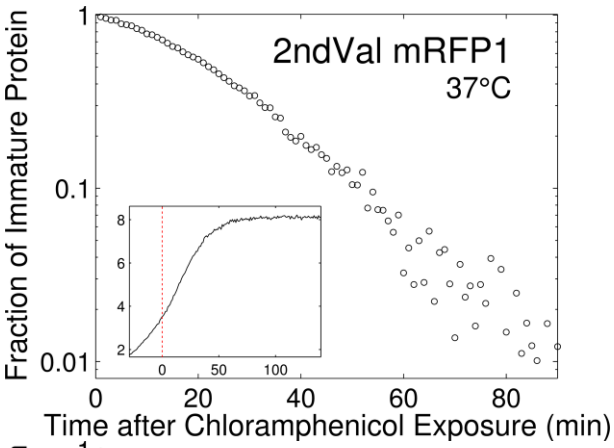
2ndVal mRFP1
37°C
Fraction of Immature Protein
Time after Chloramphenicol Exposure (min)

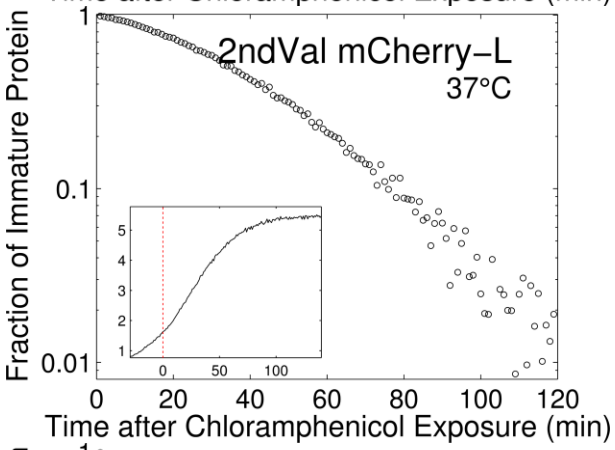
2ndVal mCherry−L
37°C
Fraction of Immature Protein
Time after Chloramphenicol Exposure (min)

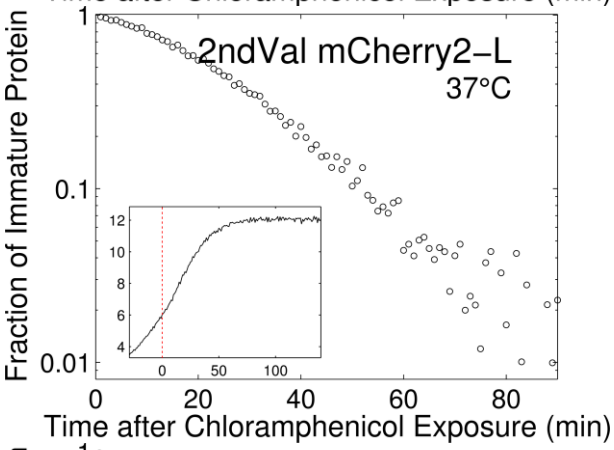
2ndVal mCherry2−L
37°C
Fraction of Immature Protein
Time after Chloramphenicol Exposure (min)

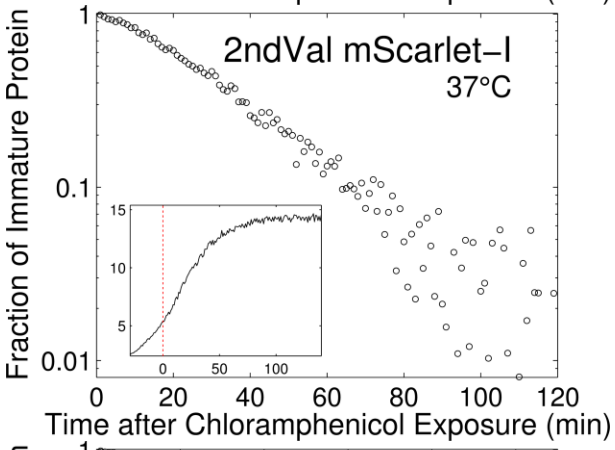
2ndVal mScarlet−I
37°C
Fraction of Immature Protein
Time after Chloramphenicol Exposure (min)

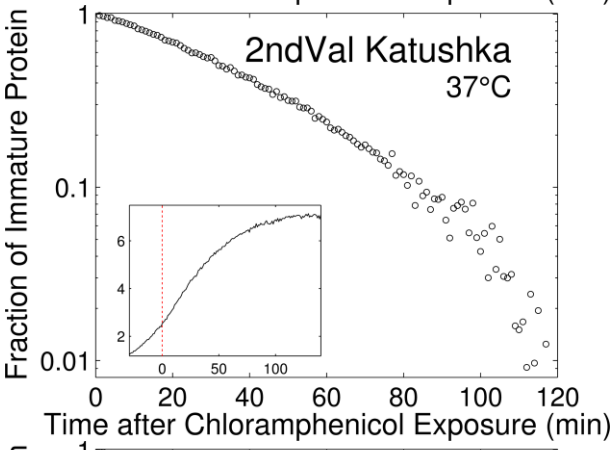
2ndVal Katushka
37°C
Fraction of Immature Protein
Time after Chloramphenicol Exposure (min)

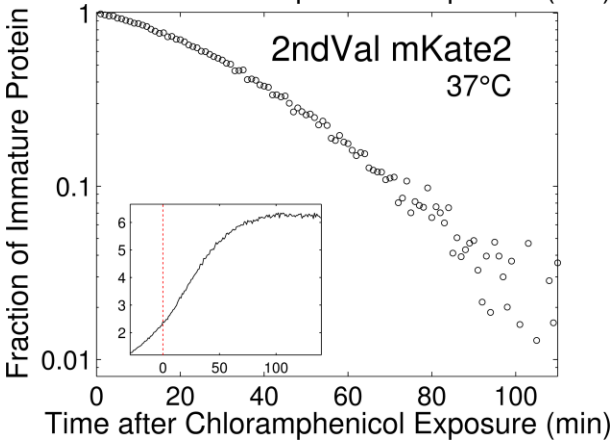
2ndVal mKate2
37°C
Fraction of Immature Protein
Time after Chloramphenicol Exposure (min)

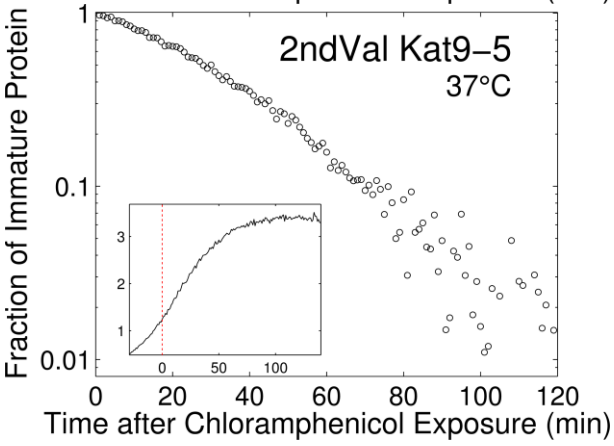
2ndVal Kat9−5
37°C
Fraction of Immature Protein
Time after Chloramphenicol Exposure (min)

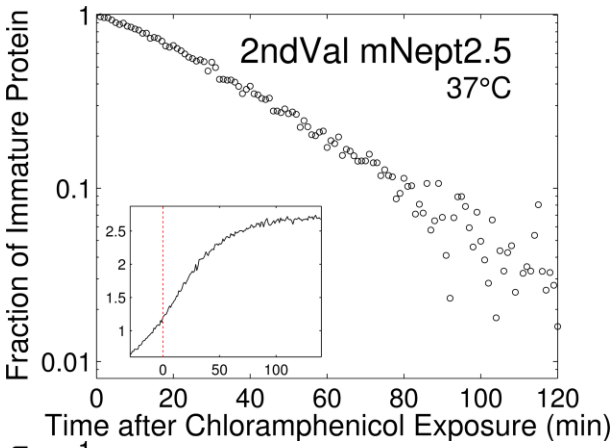

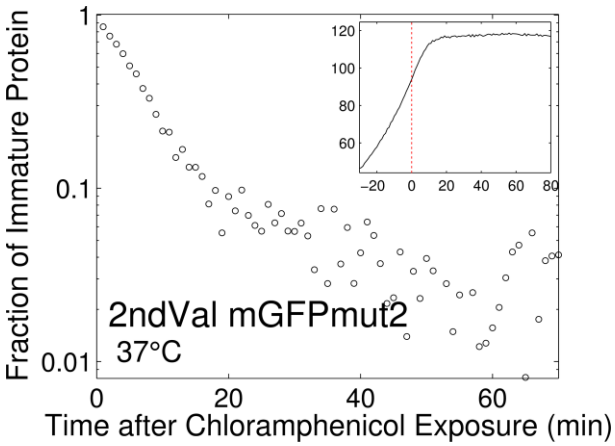

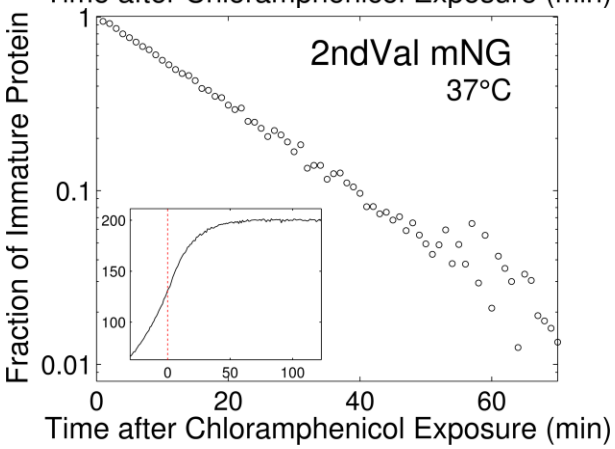

10 Supplementary References

1. Tsien RY (1998) The green fluorescent protein. *Annu Rev Biochem* 67:509-544.
2. Shaner NC, Steinbach PA, & Tsien RY (2005) A guide to choosing fluorescent proteins. *Nat Methods* 2(12):905-909.
3. Kremers GJ, Goedhart J, van Munster EB, & Gadella TW, Jr. (2006) Cyan and yellow super fluorescent proteins with improved brightness, protein folding, and FRET Forster radius. *Biochemistry* 45(21):6570-6580.
4. Markwardt ML*, et al.* (2011) An improved cerulean fluorescent protein with enhanced brightness and reduced reversible photoswitching. *PLoS One* 6(3):e17896.
5. Rizzo MA, Springer GH, Granada B, & Piston DW (2004) An improved cyan fluorescent protein variant useful for FRET. *Nat Biotechnol* 22(4):445-449.
6. Heim R & Tsien RY (1996) Engineering green fluorescent protein for improved brightness, longer wavelengths and fluorescence resonance energy transfer. *Curr Biol* 6(2):178-182.
7. Llopis J, McCaffery JM, Miyawaki A, Farquhar MG, & Tsien RY (1998) Measurement of cytosolic, mitochondrial, and Golgi pH in single living cells with green fluorescent proteins. *P Natl Acad Sci USA* 95(12):6803-6808.
8. Cubitt AB, Woollenweber LA, & Heim R (1999) Understanding structure-function relationships in the Aequorea victoria green fluorescent protein. *Methods Cell Biol* 58:19-30.
9. Nagai T*, et al.* (2002) A variant of yellow fluorescent protein with fast and efficient maturation for cell-biological applications. *Nat Biotechnol* 20(1):87-90.

10. Rekas A, Alattia JR, Nagai T, Miyawaki A, & Ikura M (2002) Crystal structure of venus, a yellow fluorescent protein with improved maturation and reduced environmental sensitivity. *J Biol Chem* 277(52):50573-50578.
11. Cox RS, 3rd, Dunlop MJ, & Elowitz MB (2010) A synthetic three-color scaffold for monitoring genetic regulation and noise. *J Biol Eng* 4:10.
12. Choi PJ, Cai L, Frieda K, & Xie S (2008) A stochastic single-molecule event triggers phenotype switching of a bacterial cell. *Science* 322(5900):442-446.
13. Bevis BJ & Glick BS (2002) Rapidly maturing variants of the Discosoma red fluorescent protein (DsRed). *Nat Biotechnol* 20(1):83-87.
14. Merzlyak EM*, et al.* (2007) Bright monomeric red fluorescent protein with an extended fluorescence lifetime. *Nat Methods* 4(7):555-557.
15. Kredel S*, et al.* (2009) mRuby, a bright monomeric red fluorescent protein for labeling of subcellular structures. *PLoS One* 4(2):e4391.
16. Bajar BT*, et al.* (2016) Improving brightness and photostability of green and red fluorescent proteins for live cell imaging and FRET reporting. *Sci Rep* 6:20889.
17. Carroll P, Muwanguzi-Karugaba J, Melief E, Files M, & Parish T (2014) Identification of the translational start site of codon-optimized mCherry in Mycobacterium tuberculosis. *BMC Res Notes* 7:366.
18. Goedhart J*, et al.* (2010) Bright cyan fluorescent protein variants identified by fluorescence lifetime screening. *Nat Methods* 7(2):137-139.
19. Goedhart J*, et al.* (2012) Structure-guided evolution of cyan fluorescent proteins towards a quantum yield of 93%. *Nat Commun* 3.
20. Costantini LM*, et al.* (2015) A palette of fluorescent proteins optimized for diverse cellular environments. *Nat Commun* 6:7670.
21. Zapata-Hommer O & Griesbeck O (2003) Efficiently folding and circularly permuted variants of the Sapphire mutant of GFP. *BMC Biotechnol* 3:5.
22. Cormack BP, Valdivia RH, & Falkow S (1996) FACS-optimized mutants of the green fluorescent protein (GFP). *Gene* 173(1):33-38.
23. Pedelacq JD, Cabantous S, Tran T, Terwilliger TC, & Waldo GS (2006) Engineering and characterization of a superfolder green fluorescent protein. *Nat Biotechnol* 24(1):79-88.
24. Nguyen AW & Daugherty PS (2005) Evolutionary optimization of fluorescent proteins for intracellular FRET. *Nat Biotechnol* 23(3):355-360.
25. Lam AJ*, et al.* (2012) Improving FRET dynamic range with bright green and red fluorescent proteins. *Nat Methods* 9(10):1005-1012.
26. Shaner NC*, et al.* (2008) Improving the photostability of bright monomeric orange and red fluorescent proteins. *Nat Methods* 5(6):545-551.
27. Strack RL*, et al.* (2008) A noncytotoxic DsRed variant for whole-cell labeling. *Nat Methods* 5(11):955-957.
28. Campbell RE*, et al.* (2002) A monomeric red fluorescent protein. *Proc Natl Acad Sci U S A* 99(12):7877-7882.
29. Shaner NC*, et al.* (2004) Improved monomeric red, orange and yellow fluorescent proteins derived from Discosoma sp red fluorescent protein. *Nat Biotechnol* 22(12):1567-1572.
30. Shen Y, Chen Y, Wu J, Shaner NC, & Campbell RE (2017) Engineering of mCherry variants with long Stokes shift, red-shifted fluorescence, and low cytotoxicity. *PLoS One* 12(2):e0171257.
31. Bindels DS*, et al.* (2017) mScarlet: a bright monomeric red fluorescent protein for cellular imaging. *Nat Methods* 14(1):53-56.
32. Shcherbo D*, et al.* (2007) Bright far-red fluorescent protein for whole-body imaging. *Nat Methods* 4(9):741-746.

33. Strack RL*, et al.* (2009) A Rapidly Maturing Far-Red Derivative of DsRed-Express2 for Whole-Cell Labeling (vol 48, pg 8279, 2009). *Biochemistry* 48(40):9704-9704.
34. Shcherbo D*, et al.* (2010) Near-infrared fluorescent proteins. *Nat Methods* 7(10):827-U1520.
35. Chu J*, et al.* (2014) Non-invasive intravital imaging of cellular differentiation with a bright red-excitable fluorescent protein. *Nat Methods* 11(5):572-578.
36. Sinnecker D, Voigt P, Hellwig N, & Schaefer M (2005) Reversible photobleaching of enhanced green fluorescent proteins. *Biochemistry* 44(18):7085-7094.
37. Shaner NC*, et al.* (2008) Improving the photostability of bright monomeric orange and red fluorescent proteins. *Nat Methods* 5(6):545-551.
38. Cranfill PJ*, et al.* (2016) Quantitative assessment of fluorescent proteins. *Nat Methods* 13(7):557-562.
39. Ward WW (2005) Biochemical and Physical Properties of Green Fluorescent Protein. *Green Fluorescent Protein*, (John Wiley & Sons, Inc.), pp 39-65.
40. Patterson GH, Knobel SM, Sharif WD, Kain SR, & Piston DW (1997) Use of the green fluorescent protein and its mutants in quantitative fluorescence microscopy. *Biophys J* 73(5):2782-2790.
41. Shcherbo D*, et al.* (2007) Bright far-red fluorescent protein for whole-body imaging. *Nat Methods* 4(9):741-746.
42. Bevis BJ & Glick BS (2002) Rapidly maturing variants of the Discosoma red fluorescent protein (DsRed). *Nat Biotechnol* 20(1):83-87.
43. Moffitt JR, Lee JB, & Cluzel P (2012) The single-cell chemostat: an agarose-based, microfluidic device for high-throughput, single-cell studies of bacteria and bacterial communities. *Lab Chip* 12(8):1487-1494.
44. Gu WJ, Zhou T, & Wilke CO (2010) A Universal Trend of Reduced mRNA Stability near the Translation-Initiation Site in Prokaryotes and Eukaryotes. *Plos Comput Biol* 6(2).
45. Kudla G, Murray AW, Tollervey D, & Plotkin JB (2009) Coding-Sequence Determinants of Gene Expression in Escherichia coli. *Science* 324(5924):255-258.
46. Hayashi F (2000) *Econometrics* (Princeton University Press, Princeton) pp xxiii, 683 p.
47. Gross LA, Baird GS, Hoffman RC, Baldridge KK, & Tsien RY (2000) The structure of the chromophore within DsRed, a red fluorescent protein from coral. *Proc Natl Acad Sci U S A* 97(22):11990-11995.
48. Abdelhamid MA*, et al.* (2014) Affinity purification of recombinant proteins using a novel silica-binding peptide as a fusion tag. *Appl Microbiol Biotechnol* 98(12):5677-5684.
49. Ishida M & Oshima T (2002) Effective structure of a leader open reading frame for enhancing the expression of GC-rich genes. *J Biochem* 132(1):63-70.